Environmental Research 261 (2024) 119719

Contents lists available at ScienceDirect

Environmental Research

journal homepage: www.elsevier.com/locate/envres

Review article

Innovative techniques for combating a common enemy forever chemicals: A comprehensive approach to mitigating per- and polyfluoroalkyl substances (PFAS) contamination

Ajibola A. Bayode [a,b,*], Stephen Sunday Emmanuel [c,**], Amos O. Akinyemi [d], Odunayo T. Ore [e], Samson O. Akpotu [f], Daniel T. Koko [b], David E. Momodu [b], Eduardo Alberto López-Maldonado [g]

[a] College of Chemical Engineering, Sichuan University of Science and Engineering, Zigong, 643000, China
[b] Department of Chemical Sciences, Faculty of Natural Sciences, Redeemer's University, P.M.B. 230, 232101, Ede, Nigeria
[c] Department of Industrial Chemistry, Faculty of Physical Sciences, University of Ilorin, P. M. B. 1515, Ilorin, Nigeria
[d] Department of Toxicology & Cancer Biology, University of Kentucky, Lexington, KY, 40536, USA
[e] Department of Chemical Sciences, Achievers University, P.M.B. 1030, Owo, Nigeria
[f] Department of Chemistry, Vaal University of Technology, Vanderbijlpark, 1900, Gauteng, South Africa
[g] Faculty of Chemical Sciences and Engineering, Autonomous University of Baja California, 22424, Tijuana, B.C., Mexico

ARTICLE INFO

Keywords:
PFAS
Adsorption
Remediation
Advanced oxidation processes
Membrane filtration

ABSTRACT

The pervasive presence of per and polyfluoroalkyl substances (PFAS), commonly referred to as "forever chemicals," in water systems poses a significant threat to both the environment and public health. PFAS are persistent organic pollutants that are incredibly resistant to degradation and have a tendency to accumulate in the environment, resulting in long-term contamination issues. This comprehensive review delves into the primary impacts of PFAS on both the environment and human health while also delving into advanced techniques aimed at addressing these concerns. The focus is on exploring the efficacy, practicality, and sustainability of these methods. The review outlines several key methods, such as advanced oxidation processes, novel materials adsorption, bioremediation, membrane filtration, and in-situ chemical oxidation, and evaluates their effectiveness in addressing PFAS contamination. By conducting a comparative analysis of these techniques, the study aims to provide a thorough understanding of current PFAS remediation technologies, as well as offer insights into integrated approaches for managing these persistent pollutants effectively. While acknowledging the high efficiency of adsorption and membrane filtration in reducing persistent organic pollutants due to their relatively low cost, versatility, and wide applicability, the review suggests that the integration of these methods could result in an overall enhancement of removal performance. Additionally, the study emphasizes the need for researcher attention in key areas and underscores the necessity of collaboration between researchers, industry, and regulatory authorities to address this complex challenge.

1. Introduction

Per- and poly-fluoroalkyl substances (PFAS) are synthetic organic compounds that have been widely employed since the 1940s in a variety of industrial and consumer products (Wang et al., 2017). Their particular qualities, including heat, water, and oil resistance, make them popular ingredients in food packaging, water-repellent fabrics, no-stick cookware, and firefighting foams (Glüge et al., 2020). PFAS are distinguished by their strong carbon-fluorine linkages, which aid in their resistance to degradation and persistence in the environment (Abunada et al., 2020; Dias et al., 2024). However, while this durability is useful in industrial applications, it also poses substantial environmental and health hazards. Research on efficient removal techniques has been spurred by the widespread concern over PFAS contamination in water bodies (Brendel et al., 2018; Hamid et al., 2018).

Per- and poly-fluoroalkyl substances (PFAS) are ubiquitous contaminants present in a range of environmental media, such as soil, surface and groundwater, and the tissues of living things (Kurwadkar

* Corresponding author. College of Chemical Engineering, Sichuan University of Science and Engineering, Zigong, 643000, China.
** Corresponding author.
E-mail addresses: bayodea@run.edu.ng (A.A. Bayode), stephenemmanuel6011@gmail.com (S.S. Emmanuel).

https://doi.org/10.1016/j.envres.2024.119719
Received 18 June 2024; Received in revised form 24 July 2024; Accepted 31 July 2024
Available online 3 August 2024

et al., 2022; Panieri et al., 2022). Because PFAS are persistent, they can build up over time and result in higher concentrations in the environment (Cousins et al., 2020; Sinclair et al., 2020). Risks of long-term exposure to this exist for both people and wildlife. Based on available evidence, PFAS has been linked to cancer, thyroid disorders, high cholesterol, obesity, liver damage, impaired fertility, and hormone suppression (Post et al., 2012; Sunderland et al., 2019). Therefore, eliminating PFAS from contaminated water sources is essential to reducing these hazards.

Owing to their chemical stability and solubility in water, PFAS are difficult to eliminate using conventional water treatment techniques (Wanninayake, 2021; Vu and Wu, 2022). Because PFAS resist degradation and persist in water, conventional methods like coagulation, flocculation, sedimentation, and biological treatment are typically ineffective against them (Merino et al., 2016). Therefore, to successfully manage PFAS contamination, innovative and specialized treatment technologies have become needed.

Three primary strategies have been the focus of recent developments in PFAS removal technologies: membrane filtration, advanced oxidation processes (AOPs), and adsorption (Yadav et al., 2022). Of these, adsorption is the most studied and makes use of substances like carbon nanotubes (CNTs), metal-organic frameworks (MOFs), covalent organic frameworks, and ion exchange resins in addition to materials like activated carbon (Zango et al., 2020; Emmanuel et al., 2024a,b,c,d,e). Because of their high surface area and porosity, which allow for efficient PFAS adsorption, granular activated carbon (GAC) and powdered activated carbon (PAC) are frequently used (Appleman et al., 2014). However, depending on the specific PFAS compound and co-contaminants, there is variation in the efficacy of activated carbon (Yuan et al., 2022a). However, the selective adsorption of negatively charged PFAS molecules by anion exchange resins is a reflection of their great potential for removing PFAS. Studies reveal that these resins are capable of removing a wide range of PFAS compounds with good removal efficiencies (Carter and Farrell, 2010; Dixit et al., 2021b). Current advancements are intended to improve resin capacity and selectivity, which will raise overall performance and cost-effectiveness. Similarly, recent developments in adsorbent materials, such as carbon nanotubes (CNTs) and metal-organic frameworks (MOFs), have shown promise in the removal of PFAS from water. MOFs can be particularly tailored to preferentially adsorb PFAS. MOFs are crystalline materials with high porosity and variable surface chemistry (Karbassiyazdi et al., 2023). Comparably, the capacity of CNTs to adsorb PFAS has been investigated. CNTs are noted for their enormous surface area and distinctive structural characteristics. These novel materials have the potential to increase the selectivity and effectiveness of PFAS removal (Felix Sahayaraj et al., 2023).

Even though tremendous progress has been achieved in creating methods for eliminating PFAS from water, further research is necessary to address several important issues. The creation of large-scale, economically viable, and environmentally friendly treatment options is a crucial objective. By doing this, we can protect the environment and public health from the risks of PFAS exposure (Brendel et al., 2018).

Many recent exciting studies have been carried out to study the removal of PFAS from waterbodies (Gagliano et al., 2020; Mojiri et al., 2023; Sun et al., 2023; Phung et al., 2024). Interestingly, some review studies have equally been carried out to highlight the removal of PFAS from waterbodies (Militao et al., 2021; Verma et al., 2021; Ambaye et al., 2022; Vu and Wu, 2022; Yadav et al., 2022; Douna and Yousefi, 2023). Many of these previous review studies have largely focused on the traditional removal of PFAS by adsorption while some have focused solely on either biological and/or electrochemical methods. However, in this study, we attempted to provide a more robust review of recent methods available for the removal of PFAS from waterbodies. To the best of our knowledge, this study represents a first attempt at undertaking a comprehensive and comparative review of recent technologies adopted for the removal of PFAS from waterbodies. In this review, we described the chemistry of emerging PFAS. In addition, the predominant uses of PFAS were elucidated whilst also describing the fate and mobility of these persistent pollutants in the environment. Furthermore, the factors influencing the choice of removal methods for PFAS were highlighted whilst also describing the various removal efficiencies of the methods. Efforts were made to elucidate the PFAS removal mechanism from a density functional theory standpoint which has not been done in any review article before on this subject. Finally, future perspectives were provided to ensure environmental sustainability and the provision of clean water resources.

1.1. Chemistry of emerging PFAS

Because of their durability and possible health effects, emerging per and polyfluoroalkyl substances (PFAS) are being increasingly discovered in different environmental matrices. This presents substantial concerns. These new compounds, which are meant to replace older, more controlled ones, frequently feature shorter carbon chains or unique functional groups, in contrast to legacy PFAS. Because of their strong carbon-fluorine linkages, these new PFAS compounds are resistant to degradation and have excellent thermal stability while being unique. This helps to explain why they have persisted in the environment for so long (Kim et al., 2023). The chemical structures of some bioaccumulative PFAS are shown in Fig. 1.

Pure PFAS compounds occur as a liquid, solid, or gas at room temperature depending on their melting and boiling temperatures (Park et al., 2020). The majority of PFAS are found in solid (crystalline or powdery) form at atmospheric conditions; however, shorter chained compounds with carbon tails ranging from four to six appear to be present in liquid form. Perfluorobutanesulfshoronic acid (PFBS) has a melting point of −21 °C, while perfluorooctanoic acid (PFOA) has a melting point that is in the range of 45–54 °C (Dhore and Murthy, 2021). The way a PFAS chemical interacts in the environment will depend on its density when it is liquid at room temperature (Rahman et al., 2014; Nguyen et al., 2020). Only a few well-researched substances, including fluorotelomer alcohols, perfluorooctane sulfonate (PFOS), and perfluorinated carboxylic acids (PFCAs), currently have experimentally measured evidence of PFAS solubility in water (Nguyen et al., 2020).

It should be mentioned that at this point, PFAS's dissociation constant and rate constant - two characteristics that indicate stability - are not well understood. According to Ateia et al. (2019), PFAS compounds contain sulphonates, sulphates, phosphates, carboxylates, and amines, among other functional groups. These functional groups control a variety of PFAS fate and transport characteristics, including dissociated and undissociated forms. Anionic or undissociated acid PFAS compounds might affect partitioning behaviour and bioaccumulative potential depending on their condition. Perfluoroalkyl acids (PFAA) are negatively charged because of their low acid dissociation constants (Ka), except for rare circumstances (acidic pH) (Shi et al., 2018; Ateia et al., 2019). Some PFAS compounds' functional groups can be separated into anions and cations in an aqueous solution at specific pH values (Wu et al., 2020). For example, PFOA dissolves in water and separates into hydrogen and perfluorooctanoate (anion). The fluoroalkyl component of ionic PFAS other than PFAAs may be linked to a zwitterion, a positively charged cation, or a negatively charged anion (Backe et al., 2013). About functional groups, PFAS can be categorized into four groups: (a) anionic, which contains an acidic functional group; (b) cationic, which contains a basic functional group); (c) zwitterionic, which contains two or more functional groups, at least one of which can form an anion and the other a cation; and (d) non-ionic, which does not dissociate (Barzen-Hanson et al., 2017; Xiao, 2017). Anionic PFAS and cationic PFAS are anticipated to have dissimilar environmental transport properties.

1.2. Overview of the fate and transport of PFAS in the environment

Per- and perfluoroalkyl substances (PFAS) are known to be generally

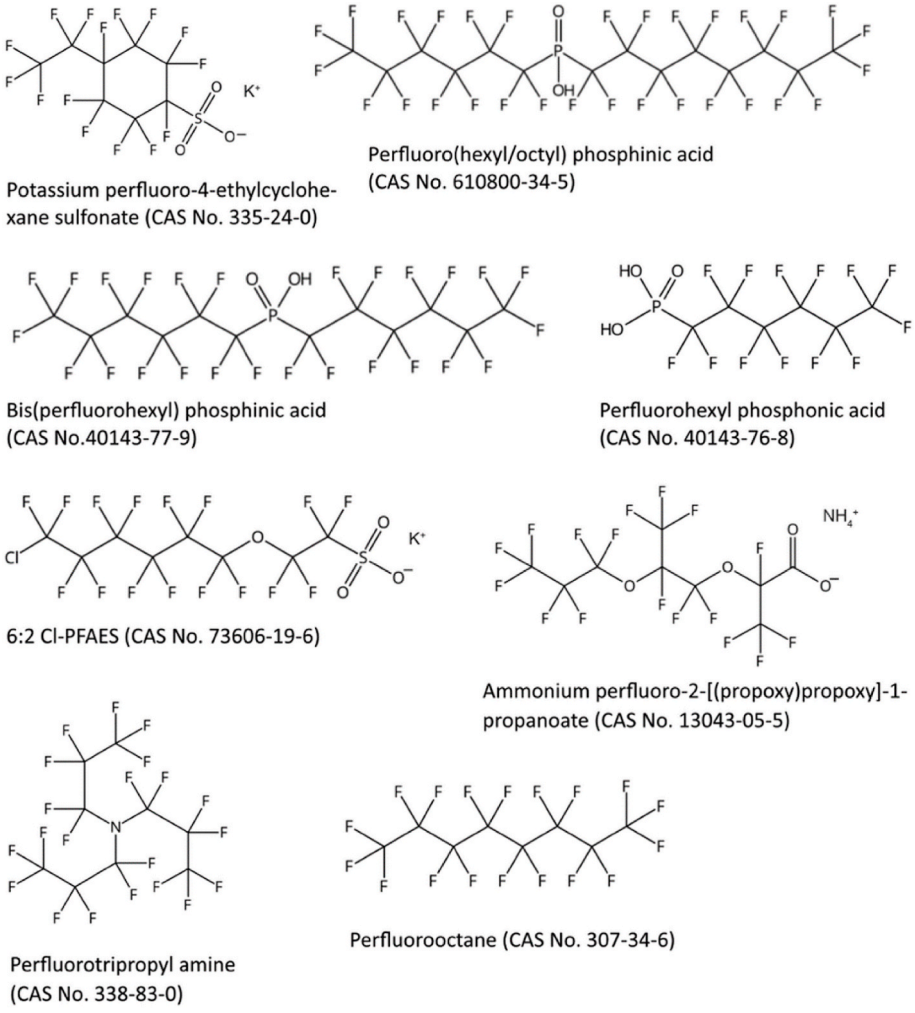

Fig. 1. Chemical structures of some bioaccumulative PFAS (Cousins et al., 2020) Copyright 2020, with open access permission from The Royal Society of Chemistry.

distributed within our surroundings due to their presence in several materials and their applications in several processes such as clothing, packaging, cosmetics, beverages, etc. (Guelfo et al., 2021; Weber et al., 2022). The fate and transport of PFAS in the environment result from intricate routes, which indicate the availability of these contaminants and their various activities after their release into different matrices (Kurwadkar et al., 2022). Inadequate reliable estimated data on the properties of PFAs and other uncertainties limit the efficiency of predicting their fate and transport within the environment using quantitative structure-activity relationship models (Nguyen et al., 2022). Therefore, considering these contaminants' different physicochemical characteristics, their fate and transfer would depend on the PFAS type, environmental pH, and the matrix involved. Various studies have shown varying distributions of PFAS based on their density (molecular weight), with longer-chain and short-chain PFAS occurring at different heights within soil sediment, as reported by Li and co-researchers. The reporters proposed that long-chain-PFAS occupy the shallower part of the soil matrix, although the shorter ones occupy a greater depth, which is influenced by the molecular weight of the past (Li et al., 2023a,b). Also, the disparities in hydrophobicity and lipophobicity within the PFAS group create numerous likely transport routes and lead to prevalent spread within our surroundings (Meegoda et al., 2020). In essence, the influences of fate and transport of PFAS could be categorized into PFAS characteristics and matrix characteristics. Explaining the processes is crucial for evaluating dangers posed by the discharge of PFAS, identifying potential exposure pathways, and evaluating treatment options (McGarr et al., 2023). According to the USA EPA, the fate and relocation of substances within areas are based on numerous elements however, predominantly on the reactions among environmental elements such as water, temperature, wind, light; and physicochemical processes which include partitioning and reactivity. For the transport of PFAS in the ecological area, some essential mechanisms have been identified, which include Partitioning between air and product (volatilization from product to air), indoor air deposition, accretion of gaseous particles, stability and migration with the earth's crust, amassing on the water surface, breakdown via hydrolysis etc., adsorption by plants and animals, among others.

An awareness of these processes is vital for determining the dangers posed by PFAS discharges, evaluating likely exposure routes, and choosing the proper techniques for their removal from the environment (McGarr et al., 2023). According to Lyu and Brusseau, the most crucial idea is knowing the outcome and transfer activities of PFAS, especially within the vadose zone, is its impact resulting in groundwater contamination, where its retention is caused by water-air interfacial adsorption (Lyu and Brusseau, 2020). The disposal of PFAS-containing products, such as firefighting foams used in military bases and other facilities in landfills, can leach into groundwater through run-off into surface water, and the primary mechanisms for their transport are advection and dispersion, same with other dissolved substances (McGuire, 2012; Rosenfeld et al., 2023).

1.3. Processes relevant to the fate and transport of PFAS

1.3.1. Phase partitioning

Partitioning is a phenomenon of distinguishing the constituents from the sample mixture by the partition of the constituents within the two phases. PFAS contains hydrophobic Partitioning towards the Organic-C and electrostatic interfaces among charged surfaces encompassing a C-F end and a non-fluorinated head comprising a polar functional group. This nature influences their transfer within different matrices by enhancing retention in sediments, parched soil, and stability in groundwater sources. An unpredictable retention level on solid materials can lead to variation in migration, where some PFAS are more rapidly conveyed than others. The tail of any PFAS is hydrophobic and generally lipophobic, i.e., doesn't react to water or non-polar material, but the polar group attracts water (hydrophilic) (Buck et al., 2011; Mussabek et al., 2019). In the event of competition among the polar and non-polar ends, it could result in extensive but irregular scattering within the surroundings. Also, the complexity of subsurface areas comprising soil materials having diverse polarities, and air-water boundaries. Multiple partitioning processes are imperative during a description of the stability and migration of PFAS. The concentration of PFAS may also be considered as they can show other behaviours with varying concentrations, such as the propensity to produce micelles towards increased amounts (Kim et al., 2015; Hidalgo and Mora-Diez, 2016; Fitzgerald et al., 2018). An investigation by Anderson and co-researchers to evaluate the impact of the partitioning course PFAS migrating in soil to groundwater within aqueous film-forming foam source zones from ongoing location evaluation in the U.S. Air Force area observed a negative slope for clay content which indicated greater declination at better percolation areas because of air water interfacial separation. They also discovered that the relationship between soil and water was influenced by the level of flushing, which suggests that mass transfer predominantly influences bulk release at meager flushed locations, thereby concluding that meta-analysis demonstrated substantial retaining of PFAS in the soil, which results from combined basic partitioning mechanisms (Anderson et al., 2019). Ebrahimi and friends examined the partitioning activities of fourteen PFAS among four 2° wastewater treatment categories based on different treatment techniques. Unfortunately, an inconsequential variation was noticed in compound-specific coefficients for the secondary treatment techniques, while they observed meaningful variation behaviour among biosolid samples. Biosolid samples that were digested anaerobically tend to have greater values compared to the aerobically digested ones, indicating that all the examined processes, including the treatment technique, could influence the leaching potentials of sewage solids (Ebrahimi et al., 2021).

1.3.2. Media-specific migration processes

In contrast to extensive phenomena like partitioning and transformation, media-specific transport of PFAS, such as transfer into semi-permeable regions, air migration, and percolating from earth to groundwater, are unique special media. Globally, there have been low amounts of pollution caused by PFAS, considering the long production time and the numerous sources that could enhance the transfer of PFAS into the environment. Variations in concentrations of this chemical could be attributed to factors such as closeness to industries, the pattern of air movement, and water distribution, among other factors. Hence, there could be no claim of universal values of PFAS pollution (deSilva, 2022; Kurwadkar et al., 2022; Purohit, 2023). Diffusion is the process that results in the movement of fluids/particles from the higher concentration region to the lower concentration area; therefore, PFAS from the sources are transferred from points where they are generated to others. Air acts as a critical passage environment towards PFAS, permitting them to diffuse in all air movement ways. This leads to universal distribution and contributes to free-PFAS adherence towards the earth and water surfaces in the locality of discharge sources, a potential issue to site surveys (Vallero, 2023; Cronin, 2024). For instance, in the investigation of PFAS from air testers collected from Northwest Europe by Barber and colleagues, it was detected that the amounts of neutral PFAS were several folds greater in the interior than outside environment, insinuating residential areas to be an essential diffuse source of these contaminants to the air. After frequent experiments for non-volatile ionic PFAS in the air samples, they strictly recommended more measurements to be carried out on ionic PFAS because they probably might have undergone atmospheric migration of gas molecules away from the source area (Barber et al., 2007). Han and co-investigators evaluated the amount and origination distribution of perfluoroalkyl acids (PFAAs) in air within China. They observed that the concentrations of the PFAS were greater folds higher than those determined in other urban locations. Still, the values were lower at point sources, suggesting diffusion from the produced areas (Han et al., 2019). Also, in another investigation by Rowe and colleagues partitioning PFAS via thermoplastic and numerous PVC liners observed substantial migration through the thermoplastic polyurethane identified by the reduction in concentration from the source and increase in concentration from the receiver over some time.

Meanwhile, the PVC liners tend to resist the diffusion of PFAS, making them excellent resisting surfaces for PFAS (Rowe et al., 2023). Ahmad and coauthors in their study to check the stability and diffusion of PFAS through high-density polyethylene (HDPE), observed a decrease in diffusion coefficient with increased molecular weight and dependent on their functional groups (Ahmad et al., 2024). Another investigation by Wang and friends to evaluate the atmospheric diffusion of PFAS evolved from fluorochemical industries and exposure risk showed a significant impact of PFAS diffusion from the industry to the atmosphere, PFOA having a higher concentration as compared to perfluoroalkyl carboxylic acids (PFCAs) (Wang et al., 2021b). This study agrees with the study by Charles E. Schaefer and friends, who also determined the aqueous diffusivities for PFAS, which showed a nonuniform trend concerning the differences in molecular weights (Schaefer et al., 2019).

Primarily for earth-groundwater transport, the fate of PFAS is substantive to percolation in the course of natural rainfall or artificial watering processes that encourage the breakdown and transfer of PFAS within a matrix system (Sepulvado et al., 2013; Ahrens and Bundschuh, 2014; Bussian et al., 2021; Sarkar et al., 2021; Sharifan et al., 2021). PFAS transfer from top-earth to groundwater is subject to numerous interrelating phenomena, that either improve or decrease its percolation amount within a period. The percolating prospect could be boosted in regions with excellent aqueous permeation capability, such as natural water sources, which include natural rain, or anthropogenic sources, such as artificial watering. Leaching potential may also be affected by the width of the unsaturated region (distance to the water table), which is common to other contaminants in shallow soils other than PFAS (Damião et al., 2023). A study by Schaefer and colleagues on the diffusion of PFAS through clay-rich soil concluded that surface diffusion plays a potentially significant part in the adsorption of PFAAs with clay-rich soils, and recommended the necessity for further investigations on the combined adsorption and diffusion of PFAAs in small permeable areas (Schaefer et al., 2021). An investigation by Borthakur and colleagues on the impact of how the discharge of soil colloidal particles during flow disturbance would increase the pore-water PFAS amounts in drenched soil. They depicted that after the disruption of flow, the PFAS amount was not diminished, demonstrating an inconsequential involvement of environmental migration. They suggested that the increase in concentration could be due to the discharge of colloid-related PFAS. They concluded that colloids might have a disproportionally more significant part in transferring PFAS in situations that discharge colloidal particles from spongy structures (Borthakur et al., 2021). The percolation and transfer of PFAS in AFFF in the unsaturated land within a firefighting teaching establishment in cold winter situations were studied by Høisæter and coinvestigators who concluded that PFOS is

intensely weakened in the unsaturated zone. Movement relies on the permeation rate, and the weakness rate appreciates with time. This was because no PFOS was detected at a distance of 60 cm in the low infiltration column, but for high infiltration, the maximum value was observed at 22–32 cm depth (Høisæter et al., 2019).

1.4. Transformation

Transformation involves the conversion of compounds or substances into other forms different from the starting materials, which for polyfluorinated PFAS are reported in the categories of biotic and abiotic transformations (O'Connor et al., 2022). Polyfluorinated PFAS are observed to be converted to PFAA precursor, referred to loosely as any PFAS material, partly due to the typically complex transformation routes towards the final PFAA compound containing some comparatively stable intermediates. Knowing the stable conversion of precursors is imperative in proposing PFAA trail advance and description which is crucial for structural area maintenance (Guelfo et al., 2021).

Biotic transformation involves the adoption of microorganisms such as strains of bacteria, fungi, and soil microorganisms, which include earthworms and plants, as reported by Bolan and colleagues (Bolan et al., 2021). Different aerobic and anaerobic bacterial species have been reported to be involved in the biotransformation of pfas. Hydrolysis, photolysis, and oxidation are abiotic phenomena that can convert precursors under ambient environmental situations. Hydrolysis of some precursors could be trailed by ensuing biotransformation, which could form PFSAs. The biotransformation of PFAA longer-chain hydrocarbon end usually requires the breakage of C–F bonds with the degradation of non-fluorinated homologues through processes such as oxidation, dealkylation, and defluorination to produce shorter-chained products (Zhang et al., 2021). In a review study by Yan and co-authors on the existence and microbial transformation of PFAS in water film-forming foam (WFFF)- affected environments using electrochemical fluorination (ECF)- and fluorotelomer (F.T.F.T.)-based WFFFs reveals WFFF to be the significant origination source of PFAS contamination, which involve 1° precursors (poly-fluoroalkyl material as WFFF components), 2° precursors (poly-fluoroalkyl transformation yields of 1° precursors), and perfluoroalkyl acids (PFAAs). They reported that the degree of biotransformation and routes for WFFF-obtained 1° and 2° precursors showed variation with diverse precursors but was regular for the PFAS present in WFFF-affected regions. For instance, easily breakable 1° precursors, like N-dimethyl ammonio propyl perfluoroalkane sulfonamide (AmPr-FASA) and n:2 fluorotelomer thioether amido sulfonate (n:2 FtTAoS), were seldom identified in WFFF-affected areas. Whereas the main 2° precursors, perfluoroalkane sulfonamides (FASAs) and n:2 fluorotelomer sulfonate (n:2 FTS), were commonly identified, that could be because of non-reactivity to bioconversion (Yan et al., 2024a). Xia and co-investigators studied the degradation of PFAS substances in wastewater effluents via photocatalysis which was compared with that of deionized water. They observed that the degradation was more favourable at pH 3.0, and the rate of degradation of PFAS in wastewater effluents was lower than that of deionized water, which may be caused by the complex composition degree of the water (Xia et al., 2023). In another study by Liu and co-investigators on the transformation of PFAS of waste collected from vehicles to landfills, which was preoccupied with PFAAs, encompassing perfluoroalkyl carboxylic acids (PFCAs) and perfluoroalkyl sulfonic acids (PFSAs). The majority of PFAS in commercial and domestic waste vehicle percolates were PFAA products, signifying product conversion to PFAAs in the landfill discharge processes. The proposed degradation routes were based on the conversion of polyfluoroalkyl phosphate diester (diPAPs) and fluorotelomer sulfonic acids (FTS) to produce PFCAs through the realization of intermediary precursors, which include fluorotelomer carboxylic acids (FTCAs) (Liu et al., 2020b).

Kolanczyk and colleagues conducted a species comparison investigation to understand the biotransformation mechanism for PFAS using fish as a case study. They considered the metabolism map for ten PFAS, and the study showed how relating the pathway mechanisms within species were enhanced via examination of the environment in which sample materials were estimated for each species. The different analytical techniques employed to detect metabolites in each study, and the number of metabolites were obtained (Kolanczyk et al., 2023). Evich and colleagues tried to propose the development of PFAS transformation species within soil New Jersey, using multi congeners, the chloro-perfluoropolyether carboxylates, with a focus on the reaction centres (chlorinated carbon and ether linkages). Although ether linkages have been proposed to be probable reaction areas, they could not find relevant literature to support the hypothesis, but rather suspected other multi-congener transformation products possessing Cl-, H-, epox- and diOH-PFAS products (Evich et al., 2022). In another study by Chen and co-investigators to examine the production of PFAS from PFAA oxides in aerated soils, observed novelty that in the existence of microorganisms in the soil, two chemicals underwent an extensive abiotic transformation. The products obtained were analogous to those obtained for biotic methods but for two PFOA and PROS, making perfluoroalkyl amine oxides an essential source of PFAA, which explains their presence in historical aqueous film-forming foam-affected areas (Chen et al., 2020). In another study, Yan and co-authors to determine the aerobic supported bioconversion of 6:2 fluorotelomer sulphonate in soils from two AFFF-affected regions observed that variation in the initial amount of sulfate and reduction of sulfate within the incubation period led to the difference in the degree of 6:2 FTS biotransformation that occurred in the two soils. They suggested from microbial community analysis that desulphobacterota microorganisms could enhance 6:2 FTS biotransformation through effective desulphonation, as well as species from the genus *Sphingomonas* that demonstrated greater impact to higher amounts of 6:2 FTS and its precursors (Yan et al., 2024b).

1.5. Uptake of PFAS by plants

PFAS reacts with blood proteins, is responsible for several pathological effects, including cancer, and occurs from the potential accumulation in agricultural produce. Transferring them to humans via the food chain remains a possible route. Some strong direct relations exist with the amount of PFAS in a location and its bioaccumulation in plants, in which the uptake relies on factors such as the level of PFAS within the earth, nature of PFAS, the length of the carbon chain, plant type, functional group, and organ. It is expected that the presence of the hydrophilic functional group in PFAS plants should be able to adsorb these compounds via their root systems and translocated to other parts like stems, leaves, and fruit systems as shown in Fig. 2A (Wang et al., 2020b; Lesmeister et al., 2021). The presence of a hydrophilic functional group in PFAS plants should likely be able to adsorb these compounds via their root systems and translocate to other parts like stems, leaves, and fruit systems (Wang et al., 2020b; Li et al., 2022). Therefore, the proximity of plants to contaminated areas or artificial watering of plants with PFAS-affected water determined the degree of accumulation, which also relies on some circumstances in locations such as soil properties (Ghisi et al., 2019). The adsorption of PFAS by plants could be studied using different techniques; Gehrenkemper and friends explored the fate of PFAS in bean plants by comparing molecular absorption spectrometry and sum parameter analysis using liquid chromatography to determine the most efficient tool. They concluded that both techniques showed relative results: M.S/M.S. was more dependable for known PFAS contamination, and MAS proved more sustainable in identifying the unknown composition of PFAS exposure (Gehrenkemper et al., 2023). The influence of dissolved organic matter (DOM) derived from soil and water on PFAS uptake was reviewed by Qi and colleagues; they observed that DOM contends with PFAS for uptake of active points available on the surface, resulting in a decrease in PFAS removal, hence enhancing discharge of PFAS to the soil. They concluded that it plays a double action in plants' uptake, breakdown, and plant PFAS adsorption, which

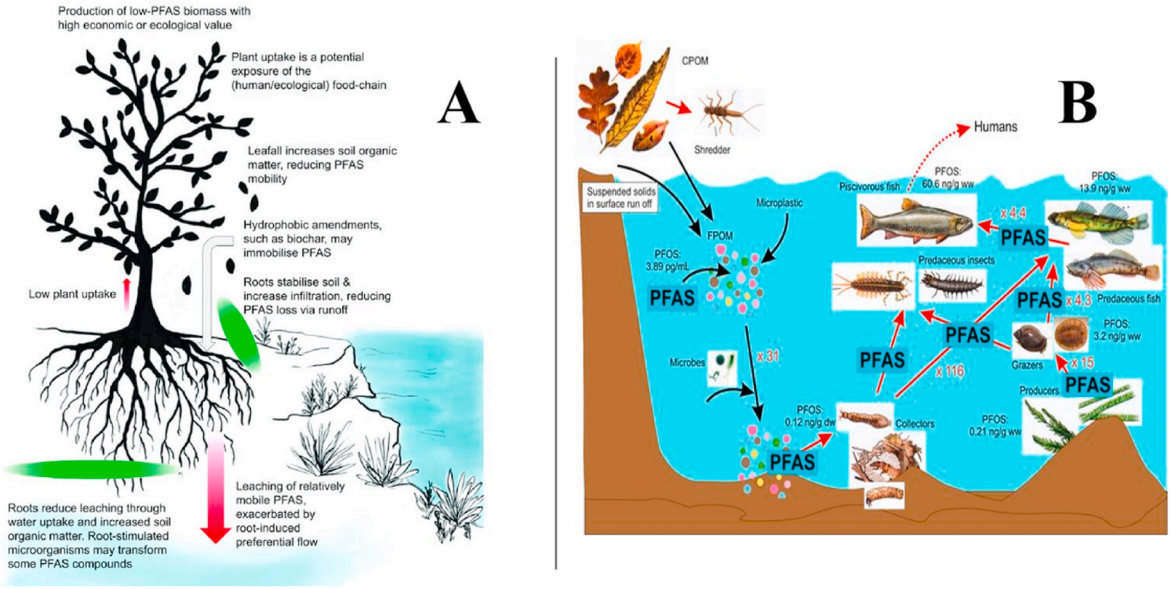

Fig. 2. Figure showing the uptake of PFAS by plants and animals (Evangelou et al., 2022). Copyright 2022, with open access permission from MDPI.

relies on the kind and the active parts on the surface (Qi et al., 2022).

1.6. Uptake by animals

The uptake of PFAS by animals, unlike plants could result from the ingestion of contaminated agricultural produce or inhalation of dust (Costello and Lee, 2020; Death et al., 2021). It has been observed to accumulate in different organs within the animal systems such as the liver, brain, muscles, kidney, and heart (Cao and Ng, 2021). In the animal system, it has been reported to be responsible for several ailments and long and short-chained PFAS have been reported to be biodistributed from mother to fetus via placenta transportation (Bartels et al., 2020). Drew and colleagues discovered numerous PFAS serums and tissues of cattle with different half-lives and observed the initial point of the age of the cattle concentration of the serum did not have any influence on their half-lives during depuration (Drew et al., 2022). The prevalence of PFAS in the system of animals has been observed to show some significant physiological changes due to their interaction with proteins-associated tissues as shown in Fig. 2B (Bangma et al., 2022). Other reported cases of PFAS in animals are presented in Table 1 below.

Table 1
Showing reports on the uptake of PFAS by different animals.

Type of PFAS	Organism/organ	Reference
Hexafluoropropylene oxide trimer acid (HFPO-TA) and hexafluoropropylene oxide dimer acid (HFPO-DA)	Mice/liver	Wen et al. (2022)
PFAS (14)	Human renal	Ryu et al. (2024)
PFAS	Chicken tissues	Fernandes et al. (2019)
PFAS	Daphnia magna	Dai et al. (2013)
PFOS and Perfluorohexanesulfonic acid	Aquatic birds/ liver	Witt et al. (2024)
PFOS, PFOA and Hexafluoropropylene Oxide Dimer Acid (GenX)	Benthic fish	Hassell et al. (2020)
PFOS	Eels, shrimps, bivalves and flounders	Zafeiraki et al. (2019)
PFAS and perfluoroalkyl carboxylic acids (PFCA)	Dairy cattle/ plasma and skin	Lupton et al. (2022)
PFOS, PFHxS, PFOA, and 6:2 FTS	*Rana pipiens* tadpoles	Hoover et al. (2017)

2. Health effects and half-life of PFAS

It is well recognized that the development of proliferating peroxisomes is how PFAS primarily manifest their toxicity. Toxic effects of PFAs have been studied in mammals, such as rodents, through experiments. However, because these organisms differ in how peroxisome proliferation is expressed, it is not fully acceptable to extrapolate the findings of this research to humans (Palmer et al., 1998). According to numerous case studies on the negative effects of PFAS exposure in people, there may be a connection between PFAS compound exposure and the development of conditions like cancer, thyroid disease, inflammatory bowel disease, high blood pressure, and others (Barry et al., 2013; Steenland et al., 2013; Vieira et al., 2013; Varjani and Chaithanya Sudha, 2018). Children are more vulnerable to PFAS contamination than adults are. This may be explained by children's faster metabolisms and constantly evolving bodies. Epidemiologic evidence was recently reviewed by (Rappazzo et al., 2017), linking exposure to PFAS during pregnancy and/or infancy associated with immunity, disease, respiratory condition, cardiovascular problems, changes in cognitive development, thyroidal, nephritic, and puberty commencement. The main way that PFAs are exposed to people among the several routes is through food and drinking water (Mishra et al., 2019). A Chinese group of women's plasma PFAS concentration has been positively correlated with eating fish and crustaceans, whereas water and soy products have been linked to reduced plasma PFAS concentrations (Zhou et al., 2019).

Additionally, PFAS have been detected in a variety of consumer products, including non-stick cookware, stain-resistant fabrics, and food packaging materials, which contribute to their widespread presence in the environment and human exposure (Seltenrich, 2020; Ramírez Carnero et al., 2021; Dueñas-Mas et al., 2023). These compounds are highly persistent, earning them the nickname "forever chemicals," due to their resistance to environmental degradation processes such as photolysis, biodegradation, and hydrolysis (Scarr and Fund, 2023; Pearson and Renfrew, 2024). One of the significant concerns regarding PFAS is their long half-life in the human body. For instance, PFOA and PFOS have half-lives in humans estimated to be around 3.8 and 5.4 years, respectively (Chi et al., 2018). This prolonged persistence can lead to bioaccumulation and potential biomagnification through the food chain, posing a risk to both human health and wildlife.

Research has also highlighted the potential endocrine-disrupting properties of PFAS, which can interfere with hormone function and

regulation. This disruption has been linked to reproductive health issues such as reduced fertility, altered menstrual cycles, and adverse pregnancy outcomes (Ding et al., 2020; Rickard et al., 2022). Moreover, exposure to PFAS has been associated with developmental effects in offspring, including lower birth weight and impaired neurodevelopment (Eick et al., 2021). Given the mounting evidence of their harmful effects, regulatory agencies worldwide are taking steps to limit PFAS exposure. For example, the European Union has implemented strict regulations on the use of certain PFAs in consumer products, and the United States Environmental Protection Agency (EPA) has established health advisories for PFOA and PFOS in drinking water (Garnett and Van Calster, 2021; Post, 2021; Zimmermann et al., 2022; Cotruvo et al., 2023).

2.1. The half-life of PFAS: persistence and implications

The half-life of a substance is the time required for its concentration to decrease by half through natural processes. For PFAS, this involves the rate at which they are metabolized and excreted by living organisms or broken down in the environment. The half-life of PFAS is influenced by several factors, including the specific chemical structure of the compound, the environmental medium (such as water, soil, or air), and the biological characteristics of the exposed organism (Krafft and Riess, 2015). In humans, the half-lives of commonly studied PFAS such as PFOA and PFOS are notably long. Studies have estimated the half-life of PFOA in humans to be approximately 3.8 years, while PFOS has an even longer half-life of around 5.4 years (Chi et al., 2018). This prolonged persistence can lead to bioaccumulation, where PFAS concentrations build up in the body over time with repeated exposure. This is particularly concerning because of the potential health effects associated with long-term PFAS exposure, including cancer, liver damage, thyroid disease, decreased fertility, and developmental issues in children (Blake and Fenton, 2020). The environmental half-lives of PFAS compounds are also significant.

PFAS are known as “forever chemicals” due to their resistance to degradation processes such as photolysis, hydrolysis, and microbial activity. For instance, in soil and water, PFAS can persist for many years, contributing to widespread environmental contamination (Abunada et al., 2020). This environmental persistence poses challenges for remediation efforts and increases the likelihood of human and wildlife exposure through contaminated water, soil, and food sources. Research has highlighted the need for effective treatment technologies to remove PFAS from drinking water and other environmental media. Methods such as granular activated carbon (GAC) filtration, ion exchange resins, and high-pressure membranes like reverse osmosis have shown promise in reducing PFAS concentrations (Crone et al., 2019). However, the high costs and technical complexities associated with these technologies underscore the importance of preventing PFAS contamination at the source. Given the persistence and potential health risks of PFAS, regulatory agencies worldwide are taking steps to limit their use and manage existing contamination. The European Union has implemented stringent regulations on certain PFAS compounds, and the United States Environmental Protection Agency (EPA) has established health advisories for PFOA and PFOS in drinking water (Cotruvo et al., 2023). These measures are critical for protecting public health and the environment from the adverse effects of PFAS exposure.

2.2. Systemic effects of PFAS

PFAS are a class of synthetic chemicals known for their widespread use in industrial and consumer products due to their unique water and oil-repellent properties (Glüge et al., 2020). However, these compounds are persistent in the environment and resist degradation, leading to their accumulation in ecosystems and potential exposure to humans (Cousins et al., 2020; Panieri et al., 2022). Once absorbed into the body through ingestion, inhalation, or dermal contact, PFAS can be distributed throughout various tissues and organs, exerting systemic effects on human health (Vujic et al., 2024). Bioaccumulation and Persistence PFAS compounds have a propensity to accumulate in the body over time, primarily in organs such as the liver, kidneys, and thyroid gland (Blake and Fenton, 2020). This bioaccumulation occurs due to the compounds’ resistance to metabolism and elimination, leading to prolonged exposure and potential adverse health effects (Panieri et al., 2022).

Endocrine Disruption Evidence suggests that PFAS may disrupt endocrine function by interfering with hormone regulation and signaling pathways (Woodruff et al., 2011; Johnson et al., 2014; Panieri et al., 2022). These compounds can bind to hormone receptors, alter hormone synthesis and metabolism, and affect downstream cellular responses (Jiang et al., 2015). Such endocrine-disrupting effects can have widespread implications for reproductive health, metabolism, and growth. Developmental Effects Exposure to PFAS during critical periods of development, such as in utero or during infancy, has been associated with adverse developmental outcomes (Zhou et al., 2023). Animal studies have shown that prenatal exposure to PFAS can result in lower birth weight, developmental delays, and neurobehavioral abnormalities (Oh et al., 2021). Similarly, human epidemiological studies have reported associations between maternal PFAS exposure and adverse birth outcomes, including preterm birth and reduced fetal growth (Bach et al., 2015). Immune System Dysfunction PFAS exposure has been linked to alterations in immune system function, including changes in immune cell activity and cytokine production (Beans, 2021). These compounds can modulate immune responses by affecting the function of immune cells such as lymphocytes, macrophages, and dendritic cells. Immune system dysfunction resulting from PFAS exposure may contribute to increased susceptibility to infections, autoimmune disorders, and inflammatory conditions (Beans, 2021). Some studies have suggested a potential association between PFAS exposure and an increased risk of certain cancers, including testicular, kidney, and prostate cancer (Steenland and Winquist, 2021). Animal studies have demonstrated the carcinogenic effects of certain PFAS compounds, particularly perfluorooctanoic acid (PFOA) and perfluorooctanesulfonic acid (PFOS), in multiple organs (Seyyedsalehi and Boffetta, 2023). However, further research is needed to fully elucidate the carcinogenic mechanisms of PFAS and their relevance to human health.

Cardiovascular Effects Emerging evidence suggests that PFAS exposure may contribute to cardiovascular disease risk factors such as elevated cholesterol levels, hypertension, and atherosclerosis (Schlezinger and Gokce, 2024). Animal studies have shown that PFAS exposure can lead to dyslipidemia, endothelial dysfunction, and oxidative stress, all of which are implicated in the development of cardiovascular disease (Boafo et al., 2023). Human epidemiological studies have also reported associations between PFAS exposure and increased risk of heart disease and stroke (Schillemans et al., 2022). In summary, PFAS exposure can have systemic effects on various organ systems and physiological processes in the body as shown in Fig. 3. Understanding these effects is crucial for assessing the health risks associated with PFAS contamination and developing strategies to mitigate exposure and protect public health.

3. Performance evaluation of methods for the removal of PFAS

Notably, conventional treatment, photocatalytic degradation, biological treatment, oxidation, sonochemical degradation, fungal degradation, ion exchange (IEX), membrane filtration, and adsorption, have been assessed and documented in the literature for eliminating PFAS from water matrices (Crone et al., 2019). However, as expected, the performances of these methods vary based on the synergy between the pragmatic experimental conditions, the material used, and bond configuration and chain length of various PFAS among other factors. Thus, the next subsections empirically discussed the performance of various PFAS cleanup techniques and elucidated the mechanism involved in the cleanup operation from a density functional theory

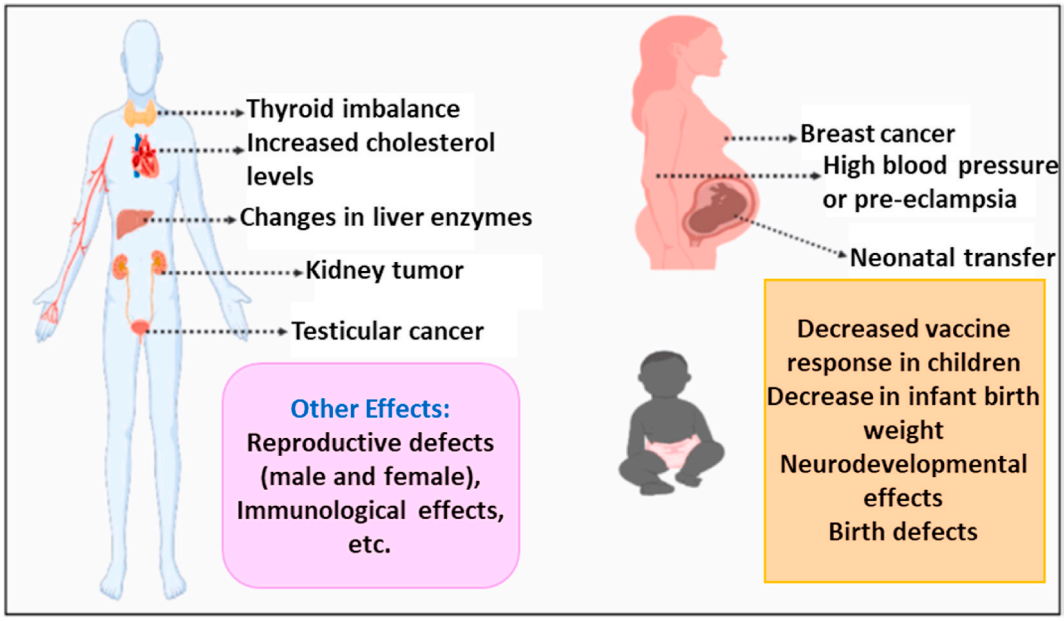

Fig. 3. Toxicities and health problems associated with PFAS exposure (Sharma et al., 2024). Copyright 2024, with open access permission from Elsevier.

(DFT) simulation standpoint.

3.1. Adsorption

Historically, adsorption is thought to be one of the oldest eco-effective and inexpensive techniques (Bayode et al., 2024; Emmanuel et al., 2024a,b,c,d,e) for removing PFAS from waterbodies or wastewater (Schröder et al., 2010; Du et al., 2014). High and selective PFAS adsorption is exhibited by effective adsorbents. Notably, activated carbon (AC) and biochar (BC) as functional adsorbents for the adsorption of PFAS have been the oldest and most researched domains. However, in recent decades, the use of nanomaterials in single or composite with AC or BC has garnered more attention. Thus, the succeeding paragraphs dealt with juxtaposing the performance of various (nano)adsorbents that have been employed for the adsorption of PFAS in recent times. For example, zirconium-based MOF was employed to clean up six PFCAs and three PFSAs from a water matrix (Li et al., 2021a,b). According to the findings, Zr-MOF has exceptional adsorption capacity (ADSCAP) of 201–604 mg/g for PFCAs, and 400–620 mg/g for PFSAs and incredibly quick adsorption kinetics with less than a minute equilibrium period. In addition, according to the DFT simulation presented in Fig. 4, the PFAS@MOF uptake process is largely governed by a mixture of hydrophobic (HPB) non-covalent PFAS–MOF contacts, electrostatic interactions (ESI), and H-bonding. Specifically, as shown in Fig. 4A, adsorption spots 1 and 2 are situated in the hexagonal and triangular pores, correspondingly. The Zr_6 node at two spots features Zr-coordinated aqua ligands that allow H-bonding interactions with PFBS, while unsaturated Zr spots additionally sponsor coordinative bonding and/or ESI. Fig. 4B and 4C, display diverse configurations of the MOF linker's pyrene motifs. At spot 1, the pyrene motifs are orthogonally coordinated to the middle of the spot, whereas at spot 2, symmetrical-positioned pyrenes form an HPB pocket. More specifically, the sorption of PFBS at spot 1 is pictured in Fig. 4D displaying PFBS–MOF bonding stabilized by robust H-bonding interactions (RSO_3···H–O), while ESI (RSO_3–Zr) and hydrophobic interactions (HPBI) (C–F chain–pyrene motif) are marginally frail. Meanwhile, Fig. 4**E** displays that PFBS sorption at spot 2 is controlled by robust coordinative bonding (RSO_3–Zr). Additionally, PFBS is cartographically restricted by the two pyrene ligands at the apex of the triangular aperture containing substantial HPBI (C–F chain–pyrene motif) and moderate H-bonding (RSO_3···H–O). A comparable trend in sorption proclivity for spot 2 is seen for all PFAS studied. Moreover, the geomorphology of Zr-MOF after PFBS uptake remains intact as seen from the SEM images displayed in Fig. 4F-I (Li et al., 2021a,b). In another typical study (Liu et al., 2015), the findings from the DFT simulation show that in conjunction with the anion-exchange mechanism, the chief mechanism of PFOA uptake by quaternized MIL-101 is a blend of ESI between the proton-rich carboxyl moieties of the terephthalic acid MOF ligand and PFOA and Lewis acid/base complexation between Cr(III) of the MOF and PFOA (Liu et al., 2015). This mechanistic elucidation is in agreement with what was expounded from the DFT simulation for the excellent sorption (>75%) of PFOA onto Fe-based MOF. In addition, as shown in Fig. 4, it was observed that PFOA molecules do not sorb in the hexagon apertures but are sorbed in the pentagonal apertures for MIL-100-Fe. Likewise, no PFOA molecules were noticed in the pentagonal apertures of MIL-101-Fe. Thus, it can be inferred that PFOA molecules tend to be sorbed in the pentagonal and triangular apertures and this shows that smaller apertures are priority sorption spots because of the more densely packed structure of pentagonal and triangular aperture architecture than that of the hexagonal one stronger interactions to PFOA (Yang et al., 2020a) (see Fig. 5).

In another research (Shaikh et al., 2023), Karanja shells AC modified by CTAB was employed for the removal of PFOA. It was found that by CTAB modification, the PFOA adsorption output of the adsorbent surged up to treble. Specifically, Karanja AC and CTAB modified versions had maximal PFOA adsorption capabilities of 157.1 mg/g and 455.8 mg/g, respectively. The adsorbent cleaned almost 90% of the PFOA as presented in Table 2 and showed good PFOA selectivity against all co-contaminants, including anions, humic acid, bentonite, and cations. The regenerant, which was 50% EtOH and 1% NH_4OH aqueous solution, recovered 80–90% of the PFOA. High PFOA ADSCAP from the river water matrix was demonstrated by the adsorbent's packed-bed column run, and the breakthrough results suited the Thomas and Yoon Nelson Model well, with R^2 values of 0.97 for both models. The findings show that, in a substantially closed-loop sustainable process, the new CTAB-Karanja-AC may be a useful sorbent for PFOA adsorptive cleanup from aquatic environments with high treatment selectivity for PFOA (Shaikh et al., 2023). In another report (Wang et al., 2021c), the ADSCAP of COF for PFAS was compared to that of AC and resin. In this work, compared to traditional activated carbons and resins, the COF-containing

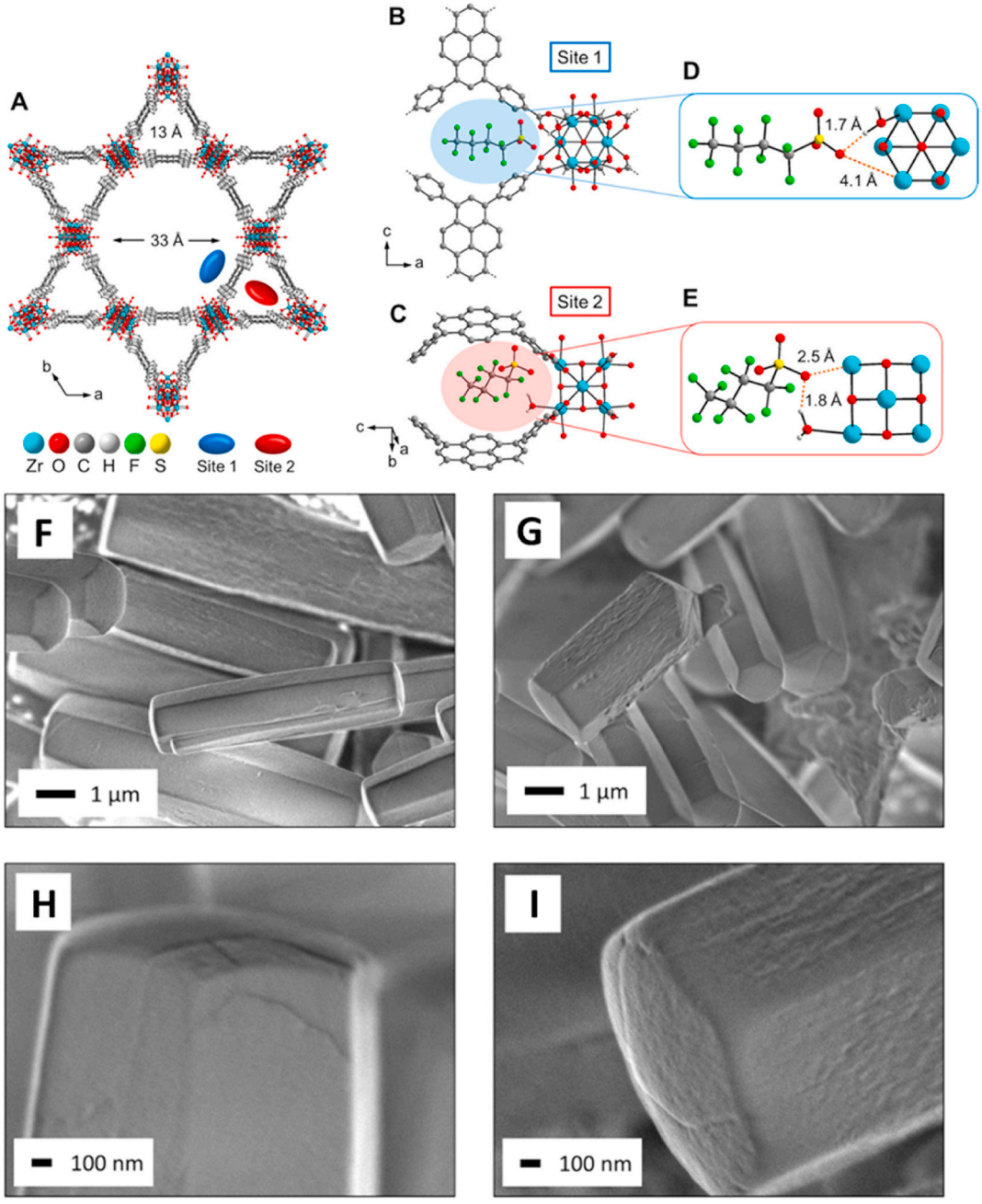

Fig. 4. Structural appearances of the Zr-MOF@PFBS sorption mechanism: (A) crystal morphology of Zr-MOF displaying the triangular and hexagonal with the corresponding sorption spots tinted as red and blue spheroid; (B, C) DFT-simulated conformation of PFBS–pyrene linker–Zr_6 node areas of Zr-MOF@PFBS at sorption spots 1 and 2, respectively; (D, E) Close view of individual sorption spots with broken lines symbolizing ESI and H-bonding of the RSO_3–Zr_6 and RSO_3···H_2O–Zr_6 motifs, correspondingly. H_2O H_2 atoms are excluded from structures for lucidity. SEM images of Zr-MOF crystallites (F and G) before (H and I) after PFBS sorption (Li et al., 2021b). Copyright 2021, with open access permission from the American Chemical Society.

quaternary ammonium demonstrated a higher ADSCAP for GenX (2.06 mmol/g) and HFPO-TA (2.16 mmol/g). It's interesting to note that the longer-chain HFPO-TA replaced the earlier sorbed GenX on the COF, and a DFT calculation helped to better clarify the underlying competitive process and afford deep acumen into the adsorption conformations and the binding interaction between PFASs and COF architectural units. Notably, according to the DFT simulation, the first phase of the PFAS adsorption process on ammonium-based COF is electrostatic attraction, followed by IEX. As shown in Fig. 6, the spatial structures of COF1-GenX and COF1-HFPO-TA were firm, and the value of ΔE binding of HFPO-TA and GenX sorbed on COF1 were −6.1 and −4.8 kJ/mol, correspondingly. These values indicate that the clean-up operation was exothermic. Additionally, COF1-HFPO-TA had a smaller ΔE binding compared to COF1-GenX, suggesting that COF1 had a higher attraction for HFPO-TA. For GenX and HFPO-TA uptake by COF2, when PFAS molecules are dispersed in water, they are initially attracted to the COF2 surface because of the ESI with the COF quaternary ammonium groups. This results in a significant decrease in system energy (Fig. 6). Following this, the PFAS molecules are firmly sorbed on the activated spots through an IEX process, which consumes energy ($\Delta E > 0$). The initial electrostatic attraction is highly exothermic and occurs easily, making the process similar for both GenX and HFPO-TA. However, the differences in their adsorption capacities on COF2 are due to varying IEX binding strengths (Fig. 6), highlighting their different adsorption behaviours. Moreover,

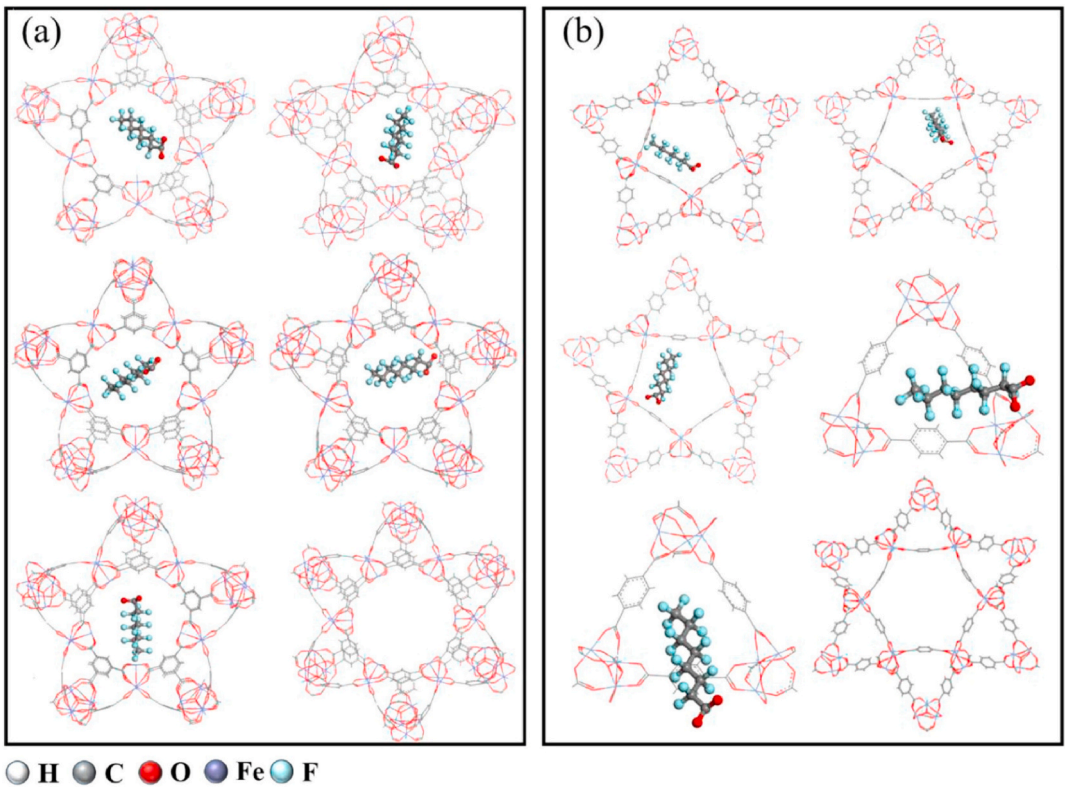

Fig. 5. The most reliable conformations for sorption of MIL-100-Fe-PFOA and MIL-101-Fe-PFOA gotten by sorption radar modules. Left: (a) MIL-100-Fe-PFOA and right (b) MIL-101-Fe-PFOA (Yang et al., 2020a). Reused with permission from Elsevier (Approval code.: 5835010047723, Copyright 2020).

+ve electrostatic potential sites are more probably to function as the active spot for PFAS molecules because they have a larger propensity to bind nucleophilic pollutants. The electrophilic portion of COF2 displayed nucleophilic PFASs molecules densely sorbed on its surface, as seen in Fig. 6e and f. This behaviour captures the nature of hydrogen bonding's (HB) electrostatic complementation. Crucially, the surface of the C-F chain end on PFAS molecules displayed a lower -ve electrostatic energy or even a +ve electrostatic energy, indicating that the oxygen-containing portion of the PFAS molecule was the important attraction spot to be sorbed by COF2. The oxygenated end and ether bond O_2 unit also demonstrated a highly -ve electrostatic surface. In addition, as shown in Fig. 6g, it is evident that the process by which HFPO-TA supplanted GenX and reclaimed the sorption spot on COF2 may be completed with low energy consumption, but roughly 10× as much energy would be required to swap GenX with PFOA (Wang et al., 2021c).

Another experiment (Wang et al., 2018b), showed that at room temperature, the elimination efficiency of PFOA and PFOS with magnetic nanoparticles-attached fluorographene-based (MNPs@FG) nanosorbent was methodically investigated. With comparatively good uptake capacities for PFOA (50.4 mg/g) and PFOS (17.2 mg/g), the nanosorbent demonstrated 92–95% and 94–97% elimination efficacies for PFOA (180 μg/L) and PFOS (180 μg/L) in 120 s, respectively. Even with naturally occurring organic materials present, the adsorption efficacy remained steady. Furthermore, the nanosorbent may significantly diminish PFOA and PFOS in ambient water from around 5 μg/L (an ecologically significant concentration) to less than 50 ng/L, which is below the health advisory standard (70 ng/L) set by the US EPA. Additionally, the spent nanosorbent was regenerated by washing with MeOH and reutilized for adsorption. Following the 5 rounds, high removal efficiency was achieved, and this remained as high as >79% and >83% for PFOA and PFOS up till the 12th cycle. Furthermore, Fig. 7c–f shows that the sorbent's shape undergoes negligible change, and some detached magnetic nanoparticles were seen (Wang et al., 2018b).

A somewhat comparable adsorption efficiency was also reported for the removal of PFOA, PFHpA, and PFHxA using bamboo-derived AC (Du et al., 2015) and for the elimination of PFOA and PFOS by triazine-based COF (Wang et al., 2016). Interestingly, from the Wang et al. study, the uptake percentage by the COF diminished slightly by just 11% and 12% for PFOS and PFOA over four adsorption-desorption rounds. Meanwhile, the % desorbed of 80–90% remained virtually unchanged between runs compared to that of AC and SWNT, dropping drastically to 40% and 50% respectively for both PFOA and PFOS (Wang et al., 2016). This is similar to the excellent regenerability (96–100% ADSCAP) demonstrated by Zr-MOF for the adsorption of PFBS in which the adsorption integrity and architectural morphology of the Zr-MOF nanosorbent remain intact (Fig. 7a and b) even after 5 rounds (Li et al., 2021a,b). The authors clarify that while a modest peak broadening of Bragg reflections may indicate a tiny shrinkage of MOF crystallite sizes owing to extended tumbling in the regeneration solvent, the PXRD patterns (Fig. 7b) reveal no loss of Bragg reflections upon regeneration, showing the structural stability of Zr-MOF. Comparing the same BET surface areas (Fig. 7a) to a control sample, there are relatively slight drops of around 4% (1 round) and 6% (5 rounds). Moreover, it was clear from the NMR spectra shown in Fig. 7g–j that the coordination of methoxy groups upon regeneration at the Zr_6 node's active spots is not a requirement for the regeneration activity. Because Cl–Zr has a stronger coordination than MeO–Zr and RSO_3–Zr, the mechanism of Zr-MOF@PFBS regeneration may therefore follow the hard and soft (Lewis) acids and bases theory, with Cl^- anions from the HCl/MeOH mixture supplanting coordinated PFBS at the Zr_6 node (Li et al., 2021a,b). Conversely, from the Du et al. study, after 5 rounds of adsorption-desorption, a significant drop in the EtOH-regenerated AC ADSCAP was recorded. The authors suggest that the adsorption of co-existing other organic compounds on bamboo-derived AC may have contributed to the progressive decline in PFCA elimination by bamboo-derived AC in recycle rounds. These compounds filled the sorption sites and were unable to be desorbed

Table 2
Summary of exemplary studies on PFAS cleanup by various techniques and materials.

PFAS removed	Material/system/method used	Maximum removal efficiency (%)	Time (Mins)	References
PFHxA	GAC/Adsorption	40	10	Hansen et al. (2010)
PFOS	NF90 membranes	96.4	1440	(Li et al., 2021a)
PFOA	CTAB-modified Karanja shells AC/Adsorption	~90	1440	Shaikh et al. (2023)
HFPO-TA	COF2/Adsorption	>99.9	–	(Wang et al., 2021c)
PFOA	Microwave–hydrothermal/persulfate oxidation	100	720	Lee et al. (2009)
PFOS	Rice straw BC-alginate composite beads/Adsorption	99	960	Militao et al. (2023)
PFOA	Al_2O_3/persulfate oxidation	100	120	Wang et al. (2019)
PFOA	NF90 membranes	97.4	1440	(Li et al., 2021a)
PFOS	Ga/TiO_2@AC/UV irradiation	75	240	Zhu et al. (2021)
PFOA	Pt–TiO_2/125 W UV irradiation	100	420	Li et al. (2016)
PFOS	NF270 membranes	>93	–	(Appleman et al., 2013a,b)
PFOS	MNPs@fluorographene/Adsorption	97	2	(Wang et al., 2018b)
PFOA	Needle-like Ga_2O_3/14 W UV irradiation	100	60	Shao et al. (2013a)
PFHxS	maize tassel AC@Ag/Adsorption	>80	1440	Omo-Okoro et al. (2021)
PFHxS	PAC/Adsorption	90	10	Hansen et al. (2010)
PFOA	NF270 membranes	>93	–	(Appleman et al., 2013a,b)
GenX	COF2/Adsorption	>93	–	(Wang et al., 2021c)
PFOA	ß-Ga_2O_3/50 W UV irradiation	100	90	Zhao et al. (2015)
PFAS	[NH_2]–COF/Adsorption	90	30	Ji et al. (2018)
PFBS	rice straw BC-alginate composite beads/Adsorption	39	960	Militao et al. (2023)
PFOA	Ga_2O_3/peroxymonosulfate UV oxidation	100	60	(Xu et al., 2020a)
PFOA	Pd–TiO_2/125 W UV irradiation	94.2	420	Li et al. (2016)
PFOS	PAC/Adsorption	97	10	Hansen et al. (2010)
PFOS	RO membranes	>99	1440	Tang et al. (2007)
PFOA	Pb-$BiFeO_3$/5 W UV irradiation	69.6	480	Shang et al. (2018)
PFHxS	NF90 membranes	99.3	1440	(Li et al., 2021a)
PFNA	PAC/Adsorption	>80	60	Son et al. (2020)
HFPO-DA	Heat/persulfate oxidation	97	2880	Ding et al. (2022)
PFAAs	Chitosan@GAC/Adsorption	39.5	72*	Liu et al. (2022)
PFOS	Nanofiltration membranes	>90	1440	Tang et al. (2007)
PFOA	In_2O_3/persulfate solar light irradiation	98.6	600	(Yuan et al., 2022b)
PFOA	PAC/Adsorption	>80	60	Son et al. (2020)
PFHxA	NF90 membranes	99.6	1440	(Li et al., 2021a)
PFBA	reed straw BC/Adsorption	92	1440	Liu et al. (2021)
PFOS	RO membrane	>99	1440	Tang et al. (2006)
PFHxA	Maize tassel AC@Ag/Adsorption	>80	1440	Omo-Okoro et al. (2021)
PFOS	poly (piperazineamide) NF membrane	91.9	–	(Wang et al., 2018a)
PFPeA	Zr-MOF/Adsorption	~99	>1	(Li et al., 2021b)
PFDcA	PAC/Adsorption	97	10	Hansen et al. (2010)
PFOA	IRA67 ion exchange resin	>80	2880	Du et al. (2015)
PFOA	FeS/persulfate oxidation	85	220	Wu et al. (2018)
PFDA	PAC/Adsorption	>80	60	Son et al. (2020)
PFBS	NF90 membranes	97.4	1440	(Li et al., 2021a)
PFOA	TiO_2-rGO/150 W mercury lamp irradiation	93	720	Gomez-Ruiz et al. (2018)
PFOS	Amb IRA-400/ion-exchange	80	240	Senevirathna et al. (2010)
PFHpA	Zr-MOF/Adsorption	~100	>1	(Li et al., 2021b)
PFOA	Fe-rGO/adsorption	>90	240	Lath et al. (2018)
PFOA	Anion exchange resin/Adsorption	96	1440	Liu et al. (2021)
PFOS	NF membranes	>90	–	Steinle-Darling and Reinhard (2008)
PFOA	In_2O_3/23 W UV irradiation	75	240	(Li et al., 2012a)
PFOS	NF270 membrane	98.6	–	Zhao et al. (2016)
PFOA	TiO_2-rGO/150 W UV irradiation	86	480	Rivero et al. (2020)
PFBS	reed straw BC/Adsorption	93	1440	Liu et al. (2021)
PFOS	Zr-MOF/Adsorption	~100	>1	(Li et al., 2021b)
PFBA	NF90 membranes	96	1440	(Li et al., 2021a)
PFOA	250 W Ultrasound/persulfate oxidation	100	360	Lei et al. (2020)
PFOA	Pt/$La_2Ti_2O_7$/CH_3OH/UV irradiation	50	1440	Chen et al. (2021)
PFOA	MNPs@fluorographene/Adsorption	95	2	(Wang et al., 2018b)
PFHxS	PAC/Adsorption	>80	60	Son et al. (2020)
PFHpA	IRA67 ion exchange resin	>90	2880	Du et al. (2015)
PFOA	aspen chips/Adsorption	~100	1440	Liu et al. (2021)
PFOA	TiO_2@oxalic acid/23 W mercury lamp irradiation	88	180	Wang and Zhang (2011)
PFBS	Zr-MOF/Adsorption	~100	>1	(Li et al., 2021b)
PFOA	Bituminous coal-based GAC/Adsorption	70	–	Siriwardena et al. (2019)
PFOS	PAC/Adsorption	>80	60	Son et al. (2020)
PFOS	ESNA1-K1 NF membrane	>90	–	Zhao et al. (2018)
PFHxA	reed straw BC/Adsorption	92	1440	Liu et al. (2021)
PFOA	NF90 membrane	~100	–	Hang et al. (2015)
PFDA	Zr-MOF/Adsorption	~100	>1	(Li et al., 2021b)
PFOA	corn cobs/Adsorption	~100	1440	Liu et al. (2021)
PFBS	poly (piperazineamide) NF membrane	48.9	–	(Wang et al., 2018a)
PFOS	DowMarathonA/ion-exchange	80	240	Senevirathna et al. (2010)
PFOA	Ag–TiO_2/125 W UV irradiation	57.7	420	Li et al. (2016)
PFOS	RO membrane	>99	1440	Tang et al. (2007)

(*continued on next page*)

Table 2 (*continued*)

PFAS removed	Material/system/method used	Maximum removal efficiency (%)	Time (Mins)	References
PFOA	Carbon aerogel/persulfate oxidation	85.7	480	Lee et al. (2022)
PFHxS	reed straw BC/Adsorption	92	1440	Liu et al. (2021)
PFOA	rGO-TiO_2/8 W UV-C lamp	99.2	480	Panchangam et al. (2018)
PFHxA	IRA67 ion exchange resin	>80	2880	Du et al. (2015)
PFNA	PAC/Adsorption	96	10	Hansen et al. (2010)
PFOA	NF270 membrane	~92.2	–	Hang et al. (2015)
PFOA	$MgAl_2O_4$@CNT/Adsorption	~100	210	Yin et al. (2023)
PFPeS	Quaternized nanocellulose/Adsorption	>90	15	(Li et al., 2023a,b)
PFHxS	Zr-MOF/Adsorption	~100	>1	(Li et al., 2021b)
PFOS	maize tassel AC@Ag/Adsorption	>80	1440	Omo-Okoro et al. (2021)
PFOA	BiOCl@Zn-Al/500 W mercury arc lamp irradiation	90	360	Yang et al. (2020b)
PFOS	NF270 membrane	~97.9	1440	Zhao et al. (2013)
PFOA	Nanospheres In_2O_3/23 W UV irradiation	100	30	(Li et al., 2012b)
PFOA	reed straw BC/Adsorption	92	1440	Liu et al. (2021)
PFOA	BiOI@Bi_5O_7I/800 W Xe irradiation	80	600	(Wang et al., 2020a)
PFHpA	Quaternized nanocellulose/Adsorption	>90	15	(Li et al., 2023a,b)
PFOA	Bamboo AC/Adsorption	>90	2880	Du et al. (2015)
PFOS	NF membrane	>99	1440	Tang et al. (2007)
PFOA	BiOCl/500 W Hg lamp irradiation	100	120	Wu et al. (2021)
PFOS	250 W Ultrasound/persulfate oxidation	100	360	Lei et al. (2020)
PFAS	Tree bark BC/Adsorption	99.6	960	Fabregat-Palau et al. (2022)
PFOA	BiOF nanosheet/500 W Hg lamp	100	360	(Wang et al., 2021a)
PFOA	BEA35 zeolite/persulfate oxidation + heat	99.8	90	Qian et al. (2022)
PFOS	poly (m-phenylene isophthalamide) hollow fiber NF membrane	95.8	–	Wang et al. (2015)
PFOA	SWCNT	>60	–	Wang et al. (2016)
PFOS	Powder AC/Adsorption	93	120	Pala et al. (2023)
PFHpA	Bamboo AC/Adsorption	>90	2880	Du et al. (2015)
PFBA	Zr-MOF/Adsorption	~90	>1	(Li et al., 2021b)
PFOA	In_2O_3/15 W UV irradiation	100	17	Li et al. (2013b)
PFOS	reed straw BC/Adsorption	93	1440	Liu et al. (2021)
PFBA	maize tassel AC@Ag/Adsorption	>80	1440	Omo-Okoro et al. (2021)
PFOA	Ti_3C_2/TiO_2/20 mW cm^{-2} UV irradiation	100	960	Song et al. (2020)
PFBS	GAC/Adsorption	71	1440	Liu et al. (2021)
PFOS	Thin film polyamide RO membrane	>99	5760	Tang et al. (2007)
PFOA	Al-based MOF	>65	>100	(Jun et al., 2019)
PFOS	PAC@polymer/Adsorption	99.2	96*	(Liu et al., 2020a)
PFAS	Thin film polyamide RO membrane	99.4	Several days	Baudequin et al. (2014)
PFOS	Thorium-based MOF/Adsorption	88.2	0.5	Li et al. (2017)
PFOS	IRA 458 resin/ion exchange	>95	240	Carter and Farrell (2010)
PFHxS	GAC/Adsorption	>70	1440	Liu et al. (2021)
PFHxA	Bamboo AC/Adsorption	>90	2880	Du et al. (2015)
PFOA	ZnO-rGO/UV irradiation/ozonation/persulfate oxidation	99.2	240	Wu et al. (2018)
PFCAs	membrane separation and electrochemical oxidation	>90	360	Soriano et al. (2020)
PFOA	Nanoplates In_2O_3/15 W UV irradiation	100	30	Li et al. (2014)
PFOS	GAC/Adsorption	79	1440	Liu et al. (2021)
PFAS	A532E resin/Ion Exchange	53.8	3600	Zaggia et al. (2016)
PFOA	GO-TiO_2/8 W UV-C lamp	93.6	480	Panchangam et al. (2018)
PFOA	GAC-Filtrasorb 400/Adsorption	>98	1440	Yao et al. (2014)
PFTS	250 W Ultrasound/persulfate oxidation	100	360	Lei et al. (2020)
PFOA	PAC	>60	>100	(Jun et al., 2019)
PFOS	SWCNT	>60	–	Wang et al. (2016)
PFOA	CNT/Adsorption	>98	240	Yao et al. (2014)
PFDA	Chitosan@GAC/Adsorption	>60	72*	Liu et al. (2022)
PFOA	GAC/Adsorption	79	1440	Liu et al. (2021)
PFAS	polystyrene-divinyl benzene resin/Ion exchange	90	1440	Liu and Sun (2021)
PFOA	Heat/persulfate oxidation	100	300	Zhang et al. (2019)
PFOS	Mg-Al-LDH/Adsorption	80.7	0.5	Li et al. (2017)
PFDA	maize tassel AC@Ag/Adsorption	>80	1440	Omo-Okoro et al. (2021)
PFOA	ß-Ga_2O_3 nanorod/50 W UV	98.8	90	Zhao et al. (2015)
PFOS	GAC-Filtrasorb 400/Adsorption	>98	1440	Yao et al. (2014)
PFOA	Fe–TiO_2/400 W UV irradiation	60	480	Chen et al. (2015)
PFAS	A592E resin/Ion exchange	99.9	15	Dixit et al. (2021a)
PFOA	Zr-MOF/Adsorption	~100	>1	(Li et al., 2021b)
PFHxS	*Pseudomonas* sp. *strain* PS27/Microbial degradation	32	14400	Presentato et al. (2020)
PFOA	Fe-TiO_2@AC/21 mW cm^{-2} UV irradiation	>90	240	Li et al. (2020)
PFOS	IRA910 resin/Ion exchange	>75	–	Maimaiti et al. (2018)
PFAS	Boron-doped diamond electrodes/electrooxidation	90	270	Urtiaga et al. (2022)
PFOA	CeO_2/In_2O_3/500 W Hg lamp irradiation	100	60	Jiang et al. (2016)
PFOA	Fe-BTC MOF/Adsorption	>75	–	Yang et al. (2020a)
PFOS	UiO-66/Adsorption	>80	–	Clark et al. (2019)
PFNA	Chitosan@GAC/Adsorption	>60	72*	Liu et al. (2022)
PFOS	CNT/Adsorption	>98	240	Yao et al. (2014)
PFOA	Pb–TiO_2/400 W UV irradiation	98	480	(Chen et al., 2016a)
PFOA	Cu–TiO_2/400 W UV irradiation	91	720	Chen et al. (2015)
PFOA	ZIF-L/Adsorption	>80	–	Chen et al. (2016b)
PFBS	IRA 458 resin/ion exchange	>95	240	Carter and Farrell (2010)

(*continued on next page*)

Table 2 (*continued*)

PFAS removed	Material/system/method used	Maximum removal efficiency (%)	Time (Mins)	References
PFHpA	maize tassel AC@Ag/Adsorption	>80	1440	Omo-Okoro et al. (2021)
PFOS	Ultrasonic irradiation	73	120	Vecitis et al. (2010)
PFOA	sheaf-like Ga_2O_3/UV	100	45	Shao et al. (2013b)
PFOA	PAC@polymer/Adsorption	85.5	96*	(Liu et al., 2020a)
PFOA	TiO_2@MWCNT/UV	~100	480	Song et al. (2012)
PFOS	IRA67/Adsorption	56.9	0.5	Li et al. (2017)
PFNA	Maize tassel AC@Ag/Adsorption	>80	1440	Omo-Okoro et al. (2021)
PFOA	In_2O_3/500 W Hg lamp irradiation	88	60	Jiang et al. (2016)
PFBS	UiO-66/Adsorption	>80	–	Clark et al. (2019)
PFOA	PAC/Adsorption	88	10	Hansen et al. (2010)
PFOA	GAC/Adsorption	58.9	1440	(Xu et al., 2020b)
PFOA	TiO_2@$HClO_4$/16 W UV-irradiation	86	420	Panchangam et al. (2009)
PFBS	Quaternized nanocellulose/Adsorption	~50	15	(Li et al., 2023a,b)
PFOS	polyamide NF membranes	99	5760	Tang et al. (2007)
PFOA	maize tassel AC@Ag/Adsorption	>80	1440	Omo-Okoro et al. (2021)
PFOA	Purolite A860 resin/Ion exchange	99	–	Dixit et al. (2019)
PFOA	In_2O_3@graphene/15 W UV irradiation	100	180	Li et al. (2013a)
PFOA	GO-P25/8 W UV-C lamp	96	480	Panchangam et al. (2018)
PFOA	IRA67 anion-exchange resin	>98	120	Yao et al. (2014)
PFHpA	PAC/Adsorption	81	10	Hansen et al. (2010)
PFNA	TiO_2@$HClO_4$/16 W UV-irradiation	99	420	Panchangam et al. (2009)
PFAO	Fe@AC/persulfate oxidation	61.7	600	Lee et al. (2020)
PFOS	MIL-101(Cr)@AC/Adsorption	80	120	Pala et al. (2023)
PFOS	triazine-based COF	>65	–	Wang et al. (2016)
PFHxA	Quaternized nanocellulose/Adsorption	~50	15	(Li et al., 2023a,b)
PFHxA	PAC/Adsorption	78	10	Hansen et al. (2010)
PFOS	Purolite A860 resin/Ion exchange	99	–	Dixit et al. (2019)
PFOA	Fe_3O_4@GAC/Adsorption	79.10	1440	(Xu et al., 2020b)
PFCAs	Fe@AC/persulfate oxidation	41.9	600	Lee et al. (2020)
PFOA	quaternized MIL-101/Adsorption	>80	–	Liu et al. (2015)
PFPeA	maize tassel AC@Ag/Adsorption	>80	1440	Omo-Okoro et al. (2021)
PFDA	TiO_2@$HClO_4$/16 W UV-irradiation	100	420	Panchangam et al. (2009)
PFOS	IRA67 anion-exchange resin	>98	120	Yao et al. (2014)
PFOA	triazine-based COF	>65	–	Wang et al. (2016)

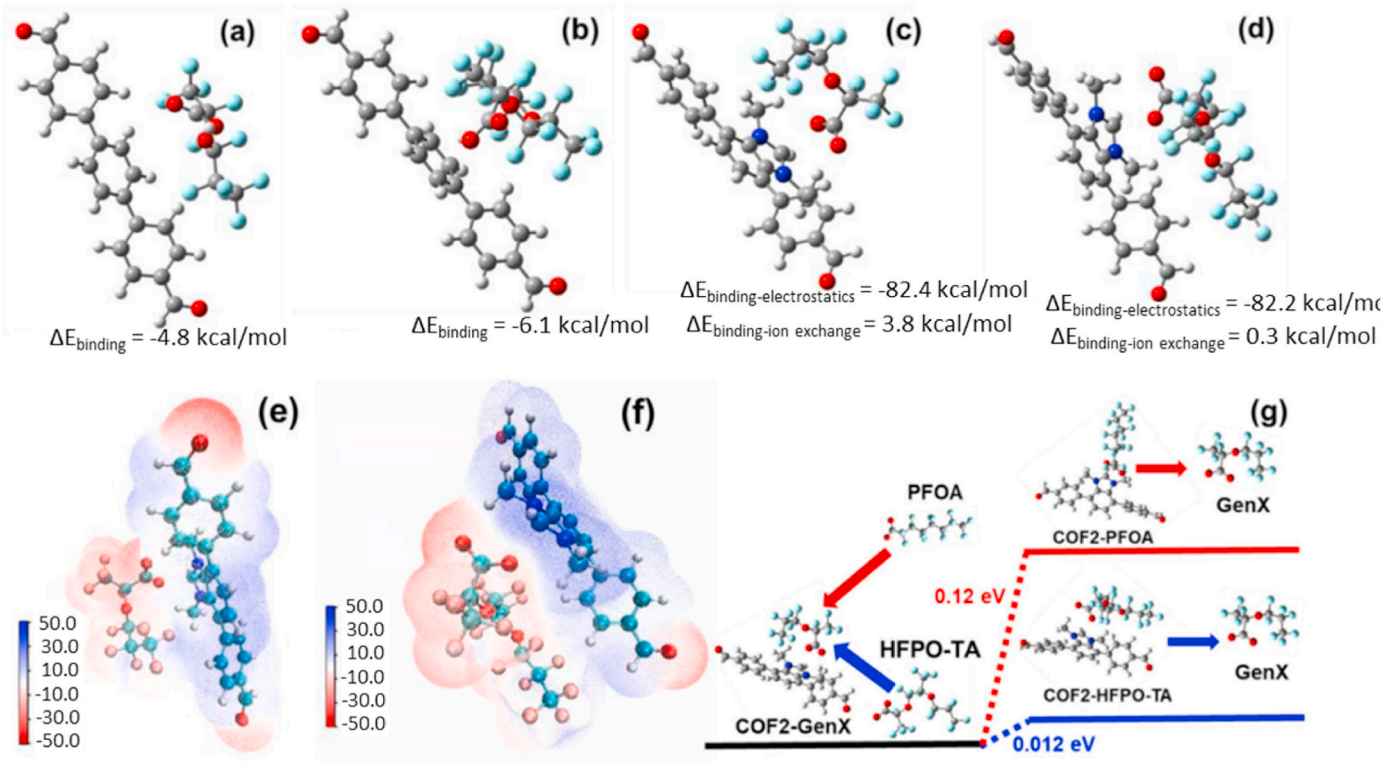

Fig. 6. DFT computed ΔE and conformations for (a) GenX and (b) HFPO-TA on the COF architecture. ΔE and conformations for (c) GenX and (d) HFPO-TA sorption on COF2 architecture through electrostatic attraction and IEX. ESP mapping after (e) GenX and (f) HFPO-TA uptake, and (g) the energy required in the substitution of GenX pre-sorbed on COF2 by PFOA and HFPO-TA (Wang et al., 2021c). Reused with permission from Elsevier (Approval code.: 5835010688154, Copyright 2020).

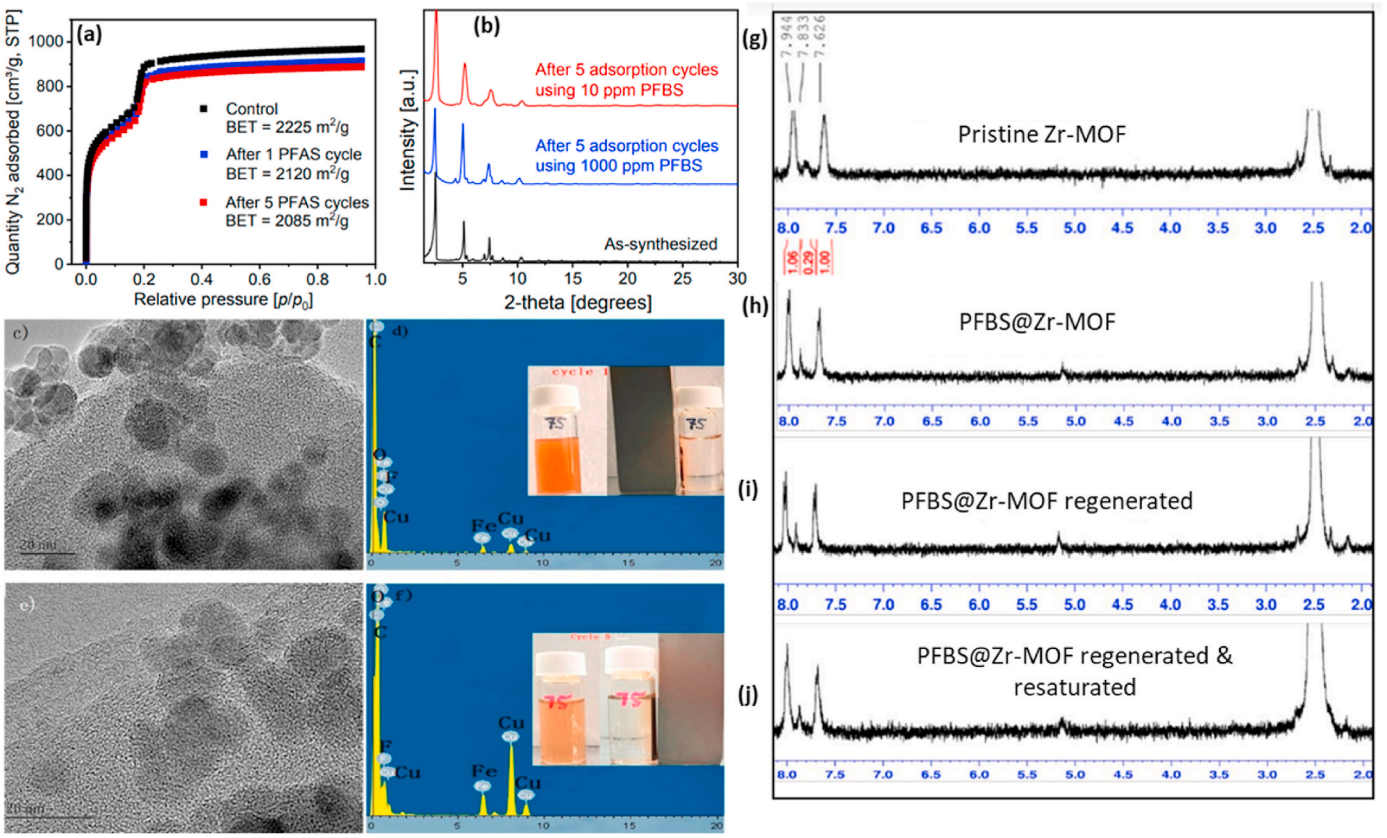

Fig. 7. (a) BET of Zr-MOF after 1 and 5 rounds of PFBS sorption, (b) PXRD patterns of Zr-MOF after 5 rounds of PFBS sorption (Li et al., 2021b). Copyright 2021, with open access permission from the American Chemical Society. (c) TEM image, and (d) EDS images of the fresh MNPs@FG nanosorbent. (e) TEM of image and (f) EDS images of the regenerated MNPs@FG nanosorbent after 5 rounds of PFOS sorption (Wang et al., 2018b). Reused with permission from Elsevier (Approval code.: 5835010979601, Copyright 2018). 1H NMR spectra of Zr-MOF sorbents: (j) as-fabricated before PFBS sorption, (h) following saturation with PFBS, (i) following regeneration with a mixture of HCl/MeOH, and (j) following resaturation with PFBS of the formerly regenerated Zr-MOF sorbent (Li et al., 2021b). Copyright 2021, with open access permission from the American Chemical Society.

during the regeneration operation (Du et al., 2015).

Notably, in another batch adsorption experiment carried out by (Riegel et al., 2023), it was shown that because of a decreasing polarity with chain length, long-chain PFAS are better absorbed by GAC than short-chain PFAS (Ochoa-Herrera and Sierra-Alvarez, 2008; Hansen et al., 2010; Medina et al., 2022). Furthermore, in another study, to juxtapose the various PFAS compounds' adsorbing capabilities, equilibrium batch tests were conducted. The sorbents' growing ADSCAP for PFAS with increasing chain length was confirmed for the sulfonic and carbonic compounds in the equilibrium batch experiments using demineralized water. In addition, higher Freundlich constant values and smaller Freundlich n values were found with longer chains and the findings of the AC experiments indicated that sorption occurred in the following order: PFOA > PHFxA > PFPeA > PFBA (Riegel et al., 2023).

In another key research finding made by (Li et al., 2023a,b), it was reported that cationic nanocellulose sorbent outperformed conventional GAC, particularly for short-chain PFASs, with outstanding elimination proficiency of over 95% for long-chain PFAS even at minimal sorbent dosages. According to the hydrophobicity trend among the PFAS molecules based on chain length and functional group, the nano cellulose sorbents with long-chain PFAs such as PFOS (559 mg/g) exhibited the highest capacity, followed by PFOA (405 mg/g), and the short-chain PFAs like PFBS (319 mg/g), and PFBA (121 mg/g) and the same trend was noted as shown in Fig. 7a when the nanosorbent was employed to clean up PFAS in polluted groundwater matrix collected from Long Island, New York (Li et al., 2023a,b). This real contaminated PFAS water cleanup for long-chain molecules is consistent with what was achieved by Li's research group (Li et al., 2021a,b) for PFAS-polluted groundwater from the U.S. Air Force Base as displayed in Fig. 8b. However, the Zr-MOF employed showed good adsorption for short-chain molecules as well (Li et al., 2021a,b).

Also, Omo-Okoro and co-workers (Omo-Okoro et al., 2021) reported on the adsorption of PFAS onto physically and chemically activated maize tassel AC@Ag. It was found that by applying chemically activated AC@Ag sorbent (81.17–83%), the percentage elimination of all 10 PFAS, including short and long chain, was greater than with physically activated AC@Ag sorbent (79.15–81%). Moreover, it is glaring that both HPB and ESI were at work during the adsorption operation with HPBI being the overriding force at an alkaline medium (pH 9). Pala's team (Pala et al., 2023) differ not in their observation as well as it was accentuated that the probable interactions between PFOS and MIL-101 (Cr)@AC are largely governed by HPB and ESI during the adsorption operation, followed by metal coordination and HB, as portrayed in Fig. 9 c. In addition, an outstanding PFOS cleanup efficiency of 80% was recorded in 120 min for the MOF/AC nanosorbent, and the EDX mapping of sulfur displayed in Fig. 9a and b following the uptake of PFOS by nanosorbent established the existence of PFOS on the surface of the MOF-AC. Similar excellent adsorption efficiency was also reported for the removal of PFNA, PFOA, PFDA, PFHxS, and PFOS in 60 min using PAC as presented in Table 2 (Son et al., 2020) and this is consistent with the ADSCAP of reed straw-derived BC for the removal of PFHxS, PFBS, PFOS, PFHxA, PFOA, PFBA but at a longer time (Liu et al., 2021) and MOF for the removal of PFOS where the authors additionally accentuated that nanosorbent with a reduced pore size or the maximum unsaturated metal sites exhibited a greater coordinative interaction with PFOS (Zhao et al., 2021). In another research, Li and co-workers (Li

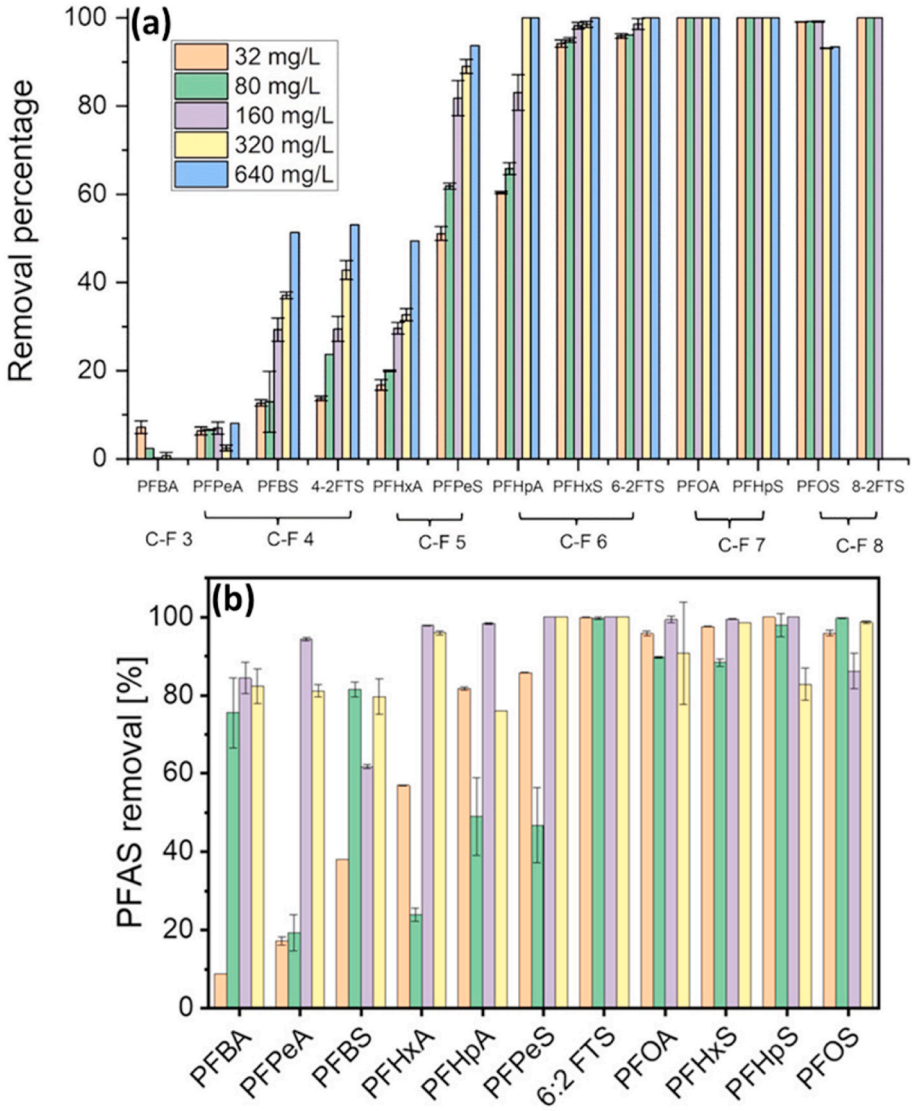

Fig. 8. % Cleanup of different PFASs in polluted groundwater matrix collected from (a) Long Island, New York by different dosages of quartenized nanocellulose (Li et al., 2023a,b), (b) U.S. Air Force Base using Zr-MOF nanosorbent (Li et al., 2021b). Copyright 2021, with open access permission from the American Chemical Society.

et al., 2017) investigated a mesoporous cationic thorium-based MOF with a high surface area of 1360 m^2/g and channels with a huge inner diameter of 2.2 nm for PFOS adsorption. Notably, the results show both high sorption selectivity of over 85% toward PFOS and rapid absorption rates. In addition, simulations utilizing quantum mechanics and molecular dynamics were employed to investigate the fundamental sorption mechanism. These theoretical results show that at various adsorption phases, driving factors such as hydrogen bonds, electrostatic interactions, hydrophobic interactions, and van der Waals interactions immobilize PFOS anions in MOF. This result is somewhat close to the 80.7% PFOS adsorption efficiency reported for Mg-Al-LDH (Li et al., 2017). In another study (Hansen et al., 2010), powder activated carbon was used to adsorb 97% PFOS in 10 min. Comparatively, under the same experimental condition, only 24% PFOS was adsorb by granular activated carbon. Interestingly, both adsorption data fitted Langmuir isotherm model (Hansen et al., 2010). Conversely, as in the case of adsorption of PFOS by granular activated carbon, multi-walled carbon nanotube, and alumina, the adsorption was confirmed to fit Freundlich isotherm and pseudo-second-order kinetic better. In addition, both granular activated carbon, and multi-walled carbon nanotube were able to remove over 98% PFOS compared to alumina that removed only 56% PFOS under the same experimental conditions (Yao et al., 2014).

3.2. *Membrane filtration technologies*

Compared to purification and separation strategies, two characteristics set membrane filtration apart: first, a small-pore feed route minimizes the total pressure drop inside the membrane, lessening the likelihood of clogging. Secondly, the membranes themselves are asymmetric. In addition, effective crossflow is critical to membrane system performance since it helps eliminate filter cake collection down to a few millimeters. The great efficiency, low energy consumption, and scalability of membrane-based separation systems make them popular in industrial water treatment and many other applications (Maroufi and Hajilary, 2023). During the membrane filtration operation, hydraulic pressure is employed to force water to permeate across the semi-permeable membrane while rejecting the undesirable solutes as retentate (Abdullah et al., 2023). Currently, four primary membrane processes—microfiltration (MF), ultrafiltration (UF), reverse osmosis (RO), and NF—are used to purify water and eliminate contaminants based on the size of its pores (Pilli et al., 2021; Maroufi and Hajilary, 2023). These methods work effectively across a range of pressure and pH

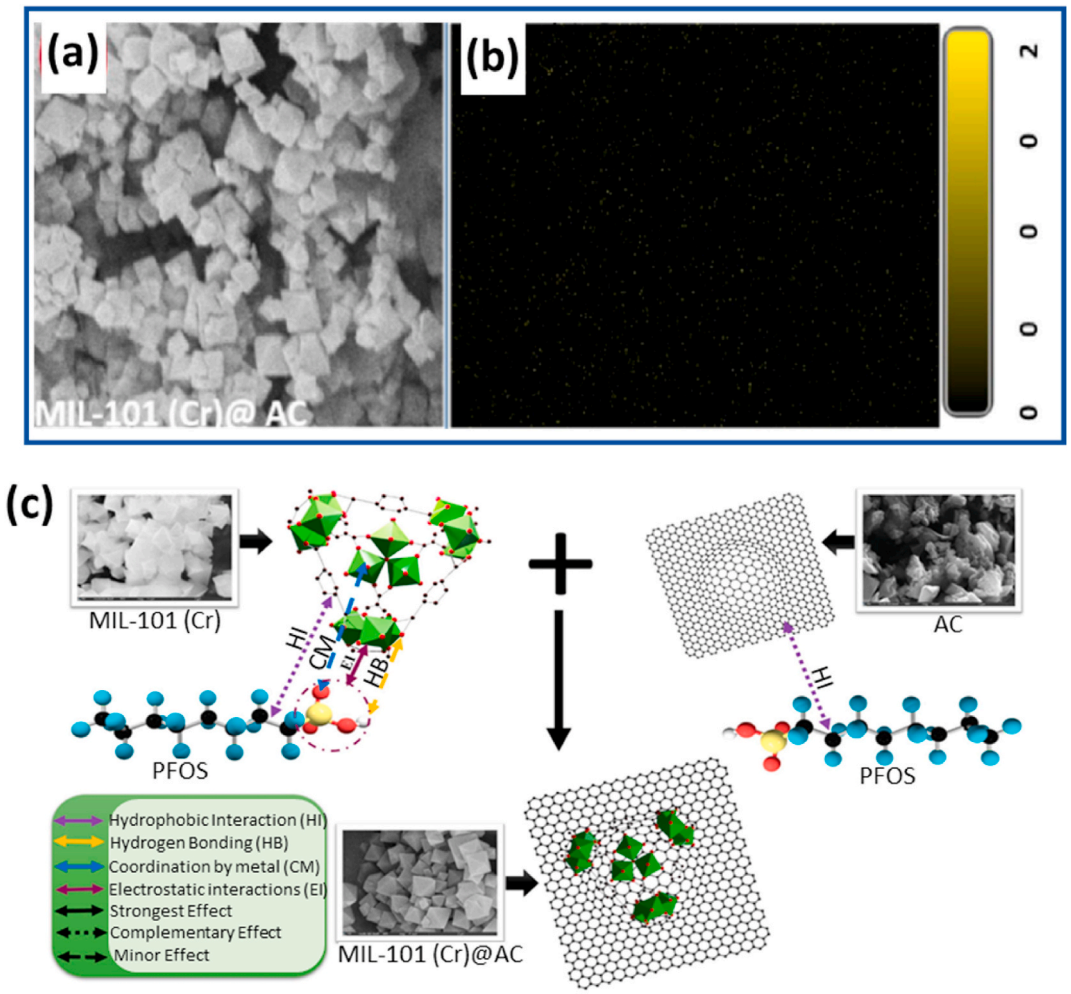

Fig. 9. (a–b) EDX mapping of sulfur following uptake of PFOS by MIL-101 (Cr) @AC. (c) Diagram illustrating potential interactions that may occur when PFOS is adsorbed on MIL-101 (Cr)@AC. The intensity of the interaction is qualitatively epitomized by the arrows between the chemical structures (Pala et al., 2023). Reused with permission from Elsevier (Approval code.: 5835021238764, Copyright 2022).

circumstances. The technique's excellent removal efficacy, independence from chemicals, mechanical toughness, chemical stability, ability to withstand intense heat, decreased need for an expert operator, and relatively low energy consumption are further advantages (Pezeshki et al., 2023). However, RO and NF discussed in the next subsections are the most researched for the removal of PFAS and this might be because their pore diameters are better suited for filtration for the elimination of almost all kinds of impurities as depicted in Fig. 10 (Pan et al., 2016).

3.3. Reverse osmosis

Reverse osmosis, in which the direction of water across a semi-permeable membrane is changed such that pure water flows from the concentrated side to the diluted side and ions are stopped from flowing through the membrane, is one of the most advanced pressure-driven membrane strategies for eliminating membrane-bound contaminants (Pezeshki et al., 2023). More specifically, in RO, organic molecules are transferred across high-pressure membranes by solute-membrane interactions mediated by steric hindrance, electrostatic, and HPBI (Kucharzyk et al., 2017). This method plays a crucial role in purification and wastewater treatment operations because of its capability and reliability in rejecting almost all sorts of contaminants including monovalent ions (Abdullah et al., 2023) and PFAS (Tang et al., 2007). In a particular report, when polyamide membranes were used for RO filtration of PFOS, almost 99% of the material was removed, with concentrations ranging from 0.5 to 1500 mg/L (Tang et al., 2007; Pilli et al., 2021). Similarly, another research team (Tang et al., 2007), looked at the extraction of PFOS from wastewater, the pollutant was extracted from using RO. Over four days, tests were conducted on 5 RO membranes with a 10 ppm PFOS inlet concentration. A thorough investigation was conducted into the membrane flux and PFOS resistance efficiency. Rejection of sodium chloride and PFOS were +vely linked. The RO membranes had rejection efficiencies of more than 99%. This outstanding PFOS rejection is in parallel with what has been reported in the earlier year (Tang et al., 2006) by the same research group. Notably, for four membranes used, strong rejection was seen across a broad range of feed concentrations and the rejection surpassed 99% at feed concentrations greater than 1 ppm. Specifically, except for feed quantities of 1600 ppm when 5% isopropyl alcohol was also present, rejection rose with increasing PFOS concentrations. This is comparable to the outcome that was reported by (Baudequin et al., 2014) using a thin film polyamide membrane for reverse osmosis. After carrying out the experiments for several days on firefighting waters containing fluorinated surfactants, a rejection efficiency of 99.4% was achieved (Baudequin et al., 2014). In addition, at feed PFOS values of 2.5 ppm and below, no appreciable decrease in permeability was seen. On the other hand, permeability varies with time for feed concentrations between 10 and 500 ppm. Even at 500 ppm PFOS, when the feed solution was almost saturated, a respectable flux was still attainable. However, permeability dropped as PFOS content rose. The PFOS molecules' trapping in the

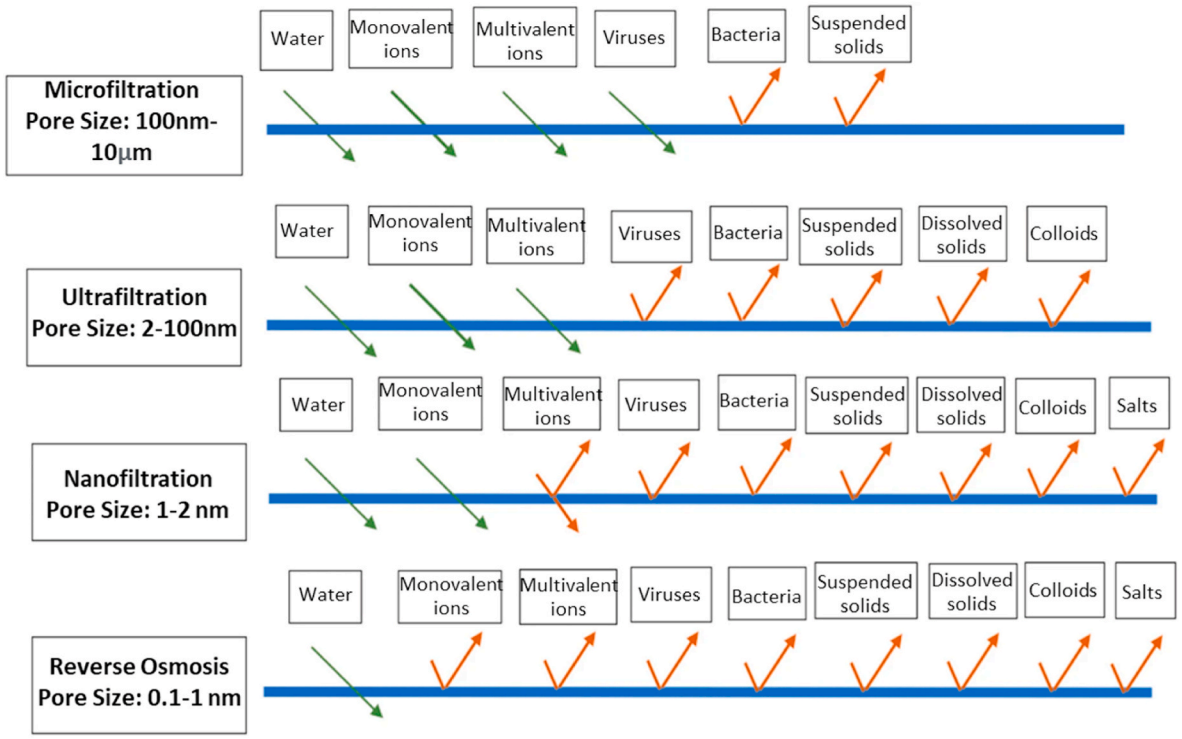

Fig. 10. The categorization of membranes used in water purification based on pore size and residual species (Maroufi and Hajilary, 2023). Reused with permission from Springer Nature (Approval code.: 501921599, Copyright 2023).

polyamide layer and subsequent buildup on the membrane surfaces are most likely responsible for the flux reduction (Tang et al., 2006).

3.4. Nanofiltration

The use of nanofiltration membranes (NFM) to provide high-quality drinking water and remove pollutants from aquatic bodies is a cutting-edge, practical, affordable, environmentally and economically beneficial option (Mallya et al., 2023). This method has been employed to clean up PFAS from time to time. In a work reported by Mu's research group (Li et al., 2021a,b), six PFCs with various head groups and C-F chains were eliminated by employing a loose NFM and a tight NFM. The tight membrane's rejection rate rose by 0.8%–7.4% while the loose membrane's rejection rate climbed by 2.2%–36.0%, according to the outcomes of electrostatic repulsion. HPBI and HB, two non-ESI, reduced the rejection rates of the tight and loose membranes by 9.5%–23.6% and 1.2%–10.3%, accordingly. To learn more about the process behind the courses of interactions between NFMs and PFCs—which are described as stable, anionic forms that occur in aqueous environments—DFT computation was used and presented in Fig. 11 is the DFTcomputed

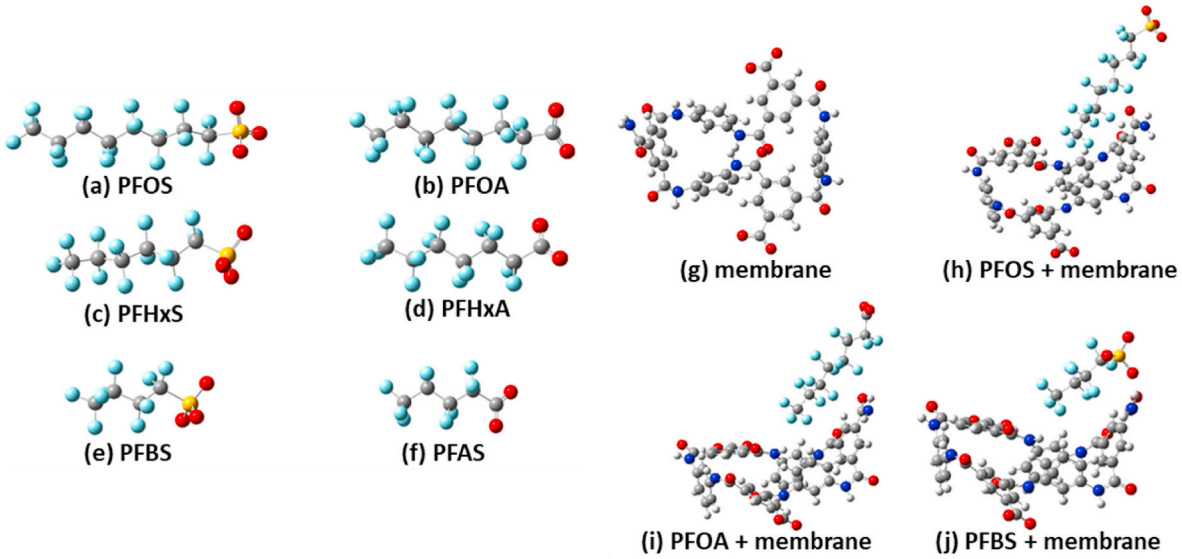

Fig. 11. Structure of (a) PFOS, (b) PFOA, (c) PFHxS, (d) PFHxA, (e) PFBS and (f) PFBA. (g) Simulated structure of NFM. DFT geometry of (h) PFOS bond with NFM. (i) PFOA bond with NFM and (j) PFBS bond with NFM. Dark blue, blue, red, yellow, and dark grey, circles represent N, F, O, S, H, and C, atoms, correspondingly (Li et al., 2021a). Reused with permission from Elsevier (Approval code.: 5835030389216, Copyright 2020).

PFCs ion geometries in an aqueous solution. The positively charged group on the membrane surface caused the PFC head groups to be forced away, as seen by the structure of Fig. 11 h, **i**, and **j**. By contrast, the C-F chain would be on the membrane surface because of H-bonding from the surrounding water molecules and HPBI and these results imply that H-bonds and HPBI are the primary ways in which PFCs interact with NFMs (Li et al., 2021a,b). In another study (. Appleman et al., 2013a,b), the efficiency of NF in cleaning a suite of PFAAs from an aquatic matrix was experimented with using deionized water and artificial groundwater, virgin flat-sheet NFMs (NF270, Dow/Filmtec) were evaluated at permeate fluxes of 17–75 L/m^2/h. Tests were conducted using constant permeate flow settings to examine the impact of humic acid-induced membrane fouling on PFAA rejection. Under all testing circumstances, both virgin and contaminated NF270 membranes showed >93% elimination for all PFAAs (Appleman et al., 2013a,b). This remarkable PFAA removal output is consistent with the one achieved by (Hang et al., 2015) where the efficiency of two market-ready NFMs (NF90 and NF270), were assessed and the outcomes demonstrated that the NF90 membrane afforded an excellent PFOA rejection of practically 100% while NF270 offered a rejection of about 92.2% at a PFOA concentration below 800 mg/L (Hang et al., 2015). In another study (Steinle-Darling and Reinhard, 2008), four nanofiltration membranes (NF270, NF200, DK, and DL) were used to assess the rejections of 15 perfluorochemicals. For MW (molecular weight) > 300 g/mol, rejections for anionic species were more than 95%. As few as 42% (DL membrane) of FOSA (MW = 499 g/mol), which is uncharged at the pH of 5.6, were rejected. Surprisingly, rejection may be reduced by up to 35% when the pH is lowered to less than 3, which increases the MWCO of NF270 by more than 200 g/mol. Rejections can be reduced by less than 1% when the ionic strength is increased by 2500 mg/L of NaCl equivalent. It was deduced that two distinct sorption operations are important according to rejection kinetics and the amount of sorption: charged species adsorb rapidly to the membrane surface, but the uncharged FOSA absorbs inside the membrane matrix in a far slower process (Steinle-Darling and Reinhard, 2008).

Notably, researchers have used the NFM to filter out PFAS from the water matrix. Nevertheless, the filtration capacity of NFMs is influenced by the physicochemical characteristics of PFAs (Appleman et al., 2013a, b; Pilli et al., 2021). For example, Appleman and co-workers (Appleman et al., 2013a,b) discovered that membrane fouling can affect the effectiveness of PFAA removal using NF, however, by implementing techniques including pre-treatment procedures, membrane surface modification, and periodic cleaning protocols, the fouling effect can be reduced. In addition, to boost the effectiveness of PFAA removal through NF, a steady and optimum permeate flux should be maintained (Appleman et al., 2013a,b; Pilli et al., 2021). Also, dissolved organic matter (DOM) can have a big impact on how well PFAAs are removed during NF (Appleman et al., 2013a,b). The rejection of PFAAs can be impacted by DOM's competition with PFAAs for adsorption sites both on the membrane matrix and in the membrane's outermost layer. Additionally, it has been discovered that co-existence ions like Ca^{2+} and Fe^{3+} coordinate with the -SO_3 groups of the PFOS molecule, which in turn affects the rejection characteristics of the NFM (Zhao et al., 2018). In particular research (Zhao et al., 2018), To separate PFOS compounds in the presence of three cations (Na^+, Ca^{2+}, and Fe^{3+}) as well as three anions (Cl^-, SO_4^{2-}, and PO_4^{3-}) a commercial NFM (ESNA1-K1) was employed. With 2 mM Na^+, Ca^{2+}, and Fe^{3+}, respectively, the PFOS rejection rose from 92.65% to 94.74%, 97.14%, and 97.94%. The percentage of PFOS rejection rose to 94.74% and 97.60%, respectively, as the concentrations of anions, such as SO_4^{2-}, and PO_4^{3-}, reached 2 mM. Three distinct cations' interactions with the PFOS molecule were examined using the DFT. It showed that each Ca^{2+} or Fe^{3+} ion preferred to coordinate with two PFOS molecules, but a single Na^+ ion could only interact with one PFOS molecule. Specifically, the computed geometries and the architectural parameters are displayed in Fig. 12. More specifically, the configurations of $[Ca\ (H_2O)_6]^{2+}$ and $[Fe(H_2O)_6]^{3+}$, which represent the stable species of Ca^{2+} and Fe^{3+} cations in the aqueous solution, respectively, are shown in Fig. 12a and **b**. According to a frontier orbital study, the -SO_3 group was the active site that could bind to positi vely charged cations including Na^+, $Ca^{2+,}$ and Fe^{3+} cations, and it was also reported that the HOMO of the anionic PFOS surfactant predominantly localized on the head of the sulphonate group (Fig. 12c).

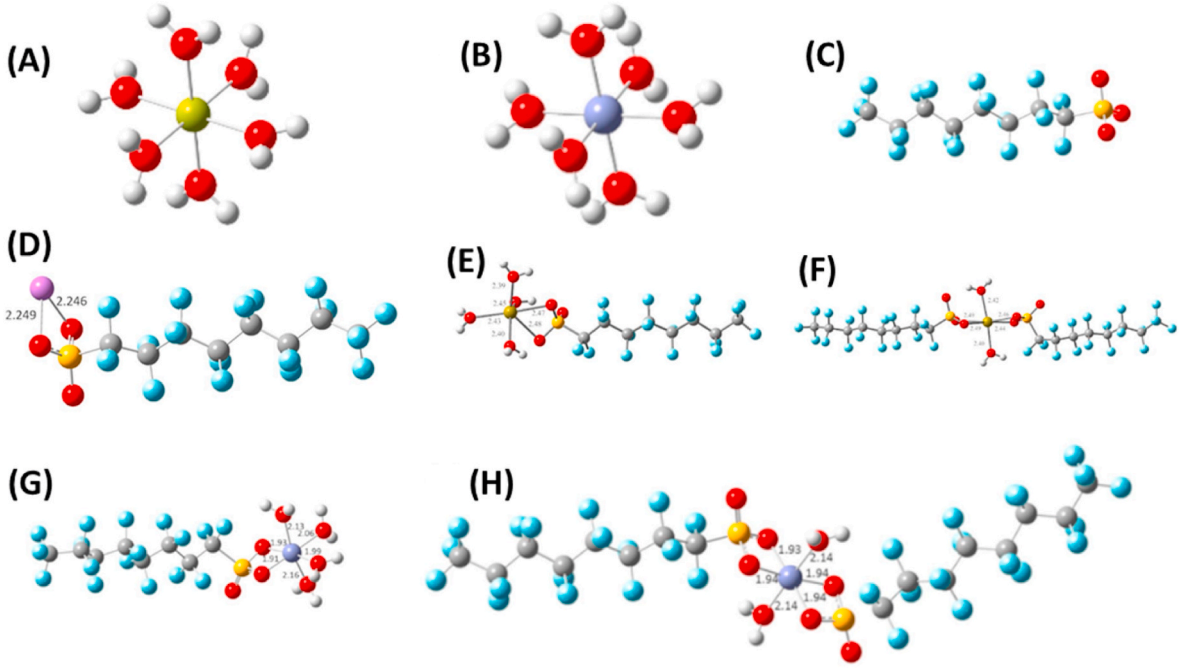

Fig. 12. The spatial architectures of PFOS and its compounds as computed by DFT: (a)$[Ca(H_2O)_6]^{2+}$, (b) $[Fe(H_2O)_6]^{3+}$, (c) the HOMO orbitals of PFOS, (d) the geometry of a Na + ion bound to single PFOS, (E) the geometry of a Ca2+ ion bound to single PFOS, (F) the geometry of a Ca2+ ion bound to deuce PFOS, (G) the geometry of a Fe3+ ion bound to single PFOS molecule and (H) the geometry of a Fe3+ ion bound to deuce PFOS molecules (Zhao et al., 2018). Reused with permission from Elsevier (Approval code.: 5835030714869, Copyright 2018).

One or two anionic PFOS molecules might attach to the Ca^{2+} and Fe^{3+} ions, forming a bridge architecture (Zhao et al., 2018). A similar effect of Ca^{2+} on the use of NFM for the removal of PFOS was also reported (Zhao et al., 2013). The findings demonstrate that, at the same pressure, PFOS rejection rose as calcium concentration did. When the calcium concentration exceeded 1 mM, the PFOS rejection was more than 98%. The structural characteristics and configurations of PFOS interacting with Ca^{2+} ions are computed using DFT and are shown in Fig. 13. The HOMO of the PFOS anion was nearly entirely localized on the sulfonate headgroup, according to frontier orbital analysis (Fig. 13a). According to the HOMO distribution, the reactive spots in aqueous solutions that formed bonds with positively charged calcium ions were the $–SO_3$ groups. The DFT results demonstrated that the molecular polarity (μ from 23.1 to 35.9) was improved by the creation of the $CF_3(CF_2)_7SO_3Ca^+$ structure (i.e., Ca^{2+} ion coupled with one PFOS molecule, Fig. 13b), which was advantageous for interacting with the charged membrane surface. In a pH 7.0 environment, Ca^{2+} ions neutralized the negatively charged NF270 membrane as well as PFOS anions, which encouraged the sorption of PFOS on membrane surfaces. Conversely, the bivalent calcium ions have the potential to form a neutral $CF_3(CF_2)_7SO_3CaO_3S(CF_2)_7CF_3$ bridging architecture by bonding with two PFOS anions. The negative sulfonate group's charge-charge repulsion was negated by the Ca^{2+} ion, which then created a strong attraction at Ca–O(S) distances of around 2.47 Å. The Ca-bridging structure seen in Fig. 13c was formed as a result of this attraction, which was sufficiently powerful to bind the PFOS molecules together. Additionally, it was confirmed by DFT micro-computation that complexation—which led to a bigger molecular size and more noticeable sieving mechanism—was one of the causes of the rise in rejection. These results generally corroborate our DFT simulation, which showed that the calcium-bridging effect causes an increase in the size of PFOS molecules and their adsorption on the membrane (Zhao et al., 2013). It can be accentuated that optimizing the nanofiltration process requires an understanding of the properties of the aqueous matrix, including the concentration and composition of co-existing ions and DOM. In addition, nanofiltration can be improved by employing methods including DOM characterization, sophisticated water quality analysis, and the creation of customized treatment plans according to the unique water matrix (Appleman et al., 2013a,b).

3.5. Ion exchange

Ion exchange techniques replace target ions inside a mixture with interchangeable ions with charges to remove PFAS from water (Rahman et al., 2014). Anion exchange is the reversible transfer of counter ions with a negative charge like OH^-, Cl^-, and HCO^{3-}, from a polymeric resin's surface to the surrounding aqueous matrix (Levchuk et al., 2018). A great deal of research has been done on the effectiveness of anionic and non-anionic IX resins in eliminating PFAS (Dixit et al., 2021b). It has been observed that IX performance is comparable to other pollutant cleanup methods, especially for short-chained PFAS, including adsorption using activated carbon and advanced oxidation procedures (Gagliano et al., 2020; Dixit et al., 2021b). PFAS absorption on a variety of adsorbents has been connected to many processes, including ESI, HB, HPB effects, van der Waals forces, and π-π bonding (Appleman et al., 2014; Lu et al., 2016; McCleaf et al., 2017; Gagliano et al., 2020; Dixit et al., 2021b). In ESI charged particles are attracted to and repelled by one another in this mechanism. When it comes to IEX, ESI is crucial because it occurs when the resin's surface charge interacts with the charged ions in the solution, causing an exchange of ions (Gagliano et al., 2020). The propensity of HPB molecules to combine in aqueous solutions is known as HPBI. When it comes to IEX, HPB effects can help the resin absorb non-polar or HPB substances, especially when water is present (Levchuk et al., 2018; Dixit et al., 2021b). van der Waals forces are produced when molecules' temporary dipole moments occur. van der Waals forces could be involved in IEX by attracting the target ions or compounds to the resin and promoting their uptake (Du et al., 2014).

HB is a possible pathway for PFAS intake through the IX process. In this, the oxygen atoms in the PFAS functional heads can act as acceptors and form bonds with the resin polymer's hydrogen atoms. Several research initiatives have examined the presence of HB in the process of removing PFAS from carbon-based media and other sorbent substances including inorganic oxides (Deng et al., 2012; Lu et al., 2016). Nevertheless, research on the amount of HB that occurs throughout the IX process has not yet been published (Dixit et al., 2021b). Experimental evidence has shown that the electrostatic forces acting throughout the IX process have been verified by the effect of altering solution pH affecting PFAS absorption. The uptake of anionic PFAS is directly impacted by altering the surface charge on IX by the protonation of surface chemical moieties in reaction to variations in pH levels. Moreover, PFAS migrate toward non-polar HPB surfaces with the help of entropy, which results in the HPB effect (Du et al., 2014; Gagliano et al., 2020). PFAS may face competition for active IX absorption sites from inorganic ions like sulphates, phosphates, and nitrates, as well as organic compounds like fulvic acids and humic fractions. The effectiveness of PFAS absorption in natural waterways is impacted by this competition (Dixit et al., 2021b). For example, in a particular study (Dixit et al., 2019), two of the most

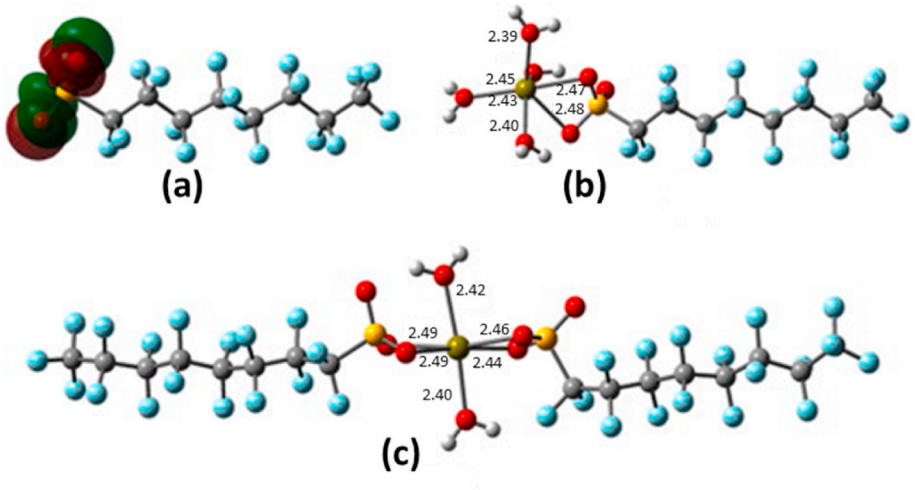

Fig. 13. (a) Structure and HOMO orbitals of PFOS molecule; (b) Geometry of calcium ion connected with single PFOS molecule; and (c) Geometry of Calcium ion connected with deuce PFOS molecules. Red, yellow, blue, dark yellow, and grey circles correspondingly represent O, S, F, Ca, and C atoms (Zhao et al., 2013). Reused with permission from Elsevier (Approval code.: 5835031221332, Copyright 2013).

persistent PFAS, PFOA and PFOS were eliminated using Purolite A860 resin (a very basic anion exchange resin). To assess the competitive absorption between OM and PFAS, the equivalent background concentration was utilized. It was found that IX succeeded in removing all PFAS and more than 60% of the dissolved organic carbon (DOC) at the same time. The presence of greater molecular weight organic components and humic was similarly associated with evidence of pore obstruction and size exclusion. The study's findings show that IX has a lot of promise for removing OM and PFAS together in situations involving drinking and potable water treatment (Dixit et al., 2019). In like manner, PFOS and PFBS removal from water using GAC and IRA-458 IEX resin was studied. According to kinetic tests, the GAC needed around 50 h and the resin about 10 h to reach the uptake equilibrium. More specifically, as presented in Table 2, over 95% of the PFOS and PFBS were eliminated in 240 min. According to sorption isotherms, the absorption of PFOS and PFBS was endothermic and facilitated by HPB effects on the GAC as well as a combination of IEX and HPB adsorption on the resin. The ionic makeup of the solution had a significant impact on the aqueous solubility of PFOS. The resin's absorption of PFOS and PFBS was hysteretic and almost completely irreversible when employing traditional regeneration techniques (Carter and Farrell, 2010). In another experiment, the ADSCAP of A532E was nearly equivalent to that of bituminous-coal derived GAC when evaluated for PFBS removal (4.7 μg/g and 4.1 μg/g, respectively), according to results from fixed-bed column testing (Zaggia et al., 2016). Also, in another research, anion-exchange resins were used to remove PFASs, and the impact of co-existing compounds on this process was investigated, as well as the competitive adsorption of PFASs. The representative PFAS used was PFHxS, and resin IRA910 was found to be efficient in removing PFHxS. PFHxS substituted the adsorbed PFASs with shorter C-F chains on the IRA910 when it was co-eliminated with other PFASs in a bisolute system, however, PFOS was not replaced by PFHxS. The sequence of the decline in competitive adsorption among PFASs was PFOS > PFHxS > PFOA > PFBS > PFHxA > PFBA. This decline was strongly associated with the hydrophobicity and functional groups of PFASs. Ionic organic compounds can decrease sorption quantity and have a concentration-dependent effect on PFHxS sorption, but nonionic organic compounds are unable to impede PFHxS clearance. The clearance effectiveness of PFHxS was marginally reduced by the presence of inorganic anions, and the impacts of various inorganic anions were comparable because of several factors including competitive anion, screening effect, and salting-out effect during the adsorption operation (Maimaiti et al., 2018). Another Research group (McCleaf et al., 2017) reported rapid breakthrough and poor removal percentage for short-chain PFCAs on AE resin (A600, polystyrene-DVB gel-type) in their fixed-bed column studies. After 50,704 BVs (Bed Volume), the eliminating ability of the short-chained PFCAs tested was approximately 11% on an A600 column. Similar to the (Zaggia et al., 2016) report, PFBS was more effectively removed by the same anion exchange resin than by other short-chain compounds, with a removal efficiency of about 55% (McCleaf et al., 2017). Using superior resins like polystyrene-divinyl benzene instead of polymethacrylate and polyacrylic resins effectively eliminated 90% of PFAS in 24 h. The resin's efficiency stems from the fact that PFAS chain length, charge, and connected chemical moiety do not alter functioning as contact duration increases by 2 h. Furthermore, spent resin can be readily renewed using solutions of NaCl and NH_4Cl; however, the effectiveness of the regenerated resin for long-chain PFAS cannot be established (Liu and Sun, 2021).

3.6. Microbial degradation

The various benefits of biological remediation, such as reduced capital and operating costs and little soil and water exploitation through the use of cutting-edge technologies, make it the ideal method for removing contaminants (Pan et al., 2016; Kucharzyk et al., 2017; Pilli et al., 2021).

There are several contradictory findings and a paucity of studies that have examined the microbial degradation of PFASs, all of which point to the necessity for additional research to completely comprehend the biotic transformations of those substances (Kucharzyk et al., 2017).

For a primary attack to take place during the microbial cleavage of fluorinated alkyl compounds, the alkyl chain must include a minimum of one hydrogen atom (Prevedouros et al., 2006). Fluorine atoms' capacity to create a thick, HPB coating that envelops carbon-carbon bonds and inhibits oxidative degradation makes it more difficult to replace them oxidatively (Rayne and Forest, 2009). This unique component of the fluorine-saturated carbon chain provides environmental protection against oxidation or can be utilized by microorganisms as a supply of carbon and energy (Colosi et al., 2009).

It has been demonstrated that certain bacterial strains can break down PFASs in aerobic environments. H-PFOS and 2,2,2-trifluoroethane were among the sulfonates that Pseudomonas strain D2 largely decomposed with hydrogen by defluorination (Key et al., 1998), under limited sulfur and aerobic circumstances. Six compounds were produced by the defluorination reaction; all of them included fluorine and oxygen but no sulfur. *Pseudomonas butanova* was able to break down the precursor of 6–2 fluorotelomer alcohols (6-2 FTOH) in another investigation, but not that of 8–2 FTOH. *Actinobacteria* may also be able to proliferate on 8-2 FTOH (Kim, 2012; Kucharzyk et al., 2017). PFASs have also been studied in anaerobic transformation, however, the emphasis has been on polyfluorinated compounds. For instance, anaerobic (methanogenic) bioreactors loaded with community-sourced trash have been shown to contain known biodegradation intermediates and exhibit higher PFAS leakage in comparison to abiotic controls (Allred et al., 2015; Kucharzyk et al., 2017).

3.7. Fungal degradation

Experiments have been carried out to address the fungal breakdown of 6:2 FTOH. This experiment looked into the possibility of fungal biodegradation of 6:2 FTOH. The capacity of the bacterium *Phanerochaete chrysosporium* to convert roughly 50% of 6:2 FTOH was specifically examined. In this experiment, several medium components were used, and the fungal breakdown of 6:2 FTOH was monitored for a predetermined amount of time. The experiment's findings provide light on the possibility of fungus, specifically *Phanerochaete chrysosporium*, biodegrading 6:2 FTOH. Additionally, two strains of aerobic bacteria and five fungal strains that were obtained from an area contaminated with aqueous firefighting foam (AFFF) were used to evaluate the biodegradation capability of PFASs. The results showed that *P. chrysosporium* could convert almost half of the 6:2 FTOH and 70% of the 8:2 FTOH in 28 days (Tseng, 2012). In a different study (Colosi et al., 2009), the possibility of enzyme-catalyzed oxidative humidification (ECOHR) was considered. PFOA breakdown was facilitated by lignin peroxidase, manganese peroxidase, and laccase catalysis, which led to a thirty percent decrease in PFOA concentrations (Leonowicz et al., 1999). According to (Pilli et al., 2021), laccase-mediated ECOHR and laccase immobilized by GAC demonstrated over thirty percent PFOA mineralization and a twenty-five percent decrease, respectively, indicating their possibility for PFOA degradation. Fungal enzyme-based oxidative coupling processes mediated by laccases can also be utilized to remediate PFAs and other organic contaminants (Pan et al., 2016). Encapsulated ligninolytic enzymes are utilized in recent bioaugmentation research by (Mahendra et al., 2016) to biotransform PFAs.

3.8. Advanced oxidation process (AOP)

Reactive compounds that oxidize organic pollutants emit carbon dioxide or transform poisons into extremely biodegradable molecules. There are two ways to go about the contaminations' chemical oxidation: in-situ or ex-situ (Kucharzyk et al., 2017; Dombrowski et al., 2018; Coyle et al., 2021; Pilli et al., 2021). For the ex-situ mode to work well,

chemicals and soil particles must be mixed effectively (Mahinroosta and Senevirathna, 2020). In-situ oxidation entails the extraction of groundwater from one side of the polluted area and the delivery of oxidative chemicals to the other side through vertical good pressure injection (Sidebottom et al., 2016; McGregor, 2018). Because of the increased contact between the oxidant and the pollutant, permeability soils yield superior outcomes. Temperature, water content, organic matter, and other minerals and contaminants all affect how well oxidation processes work. Temperature variations should be considered while utilizing processes because the reaction rate is limited by a drop in temperature below 10 °C (Mahinroosta and Senevirathna, 2020).

Hydrogen peroxide, persulfate (PS), ozone (O_3), and potassium permanganate are all examples of chemical oxidants that can be employed alone or in combination. The carbonate matter in organic soils causes competing reactions that make treatment inefficient (Dombrowski et al., 2018; Mahinroosta and Senevirathna, 2020). Due to their high electronegativity, the fluorine atoms in PFAs' carbon structures—PFOS and PFOA, for example—cause a protracted rate of oxidation and a high energy need for the breaking of the C–F bond (Pilli et al., 2021; Kurwadkar et al., 2022). Permanganate (MnO_4^-) was utilized in a study to break down PFOS in reactors with extremely acidic conditions; after 18 days, the breakdown rate was 46.7% at 65 °C and 71.7% at 85° (Liu et al., 2012). Based on research (Hori et al., 2008; Dombrowski et al., 2018), PS ($S_2O_8^{2-}$) catalyzes the photochemical breakdown of aqueous PFCAs, including PFOA. Moreover, it has been noted that microwave-assisted PS oxidation (Lee et al., 2009) and UV radiation also degrade PFOA (Chen and Zhang, 2006). However, technologies that activate persulfate using microwaves or UV light are not suitable for in situ therapy (Dombrowski et al., 2018). Lin's team (Lin et al., 2012) found that ozone treatment at alkaline pH levels (pH = 11) degraded PFOS and PFOA by 85–100%, while no PFOS or PFOA breakdown was noted when ozonation was applied at pH values between 4 and 5. Alkaline environments are more conducive to the creation of superoxide radicals ($\bullet O_2^-$), and the writers of this work speculate that $\bullet O_2^-$ in alkaline circumstances accomplished the stated deterioration. Ozonation dose was the primary determinant of both ozonation and photocatalytic ozonation efficiency (Lin et al., 2012). A very high dose of ozone at pH 11, 8.7 g/h is capable of breaking down 99% of PFOA in 4 h. The efficacy of defluorination in photocatalytic ozonation was likewise influenced by the ozone dose and the pH of the treated aqueous mixture; however, in this instance, a lower pH promotes defluorination. As hydroxyl radicals speed up breakdown by oxidizing perfluoroalkyl radicals, photo-generating holes are crucial to the usage of an electron (e−) from the absorbed perfluorooctanoate anion in the photocatalytic ozonation breakdown process of PFOA (Trojanowicz et al., 2018). Also, because hydrogen peroxide and iron are more soluble in acidic environments than in circumneutral pH ranges, Fenton's reagent chemistry is carried out at pH 3 to 4 (Huling et al., 2006). Despite having the highest oxidation potential (2.7 eV) of all radical species suitable for in-situ chemical oxidation, hydroxyl radical is not very effective in degrading PFAS, such as PFOA and PFOS, according to the results of earlier studies (Moriwaki et al., 2005; Ahmad et al., 2012; Dombrowski et al., 2018). In a particular study, using a hydrothermal process, ZnO-rGO was effectively produced at 150 °C. PFOA degradation rate was assessed using comparative tests. The findings demonstrated that 99.2% of PFOA was destroyed in persulfate-assisted photocatalytic ozonation at room temperature using modest dosages of ozone and persulfate. When used as common oxidants in photocatalytic ozonation for PFOA degradation, sodium persulfate outperformed ammonium persulfate in terms of PFOA elimination. Common elements in natural water sources, such as chloride and humic acid, demonstrated inhibitory effects on the breakdown of PFOA. Persulfate concentration during PFOA oxidation was tracked, and the conversion of persulfate to sulfate ion was investigated. The principal intermediaries during the degradation of PFOA were PFHpA, PFHeA, PFPeA, and PFBA(Wu et al., 2018).

In another study (Zhang et al., 2019), a heat/persulfate oxidation system was used to degrade PFOA with 100% efficiency in 300 min. The findings have it that the initial e− abstraction from PFOA was the rate-limiting step, according to the DFT calculations, although a significant portion of the reaction's total ΔG was provided by the production of $SO_4^{\bullet-}$ during the breakdown of persulfate. The following actions did not affect the ΔG. In addition, the author studied interactions between protonated and deprotonated species of PFOA and $SO_4^{\bullet-}$ in order to examine e− abstraction from PFOA. The findings indicated that the most advantageous reaction was between anionic PFOA and $HSO_4^{\bullet}$, with an ΔG of 7.2 kJ/mol. This clarifies that persulfate's ability to degrade PFOA requires a low pH of less than 3.5 (Zhang et al., 2019). In another similar research (Lee et al., 2020), the viability of using PS in conjunction with iron-modified activated carbon (AC) for PFOA oxidation was assessed at temperatures that are comparatively ambient (15–45 °C). 61.7% of PFOA was broken down into fluoride ions and intermediates of short-chain PFCAs with a 41.9% defluorination efficiency at 25 °C after 600 min in the presence of Fe/AC in PS oxidation. Before PFOA is oxidized, a pre-concentration phase known as adsorption onto Fe@AC can be thought of. In addition to removing PFOA via adsorption, Fe@AC also forms sulfate radicals with PS, which hastens the breakdown and mineralization of PFOA. The activation energies of defluorination and PFOA elimination were notably decreased from 97.3 to 14.5 kJ/mol and 66.8 to 13.2 kJ/mol, respectively, using Fe/AC in the PS system. It suggests that defluorination and PFOA degradation possibly occur faster at a lower reaction temperature (Lee et al., 2020). In addition, MeOH, a recognized radical scavenger, was used in an electron-trapping experiment. It was discovered that after 600 min, the addition of MeOH significantly decreased the amount of PFOA degradation, which was 31.3% for Fe@AC/PS and 28.4% for AC/PS. The few exemplary PFAS degradation works by ozonation, and persulfate oxidation are presented in Table 2.

3.9. Electrochemical degradation

The main processes used in electrochemical oxidation to eliminate impurities are direct anodic oxidation and indirect oxidation. Impurities adsorb onto the anode surface during direct anodic oxidation, where they are eliminated by an electron transfer process (Pilli et al., 2021). Strong oxidants are produced by electrochemical processes at the cathode during indirect oxidation, which removes impurities from the solution and includes the breakdown process for PFOA and PFOS has been treated using electrochemical oxidation, according to (Pierpaoli et al., 2021).

For the removal of PFAs, researchers have mostly concentrated on boron-doped diamond (BDD) thin film, Ce/PbO_2, Ti/RuO_2, and Ti/SnO_2 among the large range of electrode components (Pt, IrO_2, and RuO_2). Under ideal circumstances, BDD thin-film electrodes can efficiently break down PFOS, PFDA, PFHxA, PFOA, PFBS, PFHxS, and PFBA. With a 2-h treatment, 97% of the PFOA was degraded (resulting in a 60% fluoride output) (Zhao et al., 2012). According to (Ochiai et al., 2011a, b), other studies using thin-film BDD electrodes have not had the same impact and have required a lot more time to decompose PFOA. The primary disadvantages of using BDD in comparison to other electrode materials are its high cost and labour-intensive manufacture (Panizza and Cerisola, 2009). The potential of cerium-doped lead dioxide film electrodes, Ti/RuO_2 (Schaefer et al., 2015), and commercially procurable Ti/SnO_2 anodes (Lin et al., 2012) for the removal of PFAs has also been investigated. According to reports, the usage of Ti/SnO_2-Sb anode has reduced PFOA by 90.3% to smaller chain PFCAs and fluoride (yielding 72.9% of fluoride) (Lin et al., 2012). One of the major drawbacks of utilizing electrochemical oxidation for the treatment of PFA-contaminated effluent combined with other hazardous compounds (e.g., hydrogen fluoride, bromate, chlorine gas) is the creation of toxic byproducts that are produced during the process (Trautmann et al., 2015) Furthermore, only two studies (Schaefer et al., 2015; Trautmann et al., 2015) have demonstrated PFA breakdown using this approach in

the presence of Aqueous film forming foams AFFF concentrate-impacted or PFA-contaminated industrial groundwater. This highlights the necessity for further study on the application of electrochemical oxidation for PFA elimination (Pilli et al., 2021).

3.10. Sonochemical destruction (sonolysis)

Hao and his team (Hao et al., 2014) described sonochemistry as the process of creating chemical reactions in a solution using a sonic field. The primary process that underpins the sonochemical breakdown of organic contaminants is water pyrolysis, which produces hydrogen atoms (H), oxygen atoms (O), and hydroxyl radicals. Vapour bubbles are created when ultrasonic radiation of aqueous solutions generates ultrasonic pressure waves. The bubble-water contact has a temperature of 600–1000 K, they experience quasi-adiabatic compression that raises interior vapour temperatures to around 4000 K (Chu et al., 2017; Trojanowicz et al., 2018). Compounds that partition at the gas-liquid interface, such as perfluorinated surfactants, or components in the bubbles' gas phase, could interact with water pyrolysis byproducts. In contrast to other components in the pretreated samples, such surface-active qualities may potentially contribute a selectivity factor to the sonolytic breakdown (Trojanowicz et al., 2018).

Ultrasound frequencies used for the sonochemical breakdown of PFASs typically vary from 20 to 1000 kHz or more than 0.5 MHz. Sonolysis has shown to be a successful technique in recent years for breaking down organic effluents including PFAS effluent into less hazardous chemicals (Kucharzyk et al., 2017). For instance, Fernandez and co-workers (Fernandez et al., 2016) examine the impact of chain length, functional head group, and substituents (-CH_2–CH_2– moiety and ether group) on the degradation percentage of various carboxylic and sulfonic PFASs, 1.7 mM total organic fluorine) using sonochemical degradation at 500 kHz. PFOS and PFOA, two common perfluoroalkyl compounds, showed defluorination rates of 3.5–3.7 μM F− min^{-1}, respectively, under these circumstances. The 1.3 and 1.9-fold lower defluorination efficiencies for perfluorohexane- and perfluorobutane sulfonate than those of PFOS suggest that the degradation efficiency of perfluoroalkyl sulfonates declined with the perfluorocarbon chain length. Sonolysis of perfluoroalkyl carboxylate resemblance with 6, 5, or 3 carbon atoms showed a comparable tendency to PFOA, with 1.1-, 1.8-, and 2.3-fold reduced defluorination rates, respectively. Additionally, it was shown that perfluoroalkyl compounds were more receptive to sonolysis than their polyfluoroalkyl counterparts with an equivalent number of C atoms (PFOS/6 [thin space (1/6-em)]: [thin space (1/6-em)]^2 fluorotelomer sulfonate ≈ 2.3 defluorination efficiency). The findings show that treating PFASs in aqueous streams using sonolysis is a potential strategy (Fernandez et al., 2016). In a study, Vecitis's team (Vecitis et al., 2010) sonochemically degraded a wide range of hydrocarbon and fluorochemical parts, including cosolvents, anionic hydrocarbon surfactants, fluorinated amphiphilic surface-active agents as well as anionic fluorinated surfactants. Sonolytic degradation of the major surfactants and PFOS occurred at a variety of aqueous dilutions, ranging from 65 mg/L to 13,100 mg/L of PFOS. Following 120 min of ultrasonic irradiation, 36% of the original moles of anionic surfactants and 73% of the first moles of PFOS were removed (Vecitis et al., 2010). The fact that PFOS's degradation rates were lower than those of the fluorinated amphiphilic surfactants indicates that part of their fluorochemical tail was still intact. Fluoride and sulfate concentrations were also tracked over time while the PFOS sonochemical breakdown process progressed. Quantitative sulfate generation indicates that the first stage of PFOS sonochemical breakdown is the loss of the sulfonyl functional group (Kucharzyk et al., 2017). Gaseous, gas-liquid transition, and bulk liquid zones are the three states of cavitation bubbles that determine how quickly organic molecules degrade by ultrasonication (Al-Hamadani et al., 2017; Pilli et al., 2021).

Highly HPB and volatile substances typically break down in the gaseous zone, whereas somewhat HPB and volatile substances break down in the gas-liquid transition and non-HPB and volatile substances may break down in bulk liquid zones (Pilli et al., 2021). When an ultrasonic frequency of 200 kHz was applied, it was discovered that PFO, PFOA, and perfluoro propionic acid (PFPrA) were the most degraded (Kucharzyk et al., 2017; Pilli et al., 2021). Notably, despite its strength, the ultrasonic reaction technique consumes a lot of energy since, when employed alone, sonication is not cost-effective concerning the total amount of energy input. In recent years, ultrasound coupled with advanced oxidation methods like persulfate oxidation have gained significant notice and demonstrated the ability to significantly enhance the rate at which pollutants like dyes, and PFAS can degrade (Hao et al., 2014).

For example, when Lei's research group (Lei et al., 2020) investigated the degradation of PFOA using a combination of ultrasonic and persulfate oxidation approaches, it was found that following a 360-min reaction, the dual-frequency ultrasonic-persulfate system's PFOA defluorination percentage was 100%. In contrast, the defluorination rates for the high-frequency US/PS, low-frequency ultrasonic-persulfate, dual-frequency ultrasonic, high-frequency ultrasonic, and low-frequency ultrasonic systems were 39.4%, 38.3%, 33.2%, 0.77%, 20.1%, and 14.6%, accordingly, These findings demonstrate that the dual-frequency ultrasonic-persulfate combination system has produced an improved PFOA defluorination result, suggesting that the two techniques might work in concert to breakdown PFOA (Lei et al., 2020).

3.11. Photocatalytic degradation

When a hv from sunlight or ultraviolet irradiation with energy equivalent to or larger than the nanocatalyst's energy gap is absorbed, photocatalysis takes place, and an electrons-holes pair is produced which in turn leads to the materialization of OH and O_2 radicals that participate in the pollutant degradation operation (Emmanuel et al., 2023; Adesibikan et al., 2024; Emmanuel et al., 2024a,b,c,d,e). Interestingly, many advances have been made in this pollutant removal technique, especially in the use of nanocomposites (Emmanuel et al., 2024a,b,c,d,e) for the degradation of PFAS. For example, Zhu et al. (2021) synthesized a novel adsorptive photocatalyst, Ga/TNTs@AC, based on activated carbon and TiO_2, and employed the composite to investigate the adsorption and photocatalytic degradation of PFOS. Notably, the Ga/TNTs@AC was able to break down 75.0% and mineralize 66.2% of pre-sorbed PFOS in 240 min under UV irradiation. The composite also demonstrated quicker adsorption kinetics and a stronger affinity for PFOS than the parent AC.

Ga/TNTs@AC is also regenerable by the effective PFOS photodegradation, enabling several uses without the need for chemical regenerants. The enhanced photoactivity is ascribed to the presence of oxygen vacancies, which not only inhibited $e-/h^+$ pair recombination but also promoted the formation of $\bullet O_2^-$. The PFOS degradation process, which begins with the cleavage of the sulfonate group and turns it into PFOA, which is then decarboxylated and defluorinated by the iterative defluorination mechanism, includes both h^+ and $\bullet O_2^-$. Both h^+ and $\bullet O_2^-$ played crucial functions in the photocatalytic degradation of PFOS, which begins with cleavage of the sulfonate group and turns it into PFOA which is subsequently decarboxylated and defluorinated by the iterative defluorination mechanism (Zhu et al., 2021). A similar scenario was also reported for the photocatalytic degradation of emerging contaminant PFOA in aqueous media by employing noble (Pt, Pd, Ag) metallic NPs modified TiO_2. In this study, a 100% degradation efficiency was achieved in 240 min (Li et al., 2016). In another experiment using BiOF photocatalysts under UV irradiation, 100% degradation of PFOA was reported. According to the author, the exposed (101 facets) BiOF photocatalyst and the right concentration of O_2 vacancy worked together to facilitate the electron passage from the defective surface to O_2. In addition, the presence of an oxygen vacancy (OV) created an intermediate band that reduced the energy needed for the electron transfer and shortened the bandgap. These two advantages facilitated the remarkable

PFOA degradation output (Wang et al., 2021a). More specifically, following the band structures and partial densities of states (PDOS) simulated by DFT as shown in Fig. 14, it was accentuated that it was effortless for the electrons excited in the VB to jump directly to the CB because BiOF VB maximum and CB minimum were positioned at the same high-symmetry points (Fig. 14a). Moreover, following the emergence of OV states, a new energy band emerged in the centre of the bandgap structure, as seen in Fig. 14b and c. Also, the PDOS shows that the 6p orbitals of Bi atoms were the primary source of the oxygen vacancy states (Fig. 14d). Notably, a key factor in the photocatalytic degradation process is the intermediate band that the OV generates. More importantly, in addition to splitting the initial band gap in half, the intermediate band serves as a "step" for the absorption of lower-energy photons. The half-filled Bi 6p state in the CB traps some of the excited electrons, reducing the energy needed for the electron transfer and narrowing the band gap of the OV-BiOF. The electron distribution maps of OV-BiOF and BiOF are displayed in Fig. 14e and **f**, which help to explain the charge transfer trend in the photocatalysts. The circles that are white, red, and blue, respectively, stand for OV, charge buildup, and charge exhaust. Oxygen's strong attraction to electrons resulted in an extraordinarily high electron cloud density surrounding O in the OV-BiOF. Additionally, a portion of the electron density moved from the Bi atoms to the abstracted oxygen atom's position on the OV surface. This demonstrates that oxygen vacancies may readily absorb electrons, preventing photoelectrons and holes from recombining and extending the lifespan of photogenerated electron-hole pairs (Wang et al., 2021a).

In another study, Gomez-Ruiz et al. (2018) used a composite catalyst made of TiO_2 and rGO which was prepared by a simple hydrothermal process, to explore the photocatalytic degradation of PFOA. Under the mercury lamp, the TiO_2-rGO nanocomposite demonstrated efficient photoactivity for PFOA degradation, reaching 93% after 12 h of irradiation. This is a significant enhancement over TiO_2 photocatalysis which gave 24 % PFOA degradation and direct photolysis which gave 58%. These results suggest that rGO, maybe as a result of serving as an electron acceptor and avoiding the high recombination electron-hole, supplied the appropriate characteristics of TiO_2-rGO. In addition, OH radical was seen to play a chief role in the photocatalytic degradation operation as shown in Fig. 15. Yang's team differed in their study as it was reported that the chief participation of h^+ gave 100% degradation of PFOA using BiOCl@Zn-Al as a photocatalyst under 500 W mercury arc lamp irradiation (Yang et al., 2020b). In the same spirit, Sheaf-like β-Ga_2O_3 was reported to outperform commercial β-Ga_2O_3 in photocatalytic efficiency due to increased adsorption and sites of reaction at the nanoplate interface, resulting in 100% photodegradation of PFOA within 45 min (Shao et al., 2013b). This claim is consistent with the findings of Wu's team (Wu et al., 2021) that the 100% PFOA photocatalytic degradation within 120 min by BiOCl NPS is primarily through the positive hole direct oxidation pathway. Using the DFT simulation, the authors further established the remarkable degradation is possible because the e−s were much easier to transfer from PFOA molecules to (0 1 0) -BiOCl-oxygen vacancy than (0 0 1)-BiOCl-oxygen vacancy as shown by the yellow areas in the former than in the later as displayed in Fig. 16g and h. In addition, the shape of the as-fabricated BiOCl samples before and following PFOA photocatalytic reactions did not significantly alter, according to the SEM images (Fig. 16a–d). Further evidence for the partial conversion of Bi^{3+} to lower charge Bi ions ($Bi^{(3-x)+}$) via localized electrons on OV was provided by the Bi 4f XPS of the as-fabricated BiOCl before and following photocatalytic degradation of PFOA (Fig. 16e and f). Both (001)-BiOCl-after and (010)-BiOCl-after showed two additional peaks. Additionally, the production of OV following the photocatalytic processes was shown by the O1s XPS (Wu et al., 2021).

In parallel to the above, BiOI@Bi_5O_7I demonstrated exceptional degradation efficiency in time, dose, initial PFOA concentration, and pH dependence manner under 800 W Xe irradiation. It was observed that the distinct band gap structure of the p-n heterojunction, which improved visible light absorbance and sped up the separation of photogenerated charge carriers, was primarily responsible for the greatly increased photocatalytic activity of the BiOI@Bi_5O_7I composite.

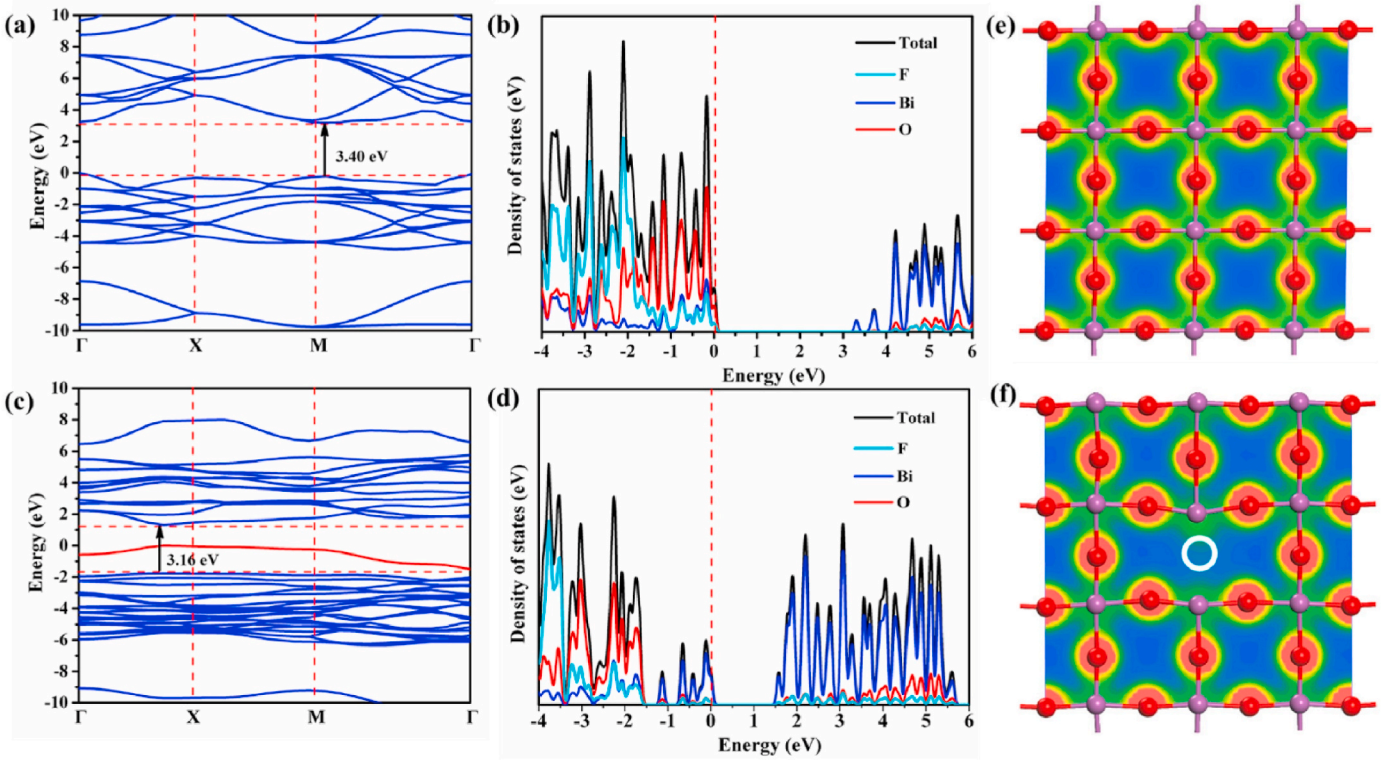

Fig. 14. (a, c) Band configuration, (b, d) partial/total densities of states, and (e, f) charge difference distributions and OV of BiOF (Wang et al., 2021c). Reused with permission from Elsevier (Approval code.: 5835031486415, Copyright 2021).

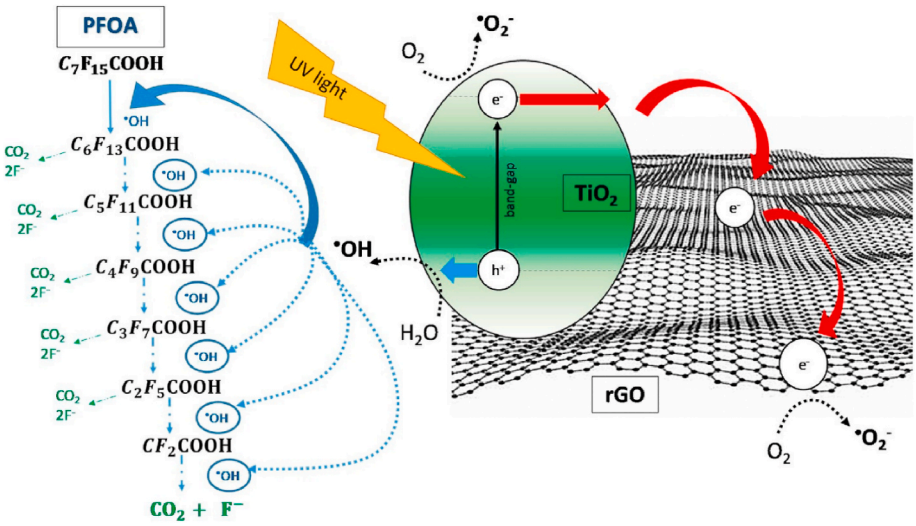

Fig. 15. Photocatalytic degradation mechanism of PFOA by TiO_2-rGO nanocomposite (Gomez-Ruiz et al., 2018). Reused with permission from Elsevier (Approval code.: 5835040533669, Copyright 2017).

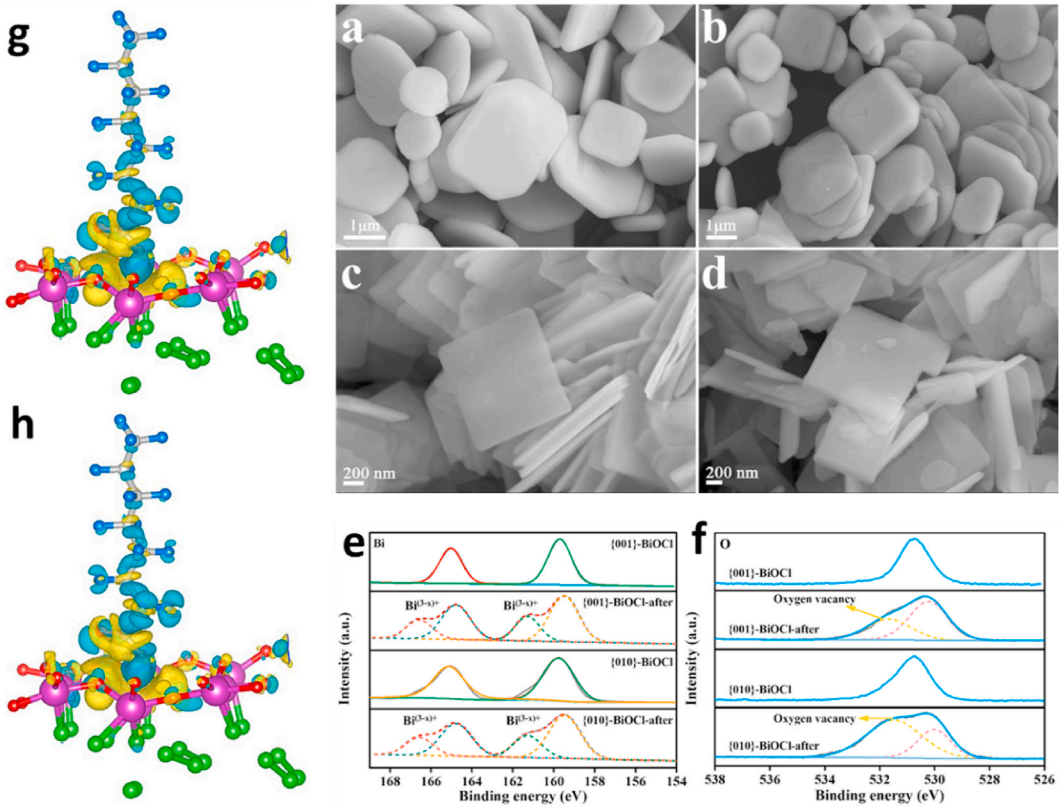

Fig. 16. SEM images of (0 0 1)-BiOCl (a: prior to; b: following) and (0 1 0)-BiOCl (c: prior to; d: following) for photocatalytic degradation of PFOA. XPS spectra for (e) Bi, 4f and (f) O, 1s of {001} or {010}-BiOCl NPs prior to and following the photocatalytic degradation of PFOA. DFT molecular architecture of (g) {0 0 1}-BiOCl facets, (h) {0 1 0}-BiOCl facets. The blue and yellow iso-surfaces represent the depletion and accumulation of charge respectively (Wu et al., 2021). Reused with permission from Elsevier (Approval code.: 5835041009977, Copyright 2021).

Specifically, when BiOI@Bi_5O_7I heterojunction nanocomposite was exposed to visible light, it generated radical •OH and other active species. These species then attacked the C−C bond between C_7F_{15} and COOH, resulting in the formation of •C_7F_{15}. After that, the •C_7F_{15} interacted with H_2O to create the unstable $C_7F_{15}OH$, which lost an HF and produced $C_6F_{13}COF$. PFHpA ($C_6F_{13}COOH$) was produced by further converting $C_6F_{13}COF$. The same degradation steps are repeated to create shorter chain molecules by continuously removing CF_2 units until harmless molecules like CO_2 and H_2O are produced at the end as shown in Fig. 17b (Wang et al., 2020a). Furthermore, according to Chen's team (Chen et al., 2021) as shown in Fig. 17c, PFOA first absorbs photogenerated e−s at the C (23)−F (11) position as indicated in the green marked area, which characterizes the C-F single bond made up of the No.23 C and the No.11 F atom. After taking on electrons, this one bond broke, resulting in the initial defluorination and the ejection of the F (11) anion (also known as hydrodefluorination). Subsequently, the C

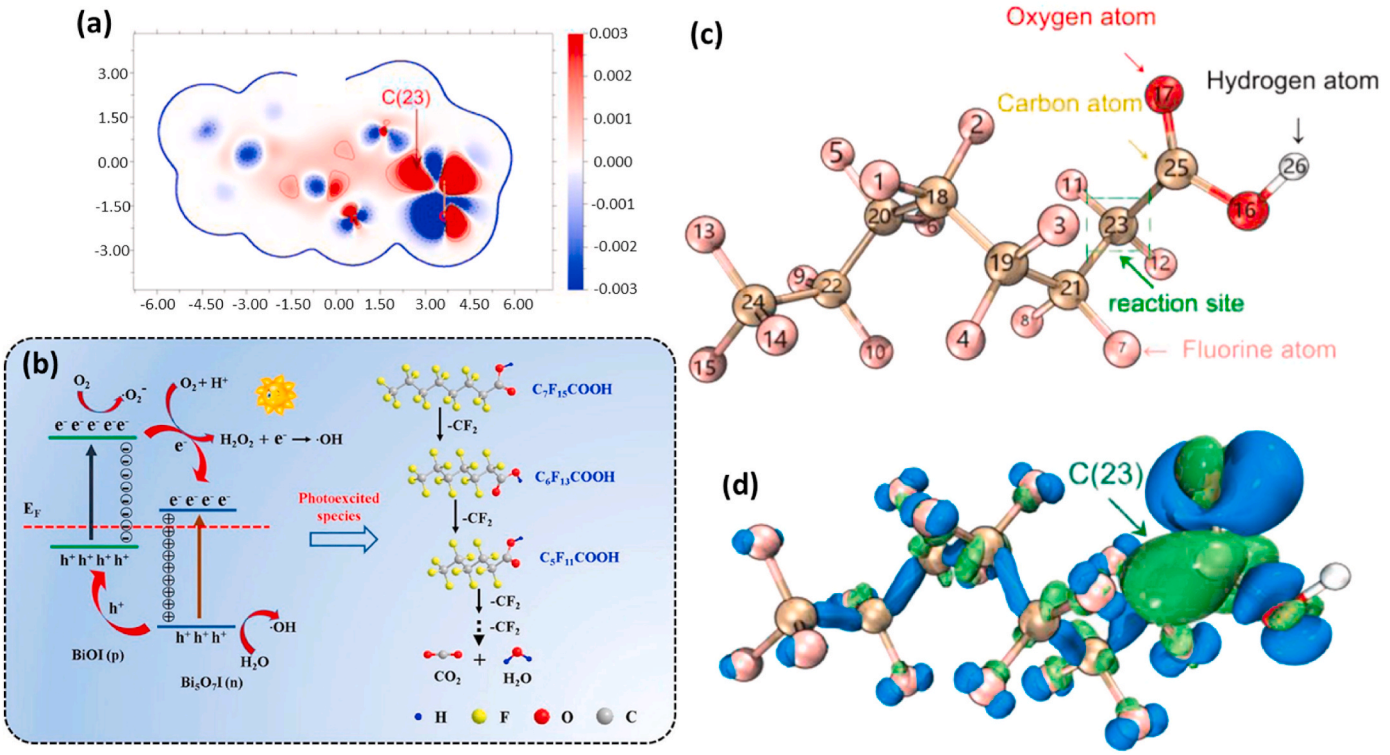

Fig. 17. (a) The Orbital-weighted duple descriptor Δf_w (r) distribution colour map for PFOA. Nucleophilic/electrophilic attack sensitivity is characterized by the blue/red colours (negative/positive values) (Chen et al., 2021). Reused with permission from Elsevier (Approval code.: 5835041385569, Copyright 2021). (b). Overview of the plausible degradation pathway of PFOA under UV light irradiation by BiOI@Bi_5O_7I p-n heterojunction photocatalyst (Wang et al., 2020a) Reused with permission from Elsevier (Approval code.: 5835050155349, Copyright 2019)., (c) Molecular 3-D configuration image of PFOA, numbers denote the tags of various atoms. The green-marked broken line border characterizes the reaction spot between PFOA and photo e−s. (d) Duple descriptor isosurfaces. Blue/Green (negative/positive values) denote the area of strong nucleophilicity and electrophilicity which favour gaining and donating electrons, respectively (Chen et al., 2021). Reused with permission from Elsevier (Approval code.: 5835041385569, Copyright 2021).

(23)-F (12) single bond underwent the same reaction, resulting in the second defluorination and the F (12) anion's discharge. Effectively describing the electronic and nucleophilic properties of various atoms in PFOA molecules is the orbital-weighted double descriptor. The capacity to receive e−s increases with the strength of the electron-philic atom. Additionally, to corroborate the findings, an examination of the nucleophilic/electrophilic reaction zones in PFOA revealed that, among the C atoms in the −C−F bonds, the C (23) atom possessed the greatest Δfw (r) of 0.02534 a.u., indicating a preference for interactions involving groups rich in e−s. Furthermore, as seen in Fig. 17a, it was discovered that the carbon atoms Δfw (r) value surged as it got closer to the C (25) in the carboxyl group. This is most likely due to the carboxyl group's potent electronegative nature, which further lowers the electron density of ortho-C atoms and encourages the transfer of electrons from C atoms to O_2 atoms. A sizable green domain encircling C (23) is seen in Fig. 17d, suggesting that Δfw (r) was positive and that this area was very electrophilic and inclined to absorb electrons. On the other hand, Fig. 17a's red and blue regions close to the C (23) atom and O (16) atom, respectively, imply that the C (23) atom is part of a common electron deficient area that easily absorbs electrons (Chen et al., 2021).

Surprisingly, in a particular study (Chen et al., 2021) only 50% degradation efficiency was obtained for the elimination of PFOA by Pt/$La_2Ti_2O_7$ under UV irradiation. However, the composite was still found to outperform the bare individual nanocomponents. Interestingly, the authors employed density functional theory to scrutinize the PFOA sorption energy on a $La_2Ti_2O_7$ or Pt/$La_2Ti_2O_7$ surface and built ternion probable sorption algorithms of PFOA on $La_2Ti_2O_7$ (101), Pt/$La_2Ti_2O_7$ (101), and Pt (111) surfaces as shown in Fig. 18. As shown in Fig. 18, the sorption energy of PFOA changes depending on its architectural locations when it adsorbs on the surfaces of Pt, $La_2Ti_2O_7$, or Pt/$La_2Ti_2O_7$. Majorly, the adsorption on the Pt/$La_2Ti_2O_7$ surface in Fig. 18 g and the perpendicular positioning of PFOA resulted in the most satisfactory sorption energy among all and binds more strongly than on bare $La_2Ti_2O_7$. However, on the Pt and $La_2Ti_2O_7$ surface, the sorption in Fig. 18a and **d** respectively, in which the carboxyl functional group principally interacts with Pt and LTO atoms led to the most satisfactory sorption energy as opposed to others in Fig. 18 that resulted in less favourable adsorption energy owing to the less reactive F_2 atoms interacting with Pt and $La_2Ti_2O_7$ atoms. Overall, the DFT simulation findings demonstrate that reductive charge transfer to the carboxyl group is caused by the favourite orientation of the PFOA interacting with the surface; additionally, the Pt/$La_2Ti_2O_7$ surface's larger charge transfer, improved adsorption energy, and lower band gap contribute to the pragmatic augmented reductive defluorination in juxtaposition to unfunctionalized $La_2Ti_2O_7$ (Chen et al., 2021).

Another jaw-dropping PFOA degradation output was recorded when the composite TiO_2 with multiwall carbon nanotube and the molecularly imprinted polymer-modified TiO_2 nanotubes were compared to pure TiO_2 under the same experimental conditions. Specifically, the multiwall carbon nanotube and the molecularly imprinted polymer-modified TiO_2 demonstrated superior PFOA photodegradation efficiency of 90% and 85% respectively within 480 min (Song et al., 2012). As can be seen in the summary made in Table 2, significant advances made in photocatalytic degradation of PFAS revealed that nanocomposites are more efficacious than the individual materials that made up the composites. Moreover, combining photocatalytic degradation with other advanced methods like ozonation has also improved the cleanup output of PFAS and thus demands more attention.

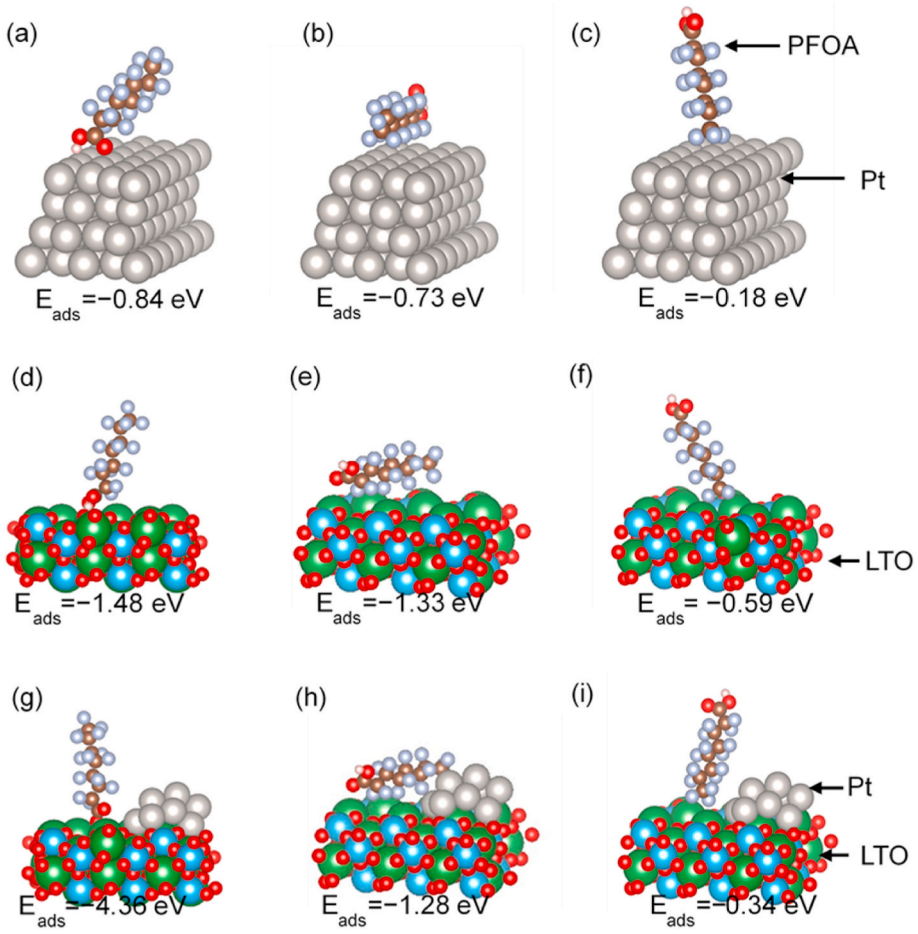

Fig. 18. The constructed PFOA adsorption by DFT simulation on Pt (111) surface (a), (b), and (c); on $La_2Ti_2O_7$ surface (d), (e), and (f); The constructed PFOA by DFT simulation without H atom adsorption on Pt/$La_2Ti_2O_7$ surface (g); The constructed PFOA adsorption by DFT simulation on Pt/$La_2Ti_2O_7$ surface (h) and (i). La, Ti O, C, H, and F atoms are denoted by green, blue, red, brown, pink, and silver, correspondingly (Chen et al., 2021). Reused with permission from Elsevier (Approval code.: 5835050572730, Copyright 2021).

4. Future perspectives

The urgent challenge of PFAS contamination requires innovative techniques for effective mitigation. Key areas for further development include the advancement of remediation technologies such as advanced oxidation processes (AOPs), bioaugmentation, and phytoremediation. Additionally, research into nanotechnology and engineered materials, including metal-organic frameworks, may enhance PFAS adsorption and degradation in contaminated environments. Efforts to identify non-fluorinated substitutes for PFAS in industrial processes and develop green chemistry alternatives for PFAS used in consumer goods are essential to prevent future contamination.

Establishing a strong international regulatory framework to restrict PFAS production and release is crucial. Harmonizing standards to encourage global cooperation is necessary for improved control measures. Policies should be implemented to reduce PFAS usage during manufacturing and incentivize end-users to adopt alternative substances. Public awareness campaigns are needed to educate communities about PFAS risks and advocate for stronger environmental protections.

Additionally, we think that the robustness of material fabrication for PFAS removal would be greatly improved by incorporating AI-assisted theoretical approaches to support the evaluation of experimental characteristics of these materials and allow scalable synthesis. Moreover, artificial intelligence may be used to create prediction models and simulations that help with experimental design, and reaction condition optimization, boosting efficiency and scalability. Researchers can more precisely regulate the size, shape, and composition of PFAS remediation materials with AI, producing higher-quality and more consistent results. This technology makes scalability more sustainable and economical by reducing the need for trial-and-error techniques and speeding up the development process (Adesibikan et al., 2024).

The development of sensitive, rapid, and cost-effective analytical methods for detecting PFAS in various matrices is imperative for sustainability. Advancements in sensor technology and portable detection devices could revolutionize real-time assessment of PFAS contamination. Multidisciplinary collaboration between chemistry, environmental science, toxicology, public health, and engineering is essential for innovative and comprehensive solutions.

Also, in the future, researchers can look into the use of a tribocatalytic/tribophotocatalytic degradation approach (Emmanuel & Adesibikan) as this area has not been researched for PFAS removal.

Exploring the use of genetically engineered microorganisms and plants for PFAS degradation, as well as harnessing synthetic biology and metabolic engineering, shows promise for breaking down PFAS into benign byproducts. Long-term, real-time monitoring programs are necessary to evaluate mitigation effectiveness and understand PFAS behaviour in the environment. Data from these programs will inform future remediation strategies and policy decisions.

5. Conclusion

In conclusion, combating PFAS pollution in wastewater requires a multidimensional approach that includes innovative technologies, stringent regulations, and engagement from the public. While adsorption, particularly with activated carbon, is highly effective, it faces problems such as energy-intensive regeneration and high operating costs. Other promising technologies include membrane filtration, improved oxidation processes, and ion exchange. Treatment decisions must take into account PFAS concentration, water quality, regulatory requirements, and site-specific considerations. Integrated techniques may provide synergistic benefits. Advances in material science and process engineering can improve PFAS removal efficiency and sustainability. Collaboration between researchers, industry, and regulatory authorities is critical to innovation and best practices. With persistent effort and comprehensive strategies, creating a PFAS-free environment is achievable.

CRediT authorship contribution statement

Ajibola A. Bayode: Writing – review & editing, Writing – original draft, Validation, Supervision, Project administration, Methodology, Investigation, Conceptualization. **Stephen Sunday Emmanuel:** Writing – review & editing, Writing – original draft, Validation, Methodology. **Amos O. Akinyemi:** Writing – original draft, Validation. **Odunayo T. Ore:** Writing – review & editing, Writing – original draft, Validation. **Samson O. Akpotu:** Writing – review & editing, Writing – original draft, Validation. **Daniel T. Koko:** Writing – review & editing, Writing – original draft, Validation, Supervision, Project administration. **David E. Momodu:** Writing – review & editing, Writing – original draft, Validation. **Eduardo Alberto López-Maldonado:** Writing – review & editing, Writing – original draft, Validation, Project administration.

Declaration of competing interest

The authors declare that they have no known competing financial interests or personal relationships that could have appeared to influence the work reported in this paper.

Data availability

No data was used for the research described in the article.

References

Abdullah, M.S., Goh, P.S., Ismail, A.F., Hasbullah, H., 2023. The treatment of endocrine-disruptive chemicals in wastewater through asymmetric reverse osmosis membranes: a review. Symmetry 15 (5), 1049.

Abunada, Z., Alazaiza, M.Y., Bashir, M.J., 2020. An overview of per-and polyfluoroalkyl substances (PFAS) in the environment: source, fate, risk and regulations. Water 12 (12), 3590.

Adesibikan, A.A., Emmanuel, S.S., Olawoyin, C.O., Ndungu, P., 2024. Cellulosic metallic nanocomposites for photocatalytic degradation of persistent dye pollutants in aquatic bodies: a pragmatic review. J. Organomet. Chem. 1010, 123087 https://doi.org/10.1016/j.jorganchem.2024.123087.

Ahmad, A., Tian, K., Tanyu, B., Foster, G.D., 2024. Sorption and diffusion of per-polyfluoroalkyl substances (PFAS) in high-density polyethylene geomembranes. Waste Manag. 174, 15–23.

Ahmad, M., Mitchell, S., Teel, A., Watts, R., 2012. Degradation of perfluorooctanoic acid (PFOA) by reactive species generated through catalyzed hydrogen peroxide propagation reactions. In: Situ Chemical Oxidation: Recent Advances, Battelle Conference, Columbus, Ohio.

Ahrens, L., Bundschuh, M., 2014. Fate and effects of poly-and perfluoroalkyl substances in the aquatic environment: a review. Environ. Toxicol. Chem. 33 (9), 1921–1929.

Al-Hamadani, Y.A., Park, C.M., Assi, L.N., Chu, K.H., Hoque, S., Jang, M., Yoon, Y., Ziehl, P., 2017. Sonocatalytic removal of ibuprofen and sulfamethoxazole in the presence of different fly ash sources. Ultrason. Sonochem. 39, 354–362.

Allred, B.M., Lang, J.R., Barlaz, M.A., Field, J.A., 2015. Physical and biological release of poly-and perfluoroalkyl substances (PFASs) from municipal solid waste in anaerobic model landfill reactors. Environ. Sci. Technol. 49 (13), 7648–7656.

Ambaye, T.G., Vaccari, M., Prasad, S., Rtimi, S., 2022. Recent progress and challenges on the removal of per-and poly-fluoroalkyl substances (PFAS) from contaminated soil and water. Environ. Sci. Pollut. Control Ser. 29 (39), 58405–58428.

Anderson, R.H., Adamson, D.T., Stroo, H.F., 2019. Partitioning of poly-and perfluoroalkyl substances from soil to groundwater within aqueous film-forming foam source zones. J. Contam. Hydrol. 220, 59–65.

Appleman, T.D., Dickenson, E.R., Bellona, C., Higgins, C.P., 2013a. Nanofiltration and granular activated carbon treatment of perfluoroalkyl acids. J. Hazard Mater. 260, 740–746.

Appleman, T.D., Dickenson, E.R.V., Bellona, C., Higgins, C.P., 2013b. Nanofiltration and granular activated carbon treatment of perfluoroalkyl acids. J. Hazard Mater. 260, 740–746. https://doi.org/10.1016/j.jhazmat.2013.06.033.

Appleman, T.D., Higgins, C.P., Quiñones, O., Vanderford, B.J., Kolstad, C., Zeigler-Holady, J.C., Dickenson, E.R., 2014. Treatment of poly-and perfluoroalkyl substances in US full-scale water treatment systems. Water Res. 51, 246–255.

Ateia, M., Alsbaiee, A., Karanfil, T., Dichtel, W., 2019. Efficient PFAS removal by amine-functionalized sorbents: critical review of the current literature. Environ. Sci. Technol. Lett. 6 (12), 688–695.

Bach, C.C., Bech, B.H., Brix, N., Nohr, E.A., Bonde, J.P.E., Henriksen, T.B., 2015. Perfluoroalkyl and polyfluoroalkyl substances and human fetal growth: a systematic review. Crit. Rev. Toxicol. 45 (1), 53–67.

Backe, W.J., Day, T.C., Field, J.A., 2013. Zwitterionic, cationic, and anionic fluorinated chemicals in aqueous film forming foam formulations and groundwater from US military bases by nonaqueous large-volume injection HPLC-MS/MS. Environ. Sci. Technol. 47 (10), 5226–5234.

Bangma, J., Guillette, T., Bommarito, P.A., Ng, C., Reiner, J.L., Lindstrom, A.B., Strynar, M.J., 2022. Understanding the dynamics of physiological changes, protein expression, and PFAS in wildlife. Environ. Int. 159, 107037.

Barber, J.L., Berger, U., Chaemfa, C., Huber, S., Jahnke, A., Temme, C., Jones, K.C., 2007. Analysis of per-and polyfluorinated alkyl substances in air samples from Northwest Europe. J. Environ. Monit. 9 (6), 530–541.

Barry, V., Winquist, A., Steenland, K., 2013. Perfluorooctanoic acid (PFOA) exposures and incident cancers among adults living near a chemical plant. Environ. Health Perspect. 121 (11–12), 1313–1318.

Bartels, J.L., Fernandez, S.R., Aweda, T.A., Alford, A., Peaslee, G.F., Garbow, J.R., Lapi, S.E., 2020. Comparative uptake and biological distribution of [18F]-labeled C6 and C8 perfluorinated alkyl substances in pregnant mice via different routes of administration. Environ. Sci. Technol. Lett. 7 (9), 665–671.

Barzen-Hanson, K.A., Roberts, S.C., Choyke, S., Oetjen, K., McAlees, A., Riddell, N., McCrindle, R., Ferguson, P.L., Higgins, C.P., Field, J.A., 2017. Discovery of 40 classes of per-and polyfluoroalkyl substances in historical aqueous film-forming foams (AFFFs) and AFFF-impacted groundwater. Environ. Sci. Technol. 51 (4), 2047–2057.

Baudequin, C., Mai, Z., Rakib, M., Deguerry, I., Severac, R., Pabon, M., Couallier, E., 2014. Removal of fluorinated surfactants by reverse osmosis–role of surfactants in membrane fouling. J. Membr. Sci. 458, 111–119.

Bayode, A.A., Emmanuel, S.S., Osti, A., Olorunnisola, C.G., Egbedina, A.O., Koko, D.T., Adedipe, D.T., Helmreich, B., Omorogie, M.O., 2024. Applications of perovskite oxides for the cleanup and mechanism of action of emerging contaminants/steroid hormones in water. J. Water Process Eng. 58, 104753.

Beans, C., 2021. How "forever chemicals" might impair the immune system. Proc. Natl. Acad. Sci. USA 118 (15), e2105018118.

Blake, B.E., Fenton, S.E., 2020. Early life exposure to per-and polyfluoroalkyl substances (PFAS) and latent health outcomes: a review including the placenta as a target tissue and possible driver of peri-and postnatal effects. Toxicology 443, 152565.

Boafo, Y.S., Mostafa, S., Obeng-Gyasi, E., 2023. Association of combined metals and PFAS with cardiovascular disease risk. Toxics 11 (12). https://doi.org/10.3390/toxics11120979.

Bolan, N., Sarkar, B., Vithanage, M., Singh, G., Tsang, D.C., Mukhopadhyay, R., Ramadass, K., Vinu, A., Sun, Y., Ramanayaka, S., 2021. Distribution, behaviour, bioavailability and remediation of poly-and per-fluoroalkyl substances (PFAS) in solid biowastes and biowaste-treated soil. Environ. Int. 155, 106600.

Borthakur, A., Wang, M., He, M., Ascencio, K., Blotevogel, J., Adamson, D.T., Mahendra, S., Mohanty, S.K., 2021. Perfluoroalkyl acids on suspended particles: significant transport pathways in surface runoff, surface waters, and subsurface soils. J. Hazard Mater. 417, 126159.

Brendel, S., Fetter, É., Staude, C., Vierke, L., Biegel-Engler, A., 2018. Short-chain perfluoroalkyl acids: environmental concerns and a regulatory strategy under REACH. Environ. Sci. Eur. 30, 1–11.

Buck, R.C., Franklin, J., Berger, U., Conder, J.M., Cousins, I.T., De Voogt, P., Jensen, A. A., Kannan, K., Mabury, S.A., van Leeuwen, S.P., 2011. Perfluoroalkyl and polyfluoroalkyl substances in the environment: terminology, classification, and origins. Integrated Environ. Assess. Manag. 7 (4), 513–541.

Bussian, B.M., Eugenio, N.R., Wilson, S.C., Ceci, A., Parelho, C., Semenov, D., Yahyaabadi, M., 2021. Main soil contaminants and their fate in the soil environment. In: Global Assessment of Soil Pollution: Report. Food and Agriculture Organization of the United Nations (FAO).

Cao, Y., Ng, C., 2021. Absorption, distribution, and toxicity of per-and polyfluoroalkyl substances (PFAS) in the brain: a review. Environ. Sci. J. Integr. Environ. Res.: Process. Impacts 23 (11), 1623–1640.

Carter, K.E., Farrell, J., 2010. Removal of perfluorooctane and perfluorobutane sulfonate from water via carbon adsorption and ion exchange. Separ. Sci. Technol. 45 (6), 762–767.

Chen, C., Ma, Q., Liu, F., Gao, J., Li, X., Sun, S., Yao, H., Liu, C., Young, J., Zhang, W., 2021. Photocatalytically reductive defluorination of perfluorooctanoic acid (PFOA) using Pt/La2Ti2O7 nanoplates: experimental and DFT assessment. J. Hazard Mater. 419, 126452 https://doi.org/10.1016/j.jhazmat.2021.126452.

Chen, H., Liu, M., Munoz, G., Duy, S.V., Sauve, S., Yao, Y., Sun, H., Liu, J., 2020. Fast generation of perfluoroalkyl acids from polyfluoroalkyl amine oxides in aerobic soils. Environ. Sci. Technol. Lett. 7 (10), 714–720.
Chen, J., Zhang, P., 2006. Photodegradation of perfluorooctanoic acid in water under irradiation of 254 nm and 185 nm light by use of persulfate. Water Sci. Technol. 54 (11–12), 317–325.
Chen, M.-J., Lo, S.-L., Lee, Y.-C., Huang, C.-C., 2015. Photocatalytic decomposition of perfluorooctanoic acid by transition-metal modified titanium dioxide. J. Hazard Mater. 288, 168–175. https://doi.org/10.1016/j.jhazmat.2015.02.004.
Chen, M.-J., Lo, S.-L., Lee, Y.-C., Kuo, J., Wu, C.-H., 2016a. Decomposition of perfluorooctanoic acid by ultraviolet light irradiation with Pb-modified titanium dioxide. J. Hazard Mater. 303, 111–118.
Chen, M.-J., Yang, A.-C., Wang, N.-H., Chiu, H.-C., Li, Y.-L., Kang, D.-Y., Lo, S.-L., 2016b. Influence of crystal topology and interior surface functionality of metal-organic frameworks on PFOA sorption performance. Microporous Mesoporous Mater. 236, 202–210. https://doi.org/10.1016/j.micromeso.2016.08.046.
Chi, Q., Li, Z., Huang, J., Ma, J., Wang, X., 2018. Interactions of perfluorooctanoic acid and perfluorooctanesulfonic acid with serum albumins by native mass spectrometry, fluorescence and molecular docking. Chemosphere 198, 442–449.
Chu, K.H., Al-Hamadani, Y.A., Park, C.M., Lee, G., Jang, M., Jang, A., Her, N., Son, A., Yoon, Y., 2017. Ultrasonic treatment of endocrine disrupting compounds, pharmaceuticals, and personal care products in water: a review. Chem. Eng. J. 327, 629–647.
Clark, C.A., Heck, K.N., Powell, C.D., Wong, M.S., 2019. Highly defective UiO-66 materials for the adsorptive removal of perfluorooctanesulfonate. ACS Sustain. Chem. Eng. 7 (7), 6619–6628.
Colosi, L.M., Pinto, R.A., Huang, Q., Weber, W.J.J., 2009. Peroxidase-mediated degradation of perfluorooctanoic acid. Environ. Toxicol. Chem.: Int. J. 28 (2), 264–271.
Costello, M.C.S., Lee, L.S., 2020. Sources, fate, and plant uptake in agricultural systems of per-and polyfluoroalkyl substances. Current Pollution Reports 1–21.
Cotruvo, J.A., Goldhaber, S.B., Cohen, A.J., 2023. EPA's unprecedented interim drinking water health advisories for PFOA and PFOS. Groundwater 61 (3), 301–303.
Cousins, I.T., DeWitt, J.C., Glüge, J., Goldenman, G., Herzke, D., Lohmann, R., Ng, C.A., Scheringer, M., Wang, Z., 2020. The high persistence of PFAS is sufficient for their management as a chemical class. Environ. Sci. J. Integr. Environ. Res.: Process. Impacts 22 (12), 2307–2312.
Coyle, C., Ghosh, R., Leeson, A., Thompson, T., 2021. US Department of Defense–funded research on treatment of per-and polyfluoroalkyl substance–laden materials. Environ. Toxicol. Chem. 40 (1), 44.
Crone, B.C., Speth, T.F., Wahman, D.G., Smith, S.J., Abulikemu, G., Kleiner, E.J., Pressman, J.G., 2019. Occurrence of per-and polyfluoroalkyl substances (PFAS) in source water and their treatment in drinking water. Crit. Rev. Environ. Sci. Technol. 49 (24), 2359–2396.
Cronin, K.S., 2024. Bystanders to a Public Health Crisis: the Failures of the US Multi-Agency Regulatory Approach to Food Safety in the Face of Persistent Organic Pollutants.
Dai, Z., Xia, X., Guo, J., Jiang, X., 2013. Bioaccumulation and uptake routes of perfluoroalkyl acids in Daphnia magna. Chemosphere 90 (5), 1589–1596.
Damião, G., Morgado, P., Silva, P., Martins, L.F., McCabe, C., Filipe, E.J., 2023. Perfluorinated pollutants in water: diffusion coefficient of perfluorosulfonic acids by molecular dynamics simulations. Fluid Phase Equil. 575, 113928.
Death, C., Bell, C., Champness, D., Milne, C., Reichman, S., Hagen, T., 2021. Per-and polyfluoroalkyl substances (PFAS) in livestock and game species: a review. Sci. Total Environ. 774, 144795.
Deng, S., Zhang, Q., Nie, Y., Wei, H., Wang, B., Huang, J., Yu, G., Xing, B., 2012. Sorption mechanisms of perfluorinated compounds on carbon nanotubes. Environ. Pollut. 168, 138–144.
deSilva, V., 2022. Pfas. In: The Challenge for Water/Wastewater Utilities. Utility Management Conference 2022.
Dhore, R., Murthy, G.S., 2021. Per/polyfluoroalkyl substances production, applications and environmental impacts. Bioresour. Technol. 341, 125808.
Dias, D., Bons, J., Kumar, A., Kabir, M.H., Liang, H., 2024. Forever chemicals, per-and polyfluoroalkyl substances (PFAS), in lubrication. Lubricants 12 (4), 114.
Ding, N., Harlow, S.D., Randolph Jr, J.F., Loch-Caruso, R., Park, S.K., 2020. Perfluoroalkyl and polyfluoroalkyl substances (PFAS) and their effects on the ovary. Hum. Reprod. Update 26 (5), 724–752.
Ding, X., Song, X., Chen, X., Ding, D., Xu, C., Chen, H., 2022. Degradation and mechanism of hexafluoropropylene oxide dimer acid by thermally activated persulfate in aqueous solutions. Chemosphere 286, 131720.
Dixit, F., Barbeau, B., Mostafavi, S.G., Mohseni, M., 2019. PFOA and PFOS removal by ion exchange for water reuse and drinking applications: role of organic matter characteristics [10.1039/C9EW00409B]. Environ. Sci. J. Integr. Environ. Res.: Water Research & Technology 5 (10), 1782–1795. https://doi.org/10.1039/C9EW00409B.
Dixit, F., Barbeau, B., Mostafavi, S.G., Mohseni, M., 2021a. PFAS and DOM removal using an organic scavenger and PFAS-specific resin: trade-off between regeneration and faster kinetics. Sci. Total Environ. 754, 142107.
Dixit, F., Dutta, R., Barbeau, B., Berube, P., Mohseni, M., 2021b. PFAS removal by ion exchange resins: a review. Chemosphere 272, 129777.
Dombrowski, P.M., Kakarla, P., Caldicott, W., Chin, Y., Sadeghi, V., Bogdan, D., Barajas-Rodriguez, F., Chiang, S.Y., 2018. Technology review and evaluation of different chemical oxidation conditions on treatability of PFAS. Remed. J. 28 (2), 135–150.
Douna, B.K., Yousefi, H., 2023. Removal of PFAS by biological methods. Asian Pacific Journal of Environment and Cancer 6 (1), 53–68.
Drew, R., Hagen, T.G., Champness, D., Sellier, A., 2022. Half-lives of several polyfluoroalkyl substances (PFAS) in cattle serum and tissues. Food Addit. Contam. 39 (2), 320–340.
Du, Z., Deng, S., Bei, Y., Huang, Q., Wang, B., Huang, J., Yu, G., 2014. Adsorption behavior and mechanism of perfluorinated compounds on various adsorbents—a review. J. Hazard Mater. 274, 443–454.
Du, Z., Deng, S., Chen, Y., Wang, B., Huang, J., Wang, Y., Yu, G., 2015. Removal of perfluorinated carboxylates from washing wastewater of perfluorooctanesulfonyl fluoride using activated carbons and resins. J. Hazard Mater. 286, 136–143. https://doi.org/10.1016/j.jhazmat.2014.12.037.
Dueñas-Mas, M.J., Ballesteros-Gómez, A., de Boer, J., 2023. Determination of several PFAS groups in food packaging material from fast-food restaurants in France. Chemosphere 339, 139734.
Ebrahimi, F., Lewis, A.J., Sales, C.M., Suri, R., McKenzie, E.R., 2021. Linking PFAS partitioning behavior in sewage solids to the solid characteristics, solution chemistry, and treatment processes. Chemosphere 271, 129530.
Eick, S.M., Enright, E.A., Geiger, S.D., Dzwilewski, K.L., DeMicco, E., Smith, S., Park, J.-S., Aguiar, A., Woodruff, T.J., Morello-Frosch, R., 2021. Associations of maternal stress, prenatal exposure to per-and polyfluoroalkyl substances (PFAS), and demographic risk factors with birth outcomes and offspring neurodevelopment: an overview of the ECHO. CA. IL prospective birth cohorts. Int. J. Environ. Res. Publ. Health 18 (2), 742.
Emmanuel, S.S., Adesibikan, A.A., Bayode, A.A., Olawoyin, C.O., Isukuru, E.J., Raji, O.Y., 2024a. A review on covalent organic frameworks with mult-site functional groups as superior adsorbents for adsorptive sequestration of radio-contaminants. J. Organomet. Chem., 123226
Emmanuel, S.S., Adesibikan, A.A., Olawoyin, C.O., Idris, M.O., 2024b. Photocatalytic degradation of maxilon dye pollutants using nano-architecture functional materials: a review. ChemistrySelect 9 (15), e202400316.
Emmanuel, S.S., Adesibikan, A.A., Saliu, O.D., Opatola, E.A., 2023. Greenly biosynthesized bimetallic nanoparticles for ecofriendly degradation of notorious dye pollutants: a review. Plant Nano Biology 3, 100024. https://doi.org/10.1016/j.plana.2023.100024.
Emmanuel, S.S., Idris, M.O., Olawoyin, C.O., Adesibikan, A.A., Aliyu, A.A., Suleiman, A. I., 2024c. Biosynthesized metallic nanoarchitecture for photocatalytic degradation of emerging organochlorine and organophosphate pollutants: a review. ChemistrySelect 9 (14), e202304956.
Emmanuel, S.S., Olawoyin, C.O., Adesibikan, A.A., Nafiu, S.A., Bayode, A.A., 2024d. Solvothermally and non-solvthermally fabricated covalent organic frameworks (COFs) for eco-friendly remediation of radiocontaminants in aquatic environments: a review. J. Organomet. Chem. 1005, 122984 https://doi.org/10.1016/j.jorganchem.2023.122984.
Emmanuel, S.S., Olawoyin, C.O., Adesibikan, A.A., Opatola, E.A., 2024e. A pragmatic review on bio-polymerized metallic nano-architecture for photocatalytic degradation of recalcitrant dye pollutants. J. Polym. Environ. 32 (1), 1–30.
Evangelou, M.W., Robinson, B.H.J.I., Health, P., 2022. The phytomanagement of PFAS-contaminated land, 19 (11), 6817.
Evich, M.G., Davis, M., Weber, E.J., Tebes-Stevens, C., Acrey, B., Henderson, W.M., Goodrow, S., Bergman, E., Washington, J.W., 2022. Environmental fate of Cl-PFPECAs: predicting the formation of PFAS transformation products in New Jersey soils. Environ. Sci. Technol. 56 (12), 7779–7788.
Fabregat-Palau, J., Vidal, M., Rigol, A., 2022. Examining sorption of perfluoroalkyl substances (PFAS) in biochars and other carbon-rich materials. Chemosphere 302, 134733.
Felix Sahayaraj, A., Joy Prabu, H., Maniraj, J., Kannan, M., Bharathi, M., Diwahar, P., Salamon, J., 2023. Metal–organic frameworks (MOFs): the next generation of materials for catalysis, gas storage, and separation. J. Inorg. Organomet. Polym. Mater. 33 (7), 1757–1781.
Fernandes, A., Lake, I., Dowding, A., Rose, M., Jones, N., Petch, R., Smith, F., Panton, S., 2019. The potential of recycled materials used in agriculture to contaminate food through uptake by livestock. Sci. Total Environ. 667, 359–370.
Fernandez, N.A., Rodriguez-Freire, L., Keswani, M., Sierra-Alvarez, R., 2016. Effect of chemical structure on the sonochemical degradation of perfluoroalkyl and polyfluoroalkyl substances (PFASs). Environ. Sci. J. Integr. Environ. Res.: Water Research & Technology 2 (6), 975–983.
Fitzgerald, N.J., Wargenau, A., Sorenson, C., Pedersen, J., Tufenkji, N., Novak, P.J., Simcik, M.F., 2018. Partitioning and accumulation of perfluoroalkyl substances in model lipid bilayers and bacteria. Environ. Sci. Technol. 52 (18), 10433–10440.
Gagliano, E., Sgroi, M., Falciglia, P.P., Vagliasindi, F.G., Roccaro, P., 2020. Removal of poly-and perfluoroalkyl substances (PFAS) from water by adsorption: role of PFAS chain length, effect of organic matter and challenges in adsorbent regeneration. Water Res. 171, 115381.
Garnett, K., Van Calster, G., 2021. The concept of essential use: a novel approach to regulating chemicals in the European Union. Transnational Environmental Law 10 (1), 159–187.
Gehrenkemper, L., Rühl, I., Westphalen, T., Simon, F., von der Au, M., Cossmer, A., Meermann, B., 2023. Investigating the uptake and fate of per-and polyfluoroalkylated substances (PFAS) in bean plants (Phaseolus vulgaris): comparison between target MS and sum parameter analysis via HR-CS-GFMAS. Environ. Sci. Eur. 35 (1), 104.
Ghisi, R., Vamerali, T., Manzetti, S., 2019. Accumulation of perfluorinated alkyl substances (PFAS) in agricultural plants: a review. Environ. Res. 169, 326–341.
Glüge, J., Scheringer, M., Cousins, I.T., DeWitt, J.C., Goldenman, G., Herzke, D., Lohmann, R., Ng, C.A., Trier, X., Wang, Z., 2020. An overview of the uses of per-and polyfluoroalkyl substances (PFAS). Environ. Sci. J. Integr. Environ. Res.: Process. Impacts 22 (12), 2345–2373.

Gomez-Ruiz, B., Ribao, P., Diban, N., Rivero, M.J., Ortiz, I., Urtiaga, A., 2018. Photocatalytic degradation and mineralization of perfluorooctanoic acid (PFOA) using a composite TiO2 −rGO catalyst. J. Hazard Mater. 344, 950–957. https://doi.org/10.1016/j.jhazmat.2017.11.048.

Guelfo, J.L., Korzeniowski, S., Mills, M.A., Anderson, J., Anderson, R.H., Arblaster, J.A., Conder, J.M., Cousins, I.T., Dasu, K., Henry, B.J., 2021. Environmental sources, chemistry, Fate, and transport of per-and Polyfluoroalkyl Substances: state of the science, key knowledge gaps, and recommendations presented at the August 2019 SETAC focus topic meeting. Environ. Toxicol. Chem. 40 (12), 3234–3260.

Hamid, H., Li, L.Y., Grace, J.R., 2018. Review of the fate and transformation of per-and polyfluoroalkyl substances (PFASs) in landfills. Environ. Pollut. 235, 74–84.

Han, D., Ma, Y., Huang, C., Zhang, X., Xu, H., Zhou, Y., Liang, S., Chen, X., Huang, X., Liao, H., 2019. Occurrence and source apportionment of perfluoroalkyl acids (PFAAs) in the atmosphere in China. Atmos. Chem. Phys. 19 (22), 14107–14117.

Hang, X., Chen, X., Luo, J., Cao, W., Wan, Y., 2015. Removal and recovery of perfluorooctanoate from wastewater by nanofiltration. Separ. Purif. Technol. 145, 120–129. https://doi.org/10.1016/j.seppur.2015.03.013.

Hansen, M.C., Børresen, M.H., Schlabach, M., Cornelissen, G., 2010. Sorption of perfluorinated compounds from contaminated water to activated carbon. J. Soils Sediments 10, 179–185.

Hao, F., Guo, W., Wang, A., Leng, Y., Li, H., 2014. Intensification of sonochemical degradation of ammonium perfluorooctanoate by persulfate oxidant. Ultrason. Sonochem. 21 (2), 554–558.

Hassell, K.L., Coggan, T.L., Cresswell, T., Kolobaric, A., Berry, K., Crosbie, N.D., Blackbeard, J., Pettigrove, V.J., Clarke, B.O., 2020. Dietary uptake and depuration kinetics of perfluorooctane sulfonate, perfluorooctanoic acid, and hexafluoropropylene oxide dimer acid (GenX) in a benthic fish. Environ. Toxicol. Chem. 39 (3), 595–603.

Hidalgo, A., Mora-Diez, N., 2016. Novel approach for predicting partition coefficients of linear perfluorinated compounds. Theor. Chem. Acc. 135, 1–11.

Høisæter, Å., Pfaff, A., Breedveld, G.D., 2019. Leaching and transport of PFAS from aqueous film-forming foam (AFFF) in the unsaturated soil at a firefighting training facility under cold climatic conditions. J. Contam. Hydrol. 222, 112–122.

Hoover, G.M., Chislock, M.F., Tornabene, B.J., Guffey, S.C., Choi, Y.J., De Perre, C., Hoverman, J.T., Lee, L.S., Sepúlveda, M.S., 2017. Uptake and depuration of four per/polyfluoroalkyl substances (PFASs) in northern leopard frog Rana pipiens tadpoles. Environ. Sci. Technol. Lett. 4 (10), 399–403.

Hori, H., Nagaoka, Y., Murayama, M., Kutsuna, S., 2008. Efficient decomposition of perfluorocarboxylic acids and alternative fluorochemical surfactants in hot water. Environ. Sci. Technol. 42 (19), 7438–7443.

Huling, S.G., Huling, S.G., Pivetz, B.E., 2006. In-situ chemical oxidation. In: Office of Research and Development, National Risk Management Laboratory.

Ji, W., Xiao, L., Ling, Y., Ching, C., Matsumoto, M., Bisbey, R.P., Helbling, D.E., Dichtel, W.R., 2018. Removal of GenX and perfluorinated alkyl substances from water by amine-functionalized covalent organic frameworks. J. Am. Chem. Soc. 140 (40), 12677–12681. https://doi.org/10.1021/jacs.8b06958.

Jiang, F., Zhao, H., Chen, H., Xu, C., Chen, J., 2016. Enhancement of photocatalytic decomposition of perfluorooctanoic acid on CeO 2/In 2 O 3. RSC Adv. 6 (76), 72015–72021.

Jiang, Q., Gao, H., Zhang, L., 2015. Metabolic effects PFAS. Toxicological Effects of Perfluoroalkyl and Polyfluoroalkyl Substances, pp. 177–201.

Johnson, P.I., Sutton, P., Atchley, D.S., Koustas, E., Lam, J., Sen, S., Robinson, K.A., Axelrad, D.A., Woodruff, T.J., 2014. The Navigation Guide—evidence-based medicine meets environmental health: systematic review of human evidence for PFOA effects on fetal growth. Environ. Health Perspect. 122 (10), 1028–1039.

Jun, B.-M., Hwang, H.S., Heo, J., Han, J., Jang, M., Sohn, J., Park, C.M., Yoon, Y., 2019. Removal of selected endocrine-disrupting compounds using Al-based metal organic framework: performance and mechanism of competitive adsorption. J. Ind. Eng. Chem. 79, 345–352. https://doi.org/10.1016/j.jiec.2019.07.009.

Karbassiyazdi, E., Kasula, M., Modak, S., Pala, J., Kalantari, M., Altaee, A., Esfahani, M. R., Razmjou, A., 2023. A juxtaposed review on adsorptive removal of PFAS by metal-organic frameworks (MOFs) with carbon-based materials, ion exchange resins, and polymer adsorbents. Chemosphere 311, 136933.

Key, B.D., Howell, R.D., Criddle, C.S., 1998. Defluorination of organofluorine sulfur compounds by Pseudomonas sp. strain D2. Environ. Sci. Technol. 32 (15), 2283–2287.

Kim, M., Li, L.Y., Grace, J.R., Yue, C., 2015. Selecting reliable physicochemical properties of perfluoroalkyl and polyfluoroalkyl substances (PFASs) based on molecular descriptors. Environ. Pollut. 196, 462–472.

Kim, M.H., 2012. Factors Affecting Biodefluorination of Fluorotelomer Alcohols (FTOHs): Degradative Microorganisms, Transformation Metabolites and Pathways, and Effects of Co-substrates.

Kim, Y., Pike, K.A., Gray, R., Sprankle, J.W., Faust, J.A., Edmiston, P.L., 2023. Non-targeted identification and semi-quantitation of emerging per-and polyfluoroalkyl substances (PFAS) in US rainwater. Environ. Sci. J. Integr. Environ. Res.: Process. Impacts 25 (11), 1771–1787.

Kolanczyk, R.C., Saley, M.R., Serrano, J.A., Daley, S.M., Tapper, M.A., 2023. PFAS biotransformation pathways: a species comparison study. Toxics 11 (1), 74.

Krafft, M.P., Riess, J.G., 2015. Per-and polyfluorinated substances (PFASs): environmental challenges. Curr. Opin. Colloid Interface Sci. 20 (3), 192–212.

Kucharzyk, K.H., Darlington, R., Benotti, M., Deeb, R., Hawley, E., 2017. Novel treatment technologies for PFAS compounds: a critical review. J. Environ. Manag. 204, 757–764.

Kurwadkar, S., Dane, J., Kanel, S.R., Nadagouda, M.N., Cawdrey, R.W., Ambade, B., Struckhoff, G.C., Wilkin, R., 2022. Per-and polyfluoroalkyl substances in water and wastewater: a critical review of their global occurrence and distribution. Sci. Total Environ. 809, 151003.

Lath, S., Navarro, D.A., Losic, D., Kumar, A., McLaughlin, M.J., 2018. Sorptive remediation of perfluorooctanoic acid (PFOA) using mixed mineral and graphene/carbon-based materials. Environ. Chem. 15 (8), 472–480. https://doi.org/10.1071/EN18156.

Lee, Y.-C., Li, Y.-f., Chen, M.-J., Chen, Y.-C., Kuo, J., Lo, S.-L., 2020. Efficient decomposition of perfluorooctanic acid by persulfate with iron-modified activated carbon. Water Res. 174, 115618.

Lee, Y.-C., Lo, S.-L., Chiueh, P.-T., Chang, D.-G., 2009. Efficient decomposition of perfluorocarboxylic acids in aqueous solution using microwave-induced persulfate. Water Res. 43 (11), 2811–2816.

Lee, Y.C., Li, Y.F., Lo, S.L., Kuo, J., Sun, W., Hu, C.Y., 2022. Decomposition of perfluorooctanic acid by carbon aerogel with persulfate. Chem. Eng. J. 430, 132900.

Lei, Y.-J., Tian, Y., Sobhani, Z., Naidu, R., Fang, C., 2020. Synergistic degradation of PFAS in water and soil by dual-frequency ultrasonic activated persulfate. Chem. Eng. J. 388, 124215.

Leonowicz, A., Matuszewska, A., Luterek, J., Ziegenhagen, D., Wojtaś-Wasilewska, M., Cho, N.-S., Hofrichter, M., Rogalski, J., 1999. Biodegradation of lignin by white rot fungi. Fungal Genet. Biol. 27 (2–3), 175–185.

Lesmeister, L., Lange, F.T., Breuer, J., Biegel-Engler, A., Giese, E., Scheurer, M., 2021. Extending the knowledge about PFAS bioaccumulation factors for agricultural plants–A review. Sci. Total Environ. 766, 142640.

Levchuk, I., Màrquez, J.J.R., Sillanpää, M., 2018. Removal of natural organic matter (NOM) from water by ion exchange–a review. Chemosphere 192, 90–104.

Li, D., Lee, C.-S., Zhang, Y., Das, R., Akter, F., Venkatesan, A.K., Hsiao, B.S., 2023a. Efficient removal of short-chain and long-chain PFAS by cationic nanocellulose [10.1039/D3TA01851B]. J. Mater. Chem. A 11 (18), 9868–9883. https://doi.org/10.1039/D3TA01851B.

Li, F., Wei, Z., He, K., Blaney, L., Cheng, X., Xu, T., Liu, W., Zhao, D., 2020. A concentrate-and-destroy technique for degradation of perfluorooctanoic acid in water using a new adsorptive photocatalyst. Water Res. 185, 116219 https://doi.org/10.1016/j.watres.2020.116219.

Li, H., Dong, Q., Zhang, M., Gong, T., Zan, R., Wang, W., 2023b. Transport behavior difference and transport model of long-and short-chain per-and polyfluoroalkyl substances in underground environmental media: a review. Environ. Pollut., 121579

Li, J., Sun, J., Li, P., 2022. Exposure routes, bioaccumulation and toxic effects of per-and polyfluoroalkyl substances (PFASs) on plants: a critical review. Environ. Int. 158, 106891.

Li, M., Sun, F., Shang, W., Zhang, X., Dong, W., Dong, Z., Zhao, S., 2021a. Removal mechanisms of perfluorinated compounds (PFCs) by nanofiltration: roles of membrane-contaminant interactions. Chem. Eng. J. 406, 126814 https://doi.org/10.1016/j.cej.2020.126814.

Li, M., Yu, Z., Liu, Q., Sun, L., Huang, W., 2016. Photocatalytic decomposition of perfluorooctanoic acid by noble metallic nanoparticles modified TiO2. Chem. Eng. J. 286, 232–238.

Li, R., Alomari, S., Stanton, R., Wasson, M.C., Islamoglu, T., Farha, O.K., Holsen, T.M., Thagard, S.M., Trivedi, D.J., Wriedt, M., 2021b. Efficient removal of per- and polyfluoroalkyl substances from water with zirconium-based metal–organic frameworks. Chem. Mater. 33 (9), 3276–3285. https://doi.org/10.1021/acs.chemmater.1c00324.

Li, X., Zhang, P., Jin, L., Shao, T., Li, Z., Cao, J., 2012a. Efficient photocatalytic decomposition of perfluorooctanoic acid by indium oxide and its mechanism. Environ. Sci. Technol. 46 (10), 5528–5534.

Li, Y., Yang, Z., Wang, Y., Bai, Z., Zheng, T., Dai, X., Liu, S., Gui, D., Liu, W., Chen, M., Chen, L., Diwu, J., Zhu, L., Zhou, R., Chai, Z., Albrecht-Schmitt, T.E., Wang, S., 2017. A mesoporous cationic thorium-organic framework that rapidly traps anionic persistent organic pollutants. Nat. Commun. 8 (1), 1354. https://doi.org/10.1038/s41467-017-01208-w.

Li, Z., Zhang, P., Li, J., Shao, T., Jin, L., 2013a. Synthesis of In2O3-graphene composites and their photocatalytic performance towards perfluorooctanoic acid decomposition. J. Photochem. Photobiol. Chem. 271, 111–116.

Li, Z., Zhang, P., Li, J., Shao, T., Wang, J., Jin, L., 2014. Synthesis of In2O3 porous nanoplates for photocatalytic decomposition of perfluorooctanoic acid (PFOA). Catal. Commun. 43, 42–46. https://doi.org/10.1016/j.catcom.2013.09.004.

Li, Z., Zhang, P., Shao, T., Li, X., 2012b. In2O3 nanoporous nanosphere: a highly efficient photocatalyst for decomposition of perfluorooctanoic acid. Appl. Catal. B Environ. 125, 350–357.

Li, Z., Zhang, P., Shao, T., Wang, J., Jin, L., Li, X., 2013b. Different nanostructured In2O3 for photocatalytic decomposition of perfluorooctanoic acid (PFOA). J. Hazard Mater. 260, 40–46. https://doi.org/10.1016/j.jhazmat.2013.04.042.

Lin, A.Y.-C., Panchangam, S.C., Chang, C.-Y., Hong, P.A., Hsueh, H.-F., 2012. Removal of perfluorooctanoic acid and perfluorooctane sulfonate via ozonation under alkaline condition. J. Hazard Mater. 243, 272–277.

Liu, C., Hatton, J., Arnold, W.A., Simcik, M.F., Pennell, K.D., 2020a. In situ sequestration of perfluoroalkyl substances using polymer-stabilized powdered activated carbon. Environ. Sci. Technol. 54 (11), 6929–6936.

Liu, C., Shih, K., Wang, F., 2012. Oxidative decomposition of perfluorooctanesulfonate in water by permanganate. Separ. Purif. Technol. 87, 95–100.

Liu, K., Zhang, S., Hu, X., Zhang, K., Roy, A., Yu, G., 2015. Understanding the adsorption of PFOA on MIL-101 (Cr)-based anionic-exchange metal–organic frameworks: comparing DFT calculations with aqueous sorption experiments. Environ. Sci. Technol. 49 (14), 8657–8665.

Liu, N., Wu, C., Lyu, G., Li, M., 2021. Efficient adsorptive removal of short-chain perfluoroalkyl acids using reed straw-derived biochar (RESCA). Sci. Total Environ. 798, 149191 https://doi.org/10.1016/j.scitotenv.2021.149191.

Liu, W., Lin, T., Zhang, X., Jiang, F., Yan, X., Chen, H., 2022. Adsorption of perfluoroalkyl acids on granular activated carbon supported chitosan: role of nanobubbles. Chemosphere 309, 136733.
Liu, Y.-L., Sun, M., 2021. Ion exchange removal and resin regeneration to treat per-and polyfluoroalkyl ether acids and other emerging PFAS in drinking water. Water Res. 207, 117781.
Liu, Y., Robey, N.M., Bowden, J.A., Tolaymat, T.M., da Silva, B.F., Solo-Gabriele, H.M., Townsend, T.G., 2020b. From waste collection vehicles to landfills: indication of per-and polyfluoroalkyl substance (PFAS) transformation. Environ. Sci. Technol. Lett. 8 (1), 66–72.
Lu, X., Deng, S., Wang, B., Huang, J., Wang, Y., Yu, G., 2016. Adsorption behavior and mechanism of perfluorooctane sulfonate on nanosized inorganic oxides. J. Colloid Interface Sci. 474, 199–205.
Lupton, S.J., Smith, D.J., Scholljegerdes, E., Ivey, S., Young, W., Genualdi, S., DeJager, L., Snyder, A., Esteban, E., Johnston, J.J., 2022. Plasma and skin per-and polyfluoroalkyl substance (PFAS) levels in dairy cattle with lifetime exposures to PFAS-contaminated drinking water and feed. J. Agric. Food Chem. 70 (50), 15945–15954.
Lyu, Y., Brusseau, M.L., 2020. The influence of solution chemistry on air-water interfacial adsorption and transport of PFOA in unsaturated porous media. Sci. Total Environ. 713, 136744.
Mahendra, S., Rome, L.H., Kickhoefer, V.A., Wang, M., 2016. Bioaugmentation with Vaults: Novel in Situ Remediation Strategy for Transformation of Perfluoroalkyl Compounds.
Mahinroosta, R., Senevirathna, L., 2020. A review of the emerging treatment technologies for PFAS contaminated soils. J. Environ. Manag. 255, 109896.
Maimaiti, A., Deng, S., Meng, P., Wang, W., Wang, B., Huang, J., Wang, Y., Yu, G., 2018. Competitive adsorption of perfluoroalkyl substances on anion exchange resins in simulated AFFF-impacted groundwater. Chem. Eng. J. 348, 494–502. https://doi.org/10.1016/j.cej.2018.05.006.
Mallya, D.S., Abdikheibari, S., Dumée, L.F., Muthukumaran, S., Lei, W., Baskaran, K., 2023. Removal of natural organic matter from surface water sources by nanofiltration and surface engineering membranes for fouling mitigation–A review. Chemosphere 321, 138070.
Maroufi, N., Hajilary, N., 2023. Nanofiltration membranes types and application in water treatment: a review. Sustainable Water Resources Management 9 (5), 142. https://doi.org/10.1007/s40899-023-00899-y.
McCleaf, P., Englund, S., Östlund, A., Lindegren, K., Wiberg, K., Ahrens, L., 2017. Removal efficiency of multiple poly-and perfluoroalkyl substances (PFASs) in drinking water using granular activated carbon (GAC) and anion exchange (AE) column tests. Water Res. 120, 77–87.
McGarr, J.T., Mbonimpa, E.G., McAvoy, D.C., Soltanian, M.R., 2023. Fate and transport of per-and polyfluoroalkyl substances (PFAS) at aqueous film forming foam (AFFF) discharge sites: a review. Soil Systems 7 (2), 53.
McGregor, R., 2018. In situ treatment of PFAS-impacted groundwater using colloidal activated carbon. Remed. J. 28 (3), 33–41.
McGuire, M., 2012. In-depth site characterization of poly-and perfluoroalkyl substances at an abandoned fire protection training area. 2012-Mine. Theses Diss. 1, 1, 3.
Medina, R., Pannu, M.W., Grieco, S.A., Hwang, M., Pham, C., Plumlee, M.H., 2022. Pilot-scale comparison of granular activated carbons, ion exchange, and alternative adsorbents for per-and polyfluoroalkyl substances removal. AWWA Water Science 4 (5), e1308.
Meegoda, J.N., Kewalramani, J.A., Li, B., Marsh, R.W., 2020. A review of the applications, environmental release, and remediation technologies of per-and polyfluoroalkyl substances. Int. J. Environ. Res. Publ. Health 17 (21), 8117.
Merino, N., Qu, Y., Deeb, R.A., Hawley, E.L., Hoffmann, M.R., Mahendra, S., 2016. Degradation and removal methods for perfluoroalkyl and polyfluoroalkyl substances in water. Environ. Eng. Sci. 33 (9), 615–649.
Militao, I.M., Roddick, F., Fan, L., Zepeda, L.C., Parthasarathy, R., Bergamasco, R., 2023. PFAS removal from water by adsorption with alginate-encapsulated plant albumin and rice straw-derived biochar. J. Water Process Eng. 53, 103616 https://doi.org/10.1016/j.jwpe.2023.103616.
Militao, I.M., Roddick, F.A., Bergamasco, R., Fan, L., 2021. Removing PFAS from aquatic systems using natural and renewable material-based adsorbents: a review. J. Environ. Chem. Eng. 9 (4), 105271.
Mishra, B., Varjani, S., Iragavarapu, G.P., Ngo, H.H., Guo, W., Vishal, B., 2019. Microbial fingerprinting of potential biodegrading organisms. Current Pollution Reports 5, 181–197.
Mojiri, A., Zhou, J.L., Ozaki, N., KarimiDermani, B., Razmi, E., Kasmuri, N., 2023. Occurrence of per-and polyfluoroalkyl substances in aquatic environments and their removal by advanced oxidation processes. Chemosphere 138666.
Moriwaki, H., Takagi, Y., Tanaka, M., Tsuruho, K., Okitsu, K., Maeda, Y., 2005. Sonochemical decomposition of perfluorooctane sulfonate and perfluorooctanoic acid. Environ. Sci. Technol. 39 (9), 3388–3392.
Mussabek, D., Ahrens, L., Persson, K.M., Berndtsson, R., 2019. Temporal trends and sediment–water partitioning of per-and polyfluoroalkyl substances (PFAS) in lake sediment. Chemosphere 227, 624–629.
Nguyen, T.M.H., Braunig, J., Kookana, R.S., Kaserzon, S.L., Knight, E.R., Vo, H.N.P., Kabiri, S., Navarro, D.A., Grimison, C., Riddell, N., 2022. Assessment of mobilization potential of per-and polyfluoroalkyl substances for soil remediation. Environ. Sci. Technol. 56 (14), 10030–10041.
Nguyen, T.M.H., Braunig, J., Thompson, K., Thompson, J., Kabiri, S., Navarro, D.A., Kookana, R.S., Grimison, C., Barnes, C.M., Higgins, C.P., 2020. Influences of chemical properties, soil properties, and solution pH on soil–water partitioning coefficients of per-and polyfluoroalkyl substances (PFASs). Environ. Sci. Technol. 54 (24), 15883–15892.
O'Connor, J., Bolan, N.S., Kumar, M., Nitai, A.S., Ahmed, M.B., Bolan, S.S., Vithanage, M., Rinklebe, J., Mukhopadhyay, R., Srivastava, P., 2022. Distribution, transformation and remediation of poly-and per-fluoroalkyl substances (PFAS) in wastewater sources. Process Saf. Environ. Protect. 164, 91–108.
Ochiai, T., Iizuka, Y., Nakata, K., Murakami, T., Tryk, D.A., Fujishima, A., Koide, Y., Morito, Y., 2011a. Efficient electrochemical decomposition of perfluorocarboxylic acids by the use of a boron-doped diamond electrode. Diam. Relat. Mater. 20 (2), 64–67.
Ochiai, T., Iizuka, Y., Nakata, K., Murakami, T., Tryk, D.A., Koide, Y., Morito, Y., Fujishima, A., 2011b. Efficient decomposition of perfluorocarboxylic acids in aqueous suspensions of a TiO2 photocatalyst with medium-pressure ultraviolet lamp irradiation under atmospheric pressure. Ind. Eng. Chem. Res. 50 (19), 10943–10947.
Ochoa-Herrera, V., Sierra-Alvarez, R., 2008. Removal of perfluorinated surfactants by sorption onto granular activated carbon, zeolite and sludge. Chemosphere 72 (10), 1588–1593.
Oh, J., Schmidt, R.J., Tancredi, D., Calafat, A.M., Roa, D.L., Hertz-Picciotto, I., Shin, H.-M., 2021. Prenatal exposure to per-and polyfluoroalkyl substances and cognitive development in infancy and toddlerhood. Environ. Res. 196, 110939.
Omo-Okoro, P.N., Curtis, C.J., Marco, A.M., Melymuk, L., Okonkwo, J.O., 2021. Removal of per-and polyfluoroalkyl substances from aqueous media using synthesized silver nanocomposite-activated carbons. Journal of Environmental Health Science and Engineering 19, 217–236.
Pala, J., Le, T., Kasula, M., Esfahani, M.R., 2023. Systematic investigation of PFOS adsorption from water by metal organic frameworks, activated carbon, metal organic framework@ activated carbon, and functionalized metal organic frameworks. Separ. Purif. Technol. 309, 123025.
Palmer, C.N., Hsu, M.-H., Griffin, K.J., Raucy, J.L., Johnson, E.F., 1998. Peroxisome proliferator activated receptor-α expression in human liver. Mol. Pharmacol. 53 (1), 14–22.
Pan, C.-G., Liu, Y.-S., Ying, G.-G., 2016. Perfluoroalkyl substances (PFASs) in wastewater treatment plants and drinking water treatment plants: removal efficiency and exposure risk. Water Res. 106, 562–570.
Panchangam, S.C., Lin, A.Y.-C., Shaik, K.L., Lin, C.-F., 2009. Decomposition of perfluorocarboxylic acids (PFCAs) by heterogeneous photocatalysis in acidic aqueous medium. Chemosphere 77 (2), 242–248.
Panchangam, S.C., Yellatur, C.S., Yang, J.-S., Loka, S.S., Lin, A.Y.C., Vemula, V., 2018. Facile fabrication of TiO2-graphene nanocomposites (TGNCs) for the efficient photocatalytic oxidation of perfluorooctanoic acid (PFOA). J. Environ. Chem. Eng. 6 (5), 6359–6369. https://doi.org/10.1016/j.jece.2018.10.003.
Panieri, E., Baralic, K., Djukic-Cosic, D., Buha Djordjevic, A., Saso, L., 2022. PFAS molecules: a major concern for the human health and the environment. Toxics 10 (2), 44.
Panizza, M., Cerisola, G., 2009. Direct and mediated anodic oxidation of organic pollutants. Chem. Rev. 109 (12), 6541–6569.
Park, M., Wu, S., Lopez, I.J., Chang, J.Y., Karanfil, T., Snyder, S.A., 2020. Adsorption of perfluoroalkyl substances (PFAS) in groundwater by granular activated carbons: roles of hydrophobicity of PFAS and carbon characteristics. Water Res. 170, 115364.
Pearson, T.W., Renfrew, D., 2024. When toxic heritage is forever: confronting PFAS contamination and toxicity as lived experience. In: Toxic Heritage. Routledge, pp. 50–61.
Pezeshki, H., Hashemi, M., Rajabi, S., 2023. Removal of arsenic as a potentially toxic element from drinking water by filtration: a mini review of nanofiltration and reverse osmosis techniques. Heliyon 9 (3), e14246.
Phung, T.V., Nguyen, T.D., Nguyen, T.N., Truong, T.K., Pham, H.V., Duong, H.A., 2024. Removal of perfluoroalkyl acids (PFAAs) from aqueous solution by water hyacinth (Eichhornia crassipes): uptake, accumulation, and translocation. Sci. Total Environ. 926, 172029.
Pierpaoli, M., Szopińska, M., Wilk, B.K., Sobaszek, M., Łuczkiewicz, A., Bogdanowicz, R., Fudala-Książek, S., 2021. Electrochemical oxidation of PFOA and PFOS in landfill leachates at low and highly boron-doped diamond electrodes. J. Hazard Mater. 403, 123606.
Pilli, S., Pandey, A.K., Pandey, V., Pandey, K., Muddam, T., Thirunagari, B.K., Thota, S. T., Varjani, S., Tyagi, R.D., 2021. Detection and removal of poly and perfluoroalkyl polluting substances for sustainable environment. J. Environ. Manag. 297, 113336.
Post, G.B., 2021. Recent US state and federal drinking water guidelines for per-and polyfluoroalkyl substances. Environ. Toxicol. Chem. 40 (3), 550–563.
Post, G.B., Cohn, P.D., Cooper, K.R., 2012. Perfluorooctanoic acid (PFOA), an emerging drinking water contaminant: a critical review of recent literature. Environ. Res. 116, 93–117.
Presentato, A., Lampis, S., Vantini, A., Manea, F., Daprà, F., Zuccoli, S., Vallini, G., 2020. On the ability of perfluorohexane sulfonate (PFHxS) bioaccumulation by two Pseudomonas sp. strains isolated from PFAS-contaminated environmental matrices. Microorganisms 8 (1), 92.
Prevedouros, K., Cousins, I.T., Buck, R.C., Korzeniowski, S.H., 2006. Sources, fate and transport of perfluorocarboxylates. Environ. Sci. Technol. 40 (1), 32–44.
Purohit, S.S., 2023. A systematic review of PFAS & subcategory chemicals: an overview of the testing methods and a comprehensive summary of the associated legislations at national & global level. Am. J. Chem. 13 (3), 49–67.
Qi, Y., Cao, H., Pan, W., Wang, C., Liang, Y., 2022. The role of dissolved organic matter during Per-and Polyfluorinated Substance (PFAS) adsorption, degradation, and plant uptake: a review. J. Hazard Mater. 436, 129139.
Qian, L., Kopinke, F.-D., Scherzer, T., Griebel, J., Georgi, A., 2022. Enhanced degradation of perfluorooctanoic acid by heat-activated persulfate in the presence of zeolites. Chem. Eng. J. 429, 132500.

Rahman, M.F., Peldszus, S., Anderson, W.B., 2014. Behaviour and fate of perfluoroalkyl and polyfluoroalkyl substances (PFASs) in drinking water treatment: a review. Water Res. 50, 318–340.

Ramírez Carnero, A., Lestido-Cardama, A., Vazquez Loureiro, P., Barbosa-Pereira, L., Rodríguez Bernaldo de Quirós, A., Sendón, R., 2021. Presence of perfluoroalkyl and polyfluoroalkyl substances (PFAS) in food contact materials (FCM) and its migration to food. Foods 10 (7). https://doi.org/10.3390/foods10071443.

Rappazzo, K.M., Coffman, E., Hines, E.P., 2017. Exposure to perfluorinated alkyl substances and health outcomes in children: a systematic review of the epidemiologic literature. Int. J. Environ. Res. Publ. Health 14 (7), 691.

Rayne, S., Forest, K., 2009. Perfluoroalkyl sulfonic and carboxylic acids: a critical review of physicochemical properties, levels and patterns in waters and wastewaters, and treatment methods. Journal of Environmental Science and Health Part A 44 (12), 1145–1199.

Rickard, B.P., Rizvi, I., Fenton, S.E., 2022. Per-and poly-fluoroalkyl substances (PFAS) and female reproductive outcomes: PFAS elimination, endocrine-mediated effects, and disease. Toxicology 465, 153031.

Riegel, M., Haist-Gulde, B., Sacher, F., 2023. Sorptive removal of short-chain perfluoroalkyl substances (PFAS) during drinking water treatment using activated carbon and anion exchanger. Environ. Sci. Eur. 35 (1), 12. https://doi.org/10.1186/s12302-023-00716-5.

Rivero, M.J., Ribao, P., Gomez-Ruiz, B., Urtiaga, A., Ortiz, I., 2020. Comparative performance of TiO2-rGO photocatalyst in the degradation of dichloroacetic and perfluorooctanoic acids. Separ. Purif. Technol. 240, 116637 https://doi.org/10.1016/j.seppur.2020.116637.

Rosenfeld, P.E., Spaeth, K.R., Remy, L.L., Byers, V., Muerth, S.A., Hallman, R.C., Summers-Evans, J., Barker, S., 2023. Perfluoroalkyl substances exposure in firefighters: sources and implications. Environ. Res. 220, 115164.

Rowe, R., Barakat, F., Patch, D., Weber, K., 2023. Diffusion and partitioning of different PFAS compounds through thermoplastic polyurethane and three different PVC-EIA liners. Sci. Total Environ. 892, 164229.

Ryu, S., Yamaguchi, E., Modaresi, S.M.S., Agudelo, J., Costales, C., West, M.A., Fischer, F., Slitt, A.L., 2024. Evaluation of 14 PFAS for permeability and organic anion transporter interactions: implications for renal clearance in humans. Chemosphere, 142390.

Sarkar, B., Mukhopadhyay, R., Ramanayaka, S., Bolan, N., Ok, Y.S., 2021. The role of soils in the disposition, sequestration and decontamination of environmental contaminants. Philosophical Transactions of the Royal Society B 376 (1834), 20200177.

Scarr, E., Fund, U.P.E., 2023. The Threat of "Forever Chemicals.

Schaefer, C.E., Andaya, C., Urtiaga, A., McKenzie, E.R., Higgins, C.P., 2015. Electrochemical treatment of perfluorooctanoic acid (PFOA) and perfluorooctane sulfonic acid (PFOS) in groundwater impacted by aqueous film forming foams (AFFFs). J. Hazard Mater. 295, 170–175.

Schaefer, C.E., Culina, V., Nguyen, D., Field, J., 2019. Uptake of poly-and perfluoroalkyl substances at the air–water interface. Environ. Sci. Technol. 53 (21), 12442–12448.

Schaefer, C.E., Drennan, D., Nickerson, A., Maizel, A., Higgins, C.P., 2021. Diffusion of perfluoroalkyl acids through clay-rich soil. J. Contam. Hydrol. 241, 103814.

Schillemans, T., Donat-Vargas, C., Lindh, C.H., de Faire, U., Wolk, A., Leander, K., Åkesson, A., 2022. Per- and polyfluoroalkyl substances and risk of myocardial infarction and stroke: a nested case-control study in Sweden. Environ. Health Perspect. 130 (3), 37007 https://doi.org/10.1289/ehp9791.

Schlezinger, J.J., Gokce, N., 2024. Perfluoroalkyl/polyfluoroalkyl substances: links to cardiovascular disease risk. Circ. Res. 134 (9), 1136–1159.

Schröder, H.F., José, H., Gebhardt, W., Moreira, R., Pinnekamp, J., 2010. Biological wastewater treatment followed by physicochemical treatment for the removal of fluorinated surfactants. Water Sci. Technol. 61 (12), 3208–3215.

Seltenrich, N., 2020. PFAS in food packaging: a hot, greasy exposure. Environ. Health Perspect. 128 (5), 054002.

Senevirathna, S.T.M.L.D., Tanaka, S., Fujii, S., Kunacheva, C., Harada, H., Shivakoti, B. R., Okamoto, R., 2010. A comparative study of adsorption of perfluorooctane sulfonate (PFOS) onto granular activated carbon, ion-exchange polymers and non-ion-exchange polymers. Chemosphere 80 (6), 647–651. https://doi.org/10.1016/j.chemosphere.2010.04.053.

Sepulvado, J.G., Blaine, A.C., Higgins, L.S.H.C.P., 2013. Occurrence and fate of poly-and perfluoroalkyl substances (pfass) in soil following the land application of municipal biosolids. SUBURFACE FATE AND TRANSPORT OF POLY-AND PERFLUOROALKYL SUBSTANCES 1001, 22.

Seyyedsalehi, M.S., Boffetta, P., 2023. Per-and poly-fluoroalkyl substances (pfas) exposure and risk of kidney, liver, and testicular cancers: a systematic review and meta-analysis. Med. Lavoro 114 (5).

Shaikh, M.A.N., Sarkar, P., Nawaz, T., 2023. PFOA remediation from aqueous media using CTAB impregnated activated carbon: a closed-loop sustainable study with comprehensive selectivity analysis. J. Water Process Eng. 54, 103965.

Shang, E., Li, Y., Niu, J., Li, S., Zhang, G., Wang, X., 2018. Photocatalytic degradation of perfluorooctanoic acid over Pb-BiFeO3/rGO catalyst: kinetics and mechanism. Chemosphere 211, 34–43. https://doi.org/10.1016/j.chemosphere.2018.07.130.

Shao, T., Zhang, P., Jin, L., Li, Z., 2013a. Photocatalytic decomposition of perfluorooctanoic acid in pure water and sewage water by nanostructured gallium oxide. Appl. Catal. B Environ. 142, 654–661.

Shao, T., Zhang, P., Li, Z., Jin, L., 2013b. Photocatalytic decomposition of perfluorooctanoic acid in pure water and wastewater by needle-like nanostructured gallium oxide. Chin. J. Catal. 34 (8), 1551–1559. https://doi.org/10.1016/S1872-2067(12)60612-3.

Sharifan, H., Bagheri, M., Wang, D., Burken, J.G., Higgins, C.P., Liang, Y., Liu, J., Schaefer, C.E., Blotevogel, J., 2021. Fate and transport of per-and polyfluoroalkyl substances (PFASs) in the vadose zone. Sci. Total Environ. 771, 145427.

Sharma, N., Kumar, V., Sugumar, V., Umesh, M., Sondhi, S., Chakraborty, P., Kaur, K., Thomas, J., Kamaraj, C., Maitra, S.S.J., Engineering, E., 2024. A Comprehensive Review on the Need for Integrated Strategies and Process Modifications for Per-And Polyfluoroalkyl Substances (PFAS) Removal: Current Insights and Future Prospects, 100623.

Shi, Y., Vestergren, R., Nost, T.H., Zhou, Z., Cai, Y., 2018. Probing the differential tissue distribution and bioaccumulation behavior of per-and polyfluoroalkyl substances of varying chain-lengths, isomeric structures and functional groups in crucian carp. Environ. Sci. Technol. 52 (8), 4592–4600.

Sidebottom, M.A., Pitenis, A.A., Junk, C.P., Kasprzak, D.J., Blackman, G.S., Burch, H.E., Harris, K.L., Sawyer, W.G., Krick, B.A., 2016. Ultralow wear Perfluoroalkoxy (PFA) and alumina composites. Wear 362, 179–185.

Sinclair, G.M., Long, S.M., Jones, O.A., 2020. What are the effects of PFAS exposure at environmentally relevant concentrations? Chemosphere 258, 127340.

Siriwardena, D.P., Crimi, M., Holsen, T.M., Bellona, C., Divine, C., Dickenson, E., 2019. Influence of groundwater conditions and co-contaminants on sorption of perfluoroalkyl compounds on granular activated carbon. Remed. J. 29 (3), 5–15.

Son, H., Kim, T., Yoom, H.-S., Zhao, D., An, B., 2020. The adsorption selectivity of short and long per- and polyfluoroalkyl substances (PFASs) from surface water using powder-activated carbon. Water 12 (11), 3287. https://www.mdpi.com/2073-4441/12/11/3287.

Song, C., Chen, P., Wang, C., Zhu, L., 2012. Photodegradation of perfluorooctanoic acid by synthesized TiO2–MWCNT composites under 365 nm UV irradiation. Chemosphere 86 (8), 853–859.

Song, H., Wang, Y., Ling, Z., Zu, D., Li, Z., Shen, Y., Li, C., 2020. Enhanced photocatalytic degradation of perfluorooctanoic acid by Ti3C2 MXene-derived heterojunction photocatalyst: application of intercalation strategy in DESs. Sci. Total Environ. 746, 141009.

Soriano, A., Schaefer, C., Urtiaga, A., 2020. Enhanced treatment of perfluoroalkyl acids in groundwater by membrane separation and electrochemical oxidation. Chemical Engineering Journal Advances 4, 100042. https://doi.org/10.1016/j.ceja.2020.100042.

Steenland, K., Winquist, A., 2021. PFAS and cancer, a scoping review of the epidemiologic evidence. Environ. Res. 194, 110690.

Steenland, K., Zhao, L., Winquist, A., Parks, C., 2013. Ulcerative colitis and perfluorooctanoic acid (PFOA) in a highly exposed population of community residents and workers in the mid-Ohio valley. Environ. Health Perspect. 121 (8), 900–905.

Steinle-Darling, E., Reinhard, M., 2008. Nanofiltration for trace organic contaminant removal: structure, solution, and membrane fouling effects on the rejection of perfluorochemicals. Environ. Sci. Technol. 42 (14), 5292–5297. https://doi.org/10.1021/es703207s.

Sun, R., Sasi, P.C., Alinezhad, A., Xiao, F., 2023. Sorptive removal of per-and polyfluoroalkyl substances (PFAS) in organic-free water, surface water, and landfill leachate and thermal reactivation of spent sorbents. Journal of Hazardous Materials Advances 10, 100311.

Sunderland, E.M., Hu, X.C., Dassuncao, C., Tokranov, A.K., Wagner, C.C., Allen, J.G., 2019. A review of the pathways of human exposure to poly-and perfluoroalkyl substances (PFASs) and present understanding of health effects. J. Expo. Sci. Environ. Epidemiol. 29 (2), 131–147.

Tang, C.Y., Fu, Q.S., Criddle, C.S., Leckie, J.O., 2007. Effect of flux (transmembrane pressure) and membrane properties on fouling and rejection of reverse osmosis and nanofiltration membranes treating perfluorooctane sulfonate containing wastewater. Environ. Sci. Technol. 41 (6), 2008–2014.

Tang, C.Y., Fu, Q.S., Robertson, A.P., Criddle, C.S., Leckie, J.O., 2006. Use of reverse osmosis membranes to remove perfluorooctane sulfonate (PFOS) from semiconductor wastewater. Environ. Sci. Technol. 40 (23), 7343–7349. https://doi.org/10.1021/es060831q.

Trautmann, A.M., Schell, H., Schmidt, K.R., Mangold, K.-M., Tiehm, A., 2015. Electrochemical degradation of perfluoroalkyl and polyfluoroalkyl substances (PFASs) in groundwater. Water Sci. Technol. 71 (10), 1569–1575.

Trojanowicz, M., Bojanowska-Czajka, A., Bartosiewicz, I., Kulisa, K., 2018. Advanced oxidation/reduction processes treatment for aqueous perfluorooctanoate (PFOA) and perfluorooctanesulfonate (PFOS)–a review of recent advances. Chem. Eng. J. 336, 170–199.

Tseng, N.S.-l., 2012. Feasibility of Biodegradation of Polyfluoroalkyl and Perfluoroalkyl Substances UCLA.

Urtiaga, A., Gomez-Lavin, S., Soriano, A., 2022. Electrochemical treatment of municipal landfill leachates and implications for poly-and perfluoroalkyl substances (PFAS) removal. J. Environ. Chem. Eng. 10 (3), 107900.

Vallero, D.A., 2023. Air Pollution Calculations: Quantifying Pollutant Formation, Transport, Transformation, Fate and Risks. Elsevier.

Varjani, S.J., Chaithanya Sudha, M., 2018. Treatment technologies for emerging organic contaminants removal from wastewater. Water remediation 91–115.

Vecitis, C.D., Wang, Y., Cheng, J., Park, H., Mader, B.T., Hoffmann, M.R., 2010. Sonochemical degradation of perfluorooctanesulfonate in aqueous film-forming foams. Environ. Sci. Technol. 44 (1), 432–438.

Verma, S., Varma, R.S., Nadagouda, M.N., 2021. Remediation and mineralization processes for per-and polyfluoroalkyl substances (PFAS) in water: a review. Sci. Total Environ. 794, 148987.

Vieira, V.M., Hoffman, K., Shin, H.-M., Weinberg, J.M., Webster, T.F., Fletcher, T., 2013. Perfluorooctanoic acid exposure and cancer outcomes in a contaminated community: a geographic analysis. Environ. Health Perspect. 121 (3), 318–323.

Vu, C.T., Wu, T., 2022. Recent progress in adsorptive removal of per-and poly-fluoroalkyl substances (PFAS) from water/wastewater. Crit. Rev. Environ. Sci. Technol. 52 (1), 90–129.
Vujic, E., Ferguson, S.S., Brouwer, K.L., 2024. Effects of PFAS on human liver transporters: implications for health outcomes. Toxicol. Sci. kfae061.
Wang, B., Lee, L.S., Wei, C., Fu, H., Zheng, S., Xu, Z., Zhu, D., 2016. Covalent triazine-based framework: a promising adsorbent for removal of perfluoroalkyl acids from aqueous solution. Environ. Pollut. 216, 884–892. https://doi.org/10.1016/j.envpol.2016.06.062.
Wang, J., Cao, C., Wang, Y., Wang, Y., Sun, B., Zhu, L., 2020a. In situ preparation of p-n BiOI@Bi5O7I heterojunction for enhanced PFOA photocatalytic degradation under simulated solar light irradiation. Chem. Eng. J. 391, 123530 https://doi.org/10.1016/j.cej.2019.123530.
Wang, J., Cao, C., Zhang, Y., Zhang, Y., Zhu, L., 2021a. Underneath mechanisms into the super effective degradation of PFOA by BiOF nanosheets with tunable oxygen vacancies on exposed (101) facets. Appl. Catal. B Environ. 286, 119911 https://doi.org/10.1016/j.apcatb.2021.119911.
Wang, J., Wang, L., Xu, C., Zhi, R., Miao, R., Liang, T., Yue, X., Lv, Y., Liu, T., 2018a. Perfluorooctane sulfonate and perfluorobutane sulfonate removal from water by nanofiltration membrane: the roles of solute concentration, ionic strength, and macromolecular organic foulants. Chem. Eng. J. 332, 787–797. https://doi.org/10.1016/j.cej.2017.09.061.
Wang, N., Lv, H., Zhou, Y., Zhu, L., Hu, Y., Majima, T., Tang, H., 2019. Complete defluorination and mineralization of perfluorooctanoic acid by a mechanochemical method using alumina and persulfate. Environ. Sci. Technol. 53 (14), 8302–8313.
Wang, P., Zhang, M., Li, Q., Lu, Y., 2021b. Atmospheric diffusion of perfluoroalkyl acids emitted from fluorochemical industry and its associated health risks. Environ. Int. 146, 106247.
Wang, T., Zhao, C., Li, P., Li, Y., Wang, J., 2015. Fabrication of novel poly(m-phenylene isophthalamide) hollow fiber nanofiltration membrane for effective removal of trace amount perfluorooctane sulfonate from water. J. Membr. Sci. 477, 74–85. https://doi.org/10.1016/j.memsci.2014.12.038.
Wang, W., Rhodes, G., Ge, J., Yu, X., Li, H., 2020b. Uptake and accumulation of per-and polyfluoroalkyl substances in plants. Chemosphere 261, 127584.
Wang, W., Xu, Z., Zhang, X., Wimmer, A., Shi, E., Qin, Y., Zhao, X., Zhou, B., Li, L., 2018b. Rapid and efficient removal of organic micropollutants from environmental water using a magnetic nanoparticles-attached fluorographene-based sorbent. Chem. Eng. J. 343, 61–68.
Wang, W., Zhou, Z., Shao, H., Zhou, S., Yu, G., Deng, S., 2021c. Cationic covalent organic framework for efficient removal of PFOA substitutes from aqueous solution. Chem. Eng. J. 412, 127509 https://doi.org/10.1016/j.cej.2020.127509.
Wang, Y., Zhang, P., 2011. Photocatalytic decomposition of perfluorooctanoic acid (PFOA) by TiO2 in the presence of oxalic acid. J. Hazard Mater. 192 (3), 1869–1875. https://doi.org/10.1016/j.jhazmat.2011.07.026.
Wang, Z., DeWitt, J.C., Higgins, C.P., Cousins, I.T., 2017. A Never-Ending Story of Per-And Polyfluoroalkyl Substances (PFASs)? ACS Publications.
Wanninayake, D.M., 2021. Comparison of currently available PFAS remediation technologies in water: a review. J. Environ. Manag. 283, 111977.
Weber, E.J., Tebes-Stevens, C., Washington, J.W., Gladstone, R., 2022. Development of a PFAS reaction library: identifying plausible transformation pathways in environmental and biological systems. Environ. Sci. J. Integr. Environ. Res.: Process. Impacts 24 (5), 689–753.
Wen, Y., Kong, Y., Peng, Y., Cui, X., 2022. Uptake, distribution, and depuration of emerging per-and polyfluoroalkyl substances in mice: role of gut microbiota. Sci. Total Environ. 853, 158372.
Witt, C.C., Gadek, C.R., Cartron, J.-L.E., Andersen, M.J., Campbell, M.L., Castro-Farias, M., Gyllenhaal, E.F., Johnson, A.B., Malaney, J.L., Montoya, K.N., 2024. Extraordinary levels of per-and polyfluoroalkyl substances (PFAS) in vertebrate animals at a New Mexico desert oasis: multiple pathways for wildlife and human exposure. Environ. Res., 118229
Woodruff, T.J., Zota, A.R., Schwartz, J.M., 2011. Environmental chemicals in pregnant women in the United States: NHANES 2003–2004. Environ. Health Perspect. 119 (6), 878–885.
Wu, C., Klemes, M.J., Trang, B., Dichtel, W.R., Helbling, D.E., 2020. Exploring the factors that influence the adsorption of anionic PFAS on conventional and emerging adsorbents in aquatic matrices. Water Res. 182, 115950.
Wu, D., Li, X., Zhang, J., Chen, W., Lu, P., Tang, Y., Li, L., 2018. Efficient PFOA degradation by persulfate-assisted photocatalytic ozonation. Separ. Purif. Technol. 207, 255–261.
Wu, Y., Hu, Y., Han, M., Ouyang, Y., Xia, L., Huang, X., Hu, Z., Li, C., 2021. Mechanism insights into the facet-dependent photocatalytic degradation of perfluorooctanoic acid on BiOCl nanosheets. Chem. Eng. J. 425, 130672 https://doi.org/10.1016/j.cej.2021.130672.
Xia, C., Qu, S., Bhattacharjee, L., Lim, X.E., Yang, H., Liu, J., 2023. Degradation of perfluoroalkyl substances using UV/Fe0 system with and without the presence of oxygen. Environ. Technol. 44 (18), 2725–2736.
Xiao, F., 2017. Emerging poly-and perfluoroalkyl substances in the aquatic environment: a review of current literature. Water Res. 124, 482–495.
Xu, B., Zhou, J.L., Altaee, A., Ahmed, M.B., Johir, M.A.H., Ren, J., Li, X., 2020a. Improved photocatalysis of perfluorooctanoic acid in water and wastewater by Ga2O3/UV system assisted by peroxymonosulfate. Chemosphere 239, 124722. https://doi.org/10.1016/j.chemosphere.2019.124722.
Xu, J., Liu, Z., Zhao, D., Gao, N., Fu, X., 2020b. Enhanced adsorption of perfluorooctanoic acid (PFOA) from water by granular activated carbon supported magnetite nanoparticles. Sci. Total Environ. 723, 137757 https://doi.org/10.1016/j.scitotenv.2020.137757.
Yadav, S., Ibrar, I., Al-Juboori, R.A., Singh, L., Ganbat, N., Kazwini, T., Karbassiyazdi, E., Samal, A.K., Subbiah, S., Altaee, A., 2022. Updated review on emerging technologies for PFAS contaminated water treatment. Chem. Eng. Res. Des. 182, 667–700.
Yan, P.-F., Dong, S., Manz, K.E., Woodcock, M.J., Liu, C., Mezzari, M.P., Abriola, L.M., Pennell, K.D., Cápiro, N.L., 2024a. Aerobic biotransformation of 6: 2 fluorotelomer sulfonate in soils from two aqueous film-forming foam (AFFF)-impacted sites. Water Res. 249, 120941.
Yan, P.-F., Dong, S., Woodcock, M.J., Manz, K.E., Garza-Rubalcava, U., Abriola, L.M., Pennell, K.D., Cápiro, N.L., 2024b. Biotransformation of 6: 2 fluorotelomer sulfonate and microbial community dynamics in water-saturated one-dimensional flow-through columns. Water Res. 252, 121146.
Yang, Y., Zheng, Z., Ji, W., Xu, J., Zhang, X., 2020a. Insights to perfluorooctanoic acid adsorption micro-mechanism over Fe-based metal organic frameworks: combining computational calculation with response surface methodology. J. Hazard Mater. 395, 122686 https://doi.org/10.1016/j.jhazmat.2020.122686.
Yang, Y., Zheng, Z., Yang, M., Chen, J., Li, C., Zhang, C., Zhang, X., 2020b. In-situ fabrication of a spherical-shaped Zn-Al hydrotalcite with BiOCl and study on its enhanced photocatalytic mechanism for perfluorooctanoic acid removal performed with a response surface methodology. J. Hazard Mater. 399, 123070 https://doi.org/10.1016/j.jhazmat.2020.123070.
Yao, Y., Volchek, K., Brown, C.E., Robinson, A., Obal, T., 2014. Comparative study on adsorption of perfluorooctane sulfonate (PFOS) and perfluorooctanoate (PFOA) by different adsorbents in water. Water Sci. Technol. 70 (12), 1983–1991. https://doi.org/10.2166/wst.2014.445.
Yin, S., López, J.F., Solís, J.J.C., Wong, M.S., Villagrán, D., 2023. Enhanced adsorption of PFOA with nano MgAl2O4@CNTs: influence of pH and dosage, and environmental conditions. Journal of Hazardous Materials Advances 9, 100252. https://doi.org/10.1016/j.hazadv.2023.100252.
Yuan, J., Mortazavian, S., Passeport, E., Hofmann, R., 2022a. Evaluating perfluorooctanoic acid (PFOA) and perfluorooctanesulfonic acid (PFOS) removal across granular activated carbon (GAC) filter-adsorbers in drinking water treatment plants. Sci. Total Environ. 838, 156406.
Yuan, Y., Feng, L., He, X., Liu, X., Xie, N., Ai, Z., Zhang, L., Gong, J., 2022b. Efficient removal of PFOA with an In2O3/persulfate system under solar light via the combined process of surface radicals and photogenerated holes. J. Hazard Mater. 423, 127176 https://doi.org/10.1016/j.jhazmat.2021.127176.
Zafeiraki, E., Gebbink, W.A., Hoogenboom, R.L., Kotterman, M., Kwadijk, C., Dassenakis, E., van Leeuwen, S.P., 2019. Occurrence of perfluoroalkyl substances (PFASs) in a large number of wild and farmed aquatic animals collected in The Netherlands. Chemosphere 232, 415–423.
Zaggia, A., Conte, L., Falletti, L., Fant, M., Chiorboli, A., 2016. Use of strong anion exchange resins for the removal of perfluoroalkylated substances from contaminated drinking water in batch and continuous pilot plants. Water Res. 91, 137–146.
Zango, Z.U., Jumbri, K., Sambudi, N.S., Ramli, A., Abu Bakar, N.H.H., Saad, B., Rozaini, M.N.H., Isiyaka, H.A., Jagaba, A.H., Aldaghri, O., 2020. A critical review on metal-organic frameworks and their composites as advanced materials for adsorption and photocatalytic degradation of emerging organic pollutants from wastewater. Polymers 12 (11), 2648.
Zhang, W., Pang, S., Lin, Z., Mishra, S., Bhatt, P., Chen, S., 2021. Biotransformation of perfluoroalkyl acid precursors from various environmental systems: advances and perspectives. Environ. Pollut. 272, 115908.
Zhang, Y., Moores, A., Liu, J., Ghoshal, S., 2019. New insights into the degradation mechanism of perfluorooctanoic acid by persulfate from density functional theory and experimental data. Environ. Sci. Technol. 53 (15), 8672–8681.
Zhao, B., Li, X., Yang, L., Wang, F., Li, J., Xia, W., Li, W., Zhou, L., Zhao, C., 2015. ß-Ga2O3 nanorod synthesis with a one-step microwave irradiation hydrothermal method and its efficient photocatalytic degradation for perfluorooctanoic acid. Photochem. Photobiol. 91 (1), 42–47.
Zhao, B., Lv, M., Zhou, L., 2012. Photocatalytic degradation of perfluorooctanoic acid with β-Ga2O3 in anoxic aqueous solution. J. Environ. Sci. 24 (4), 774–780.
Zhao, C., Hu, G., Hou, D., Yu, L., Zhao, Y., Wang, J., Cao, A., Zhai, Y., 2018. Study on the effects of cations and anions on the removal of perfluorooctane sulphonate by nanofiltration membrane. Separ. Purif. Technol. 202, 385–396. https://doi.org/10.1016/j.seppur.2018.03.046.
Zhao, C., Tang, C.Y., Li, P., Adrian, P., Hu, G., 2016. Perfluorooctane sulfonate removal by nanofiltration membrane—the effect and interaction of magnesium ion/humic acid. J. Membr. Sci. 503, 31–41. https://doi.org/10.1016/j.memsci.2015.12.049.
Zhao, C., Xu, Y., Xiao, F., Ma, J., Zou, Y., Tang, W., 2021. Perfluorooctane sulfonate removal by metal-organic frameworks (MOFs): insights into the effect and mechanism of metal nodes and organic ligands. Chem. Eng. J. 406, 126852 https://doi.org/10.1016/j.cej.2020.126852.
Zhao, C., Zhang, J., He, G., Wang, T., Hou, D., Luan, Z., 2013. Perfluorooctane sulfonate removal by nanofiltration membrane the role of calcium ions. Chem. Eng. J. 233, 224–232. https://doi.org/10.1016/j.cej.2013.08.027.
Zhou, W., Zhao, S., Tong, C., Chen, L., Yu, X., Yuan, T., Aimuzi, R., Luo, F., Tian, Y., Zhang, J., 2019. Dietary intake, drinking water ingestion and plasma perfluoroalkyl substances concentration in reproductive aged Chinese women. Environ. Int. 127, 487–494.
Zhou, Y., Li, Q., Wang, P., Li, J., Zhao, W., Zhang, L., Wang, H., Cheng, Y., Shi, H., Li, J., 2023. Associations of prenatal PFAS exposure and early childhood

neurodevelopment: evidence from the Shanghai Maternal-Child Pairs Cohort. Environ. Int. 173, 107850.
Zhu, Y., Xu, T., Zhao, D., Li, F., Liu, W., Wang, B., An, B., 2021. Adsorption and solid-phase photocatalytic degradation of perfluorooctane sulfonate in water using gallium-doped carbon-modified titanate nanotubes. Chem. Eng. J. 421, 129676 https://doi.org/10.1016/j.cej.2021.129676.
Zimmermann, L., Scheringer, M., Geueke, B., Boucher, J.M., Parkinson, L.V., Groh, K.J., Muncke, J., 2022. Implementing the EU Chemicals Strategy for Sustainability: the case of food contact chemicals of concern. J. Hazard Mater. 437, 129167.